On the Technical Challenges of Cognitive Radio in TV White Spaces



Thesis submitted to the University of Nottingham for the degree of

Master of Research (MRes)

Electrical and Electronic Engineering

by

Mir Muhammad Lodro, B.E., M.E.

Supervised by

Steve Greedy

George Green Institute for Electromagnetics Research-GGIEMR
Department of Electrical and Electronic Engineering

The University of Nottingham, University Park, UK

September 30, 2015

Abstract

Cognitive Radio (CR) has been considered as a powerful technique to increase the spectral efficiency by enabling unlicensed users to access unused spectrum opportunistically. Cognitive Radio has two important paradigms to efficiently utilise spectrum which are spectrum sensing and spectrum database. In spectrum sensing unlicensed users sense the spectrum and to detect the availability of under-utilised channels before transmission and access the channels when idle or tolerable interference to primary user (PU) is guaranteed. For the later case i.e. database paradigm of CR unlicensed users can acquire the availability of channels through spectrum database before accessing the channels. In this work, spectrum sensing part of the CR has been focused. In cognitive radio SU should yield maximum throughput and guarantee maximum PU protection. Sensing-throughput tradeoff has been studied for both single cognitive radio and cooperative cognitive radio with different fusion strategies. In cooperative cognitive radio OR and Optimal fusion strategies yielded maxim throughput than the AND strategy. Thereafter, the problem of throughput has been compared for both half-duplex cognitive radio and full-duplex cognitive radio for a given target probability of detection. It was found that there is an optimal sensing time at which a CR yields maximum throughput for a given target probability of detection. Much of the initial discussion is based on half-duplex communication cognitive radio (HDC-CR) using HDC-SS scheme. It is of special interest to derive the P_D, P_{FA} mathematical expressions for full-duplex communication cognitive radio (FDC-CR) which uses full-duplex spectrum sensing scheme to do sensing and transmission at the same time. It was found that the FDC-CR yields higher throughput for SU than the HDC-CR since FDC-CR performs sensing and data transmission at the same time therefore it gets increased data transmission time for secondary user.

Finally, this work resulted in conference papers and laid the foundation for numerous other ideas pertinent to cognitive radio for use in green wireless communication, small-cell dense wireless networks etc.

Conferences Papers

MirMuhammad Lodro, Steve Greedy, Chris Smartt, DWP Thomas, and Ana Vukovic "Sensing-Throughput Tradeoff for Cognitive Radio in TV White Spaces" in proceedings of 9th International Conference on Next Generation Mobile Applications, Services and Technologies (NGMAST2015), Emmanuel College, University of Cambridge, UK

MirMuhammad Lodro, Aziz Khuwaja, Chris Smartt "Energy-efficiency and Outage Analysis of Cooperative Green Cellular Communication Networks" was accepted in 36th IEEE Sarnoff Symposium 2015, NJIT, USA

MirMuhammad Lodro, Steve Greedy, Chris Smartt, Aziz A. Khuwaja, Ana Vukovic "A Short Review on Progress for 5G mmWave Cellular Communication Networks" was accepted in 36th IEEE Sarnoff Symposium 2015, NJIT, USA

The papers as enlisted below are under consideration for submission in one of the following conferences: 15th IEEE International Symposium on Signal Processing and Information Technology 2015, (ISSIT2015),IEEE Wireless Communication and Networking Conference (WCNC2016),IEEE International Conference on Communications, 2016 (ICC2016).

- "Multislot Sensing-throughput Tradeoff for Cooperative Cognitive Radio in TV White Space"
- "Time-slotted and Non time-slotted Multichannel Half-Duplex and Full-Duplex Communication Cognitive Radio"
- "Autocorrelation based Sensing and Sequential Detection of CP-OFDM Systems over Multipath Fading Channels"

Dedication

I dedicate this work to my father and mother and my whole family.

Declaration

This Work has been carried out by Mr. Mir Muhammad Lodro under the supervision of Dr. Steve Greedy at Department of Electrical and Electronic Engineering, The University of Nottingham, University Park, UK

Acknowledgment

I am highly thankful to my supervisors Steve Greedy and Christopher Smartt and internal assessor Prof. DWP Thomas. I am thankful to Prof. Thomas and Dr. Steve for funding my paper presentation and attendance of conference at the University of Cambridge, UK. Big thanks to Dr. Steve for his assistance, benign and supple attitude without his discretion and help this coherent assimilation of the work was not possible. I am also thankful to Dr. Alexander Kilashanikov and Prof. John Walker who became source of furthering and refining my concepts in Signal Processing and Digital Communication respectively; specially because of later's teaching style. I am exceptionally thankful to Dr. Ana Vukovic for her discussions and lectures on Wireless Communication which became an opportunity to glean the information to fill the voids of my wireless knowledge. Thanks to GGIEMR team for creating a *milieu-of-research* and confluence of ideas. Christopher's EMC machine is awesome! Thanks to Armando for unforgettable memories. I am also thankful to the University of Nottingham, England and Sukkur IBA, Sindh for funding my MRes studies in Electrical and Electronic Engineering at the University of Nottingham, UK.

Finally, I shall remain thankful to Pauline, Colin Guy and Piotr who helped me to get through the nightmare of installing correct versions of software in sequence for making Nutaq's picoSDR kit up and running.

List of Figures

1.1 Spectrum Usage Measurement over Six Locations[2] 23
1.2 Joseph Mitola's view of Cognitive Radio [4] 24
1.3 Haykin's view of CR[5] 25

2.1 A Typical Multipath Fading Scenario 29
2.2 Discrete Impulse Response of Mobile Channel 31
2.3 Typical Indoor Power Delay Profile 33
2.4 Doppler Shift Scenario 34
2.5 Frequency Flat and Frequency Selective Fading 35
2.6 Rayleigh and Rician Multipath Fading: No. of Samples=10^3 37
2.7 Gamma Distribution and Chi-squared Distribution with v Degrees of Freedom (DoF) 39
2.8 Spectrum Hole Concept 41
2.9 Spectrum Hole Concept 42
2.10 Spectrum Hole Concept 42
2.11 Receiver Operating Characteristics (ROC) Curves 44
2.12 SNR Wall versus Noise Uncertainty 46
2.13 Performance Comparison of Energy Detector and Matched Filter . . 47
2.14 Interference Temperature Model[12] 48

3.1 Nutaq's PicoSDR Teardown 52
3.2 PicoSDR Side View 54
3.3 BER performance of M-QAM and M-PSK in Rician fading with diversity order of $L = 2$ 55
3.4 PSD of OSTBC-QPSK Signal over 4x4 MIMO Channel 2-tap and 3-tap fading channel Respectively 56

3.5 BWRC's Berkeley Emulation Engine 59
3.6 BEE2 Board Layout 59
3.7 Rice University's WARP Prototype 61
3.8 White RHINO board[13] 62
3.9 RTL-SDR DVB-T, DAB+FM teardown 63
3.10 BBC Leicester FM 104.9 signal, waterfall graph,IF spectrum, MPx spectrum, and audio spectrum as received on DAB-T USB dongle at High Frequency Measurement and Characterization Lab,GGIEMR, The University of Nottingham,UK 64

4.1 Coexistence and Interference scenario of CRNs in TVWS 72
4.2 Database Architecture 73
4.3 Cognitive Radio ETSI Database Implementation 73

5.1 Null hypothesis and alternative hypothesis with increase in signal mean A, increase in sample size N and decrease in variance σ^2 . . . 79
5.2 Spectrogram and PSD of a sinusoid and AWGN noise with $\mu = 0$ and $\sigma = 1$ 80
5.3 Probability of detection for various values of probability of false alarm 83
5.4 Frame Structure used in Cognitive Radio 84
5.5 Probability of false alarm versus sensing time 88
5.6 Probability of detection versus sensing time 89
5.7 Probability of detection versus SNR 90
5.8 Minimum number of samples required versus probability of false alarm 90
5.9 Cooperative Cognitive Radio network coexisting with PU TV network 92
5.10 Secondary user maximum throughput versus sensing time 94
5.11 Probability of false alarm as a function of number of cooperative users OR fusion strategies 95
5.12 Probability of false alarm as a function of number of cooperative users AND fusion strategies 96
5.13 Average probability of detection as a function of sensing time in multi-slot sensing 101
5.14 Average probability of missed detection as a function of sensing time in multi-slot spectrum sensing 102

5.15 Average probability of false alarm as a function of sensing time with known channel coefficients . . . 103
5.16 Average probability of false alarm as a function of sensing time with unknown channel coefficients . . . 103
5.17 Normalized throughput as a function of sensing time in multislot scenario . . . 104
5.18 CDF and PDF of cumulative interference in Rayleigh fading . . . 108
5.19 Probability of beacon miss detection (Pmi) versus the distance r_i over Nakagami fading channel with different values of pathloss: $\beta = 0.001$,$\lambda = 0.01$,$\gamma = 10^{-6}$,$m = 2$,$M = 5$ . . . 109
5.20 Probability of beacon miss detection versus distance between beacon Tx and SU . . . 111
5.21 Mean of the cumulative interference versus cooperation distance with ML detection and OR sensing strategy . . . 111

6.1 OFDM Transmitter Architecture[21] . . . 115
6.2 OFDM Receiver Architecture[21] . . . 115
6.3 Consecutive OFDM subcarriers in time domain . . . 116
6.4 OFDM subcarrier spectrum . . . 117
6.5 Transmitter Architecture of NC-OFDM . . . 119
6.6 Receiver Architecture of NC-OFDM . . . 120
6.7 Peak-to-Average-Power-Ratio (PAPR) CCDF . . . 127
6.8 Peak-to-Average-Power-Ratio (PAPR) CCDF of BPSK . . . 127
6.9 PAPR Distribution in NC-OFDM Signal $\alpha = 1$ . . . 129
6.10 Throughput versus sensing time of OFDM based cognitive radio: $N_c = 8$,$N_d = 32$,$\lambda = 0.001$,$N_f = 100(N_c + N_d)$ . . . 135
6.11 Probability of detection P_D versus SNR for DVB-T standard: $T_d = 8192$,$T_c = 1024$,$\mu = 0.111$ . . . 142
6.12 Receiver Operating Characteristic (ROC) curves for DVB-T standard: $T_d = 8192$,$T_c = 1024$,$\mu = 0.111$ . . . 143
6.13 Receiver Operating Characteristic (ROC) curves for DVB-T, WLAN and LTE-A standards: $T_d = 8192$,$T_c = 1024$,$\mu = 0.111$; $T_d = 52$,$T_c = 13$,$\mu = 0.2$ and $T_d = 512$,$T_c = 36$,$\mu = 0.067$ respectively . . . 144

6.14 Multi-channel cognitive radio network model 147
6.15 Control model of non-slotted multi-channel CRN and time-slotted CRN 148
6.16 Spectrum sensing non-time slotted CRN (NTS-CRN) 148
6.17 Probability of detection of time slotted and non-time slotted full-duplex cognitive radio without self-interference 151
6.18 Probability of missed detection of time slotted and non-time slotted full-duplex cognitive radio without self-interference 152
6.19 Probability of detection of time slotted and non-time slotted full-duplex cognitive radio with and without interference 153
6.20 Probability of missed detection of time slotted and non-time slotted full-duplex cognitive radio with and without interference 154
6.21 Probability of false alarm of time slotted and non-time slotted full-duplex cognitive radio without self-interference 155
6.22 Probability of false alarm of time slotted and non-time slotted full-duplex cognitive radio with and without interference 155
6.23 Average throughput of saturated full-duplex cognitive radio 156

B.1 Nutaq's Perseus 601x Blockset and FPGA board configuration . . . 164
B.2 A set of perseus only examples as loaded on MATLAB 2011b 165
B.3 Complete QAM-64 OFDM Transceiver in Simulink 166
B.4 Configuration of Putty communication software 167
B.5 Initiating ADP CLI and connecting with perseus board 168
B.6 Complete path for launching radio420m-ofdm OFDM model 169
B.7 Complete system screen capture showing video transmission from host PC to Nutaq's PicoSDR 170

List of Tables

3.1 Computational requirements of White RHINO[13] 62

4.1 OFDM based cognitive wireless standards in TVWS 69

5.1 System Model Parameters 106

6.1 Theoretical approximation to CCDF of PAPR values[21] 126

6.2 P_D, P_{MD} and P_{FA} values for non-time slotted CRN with self-interference and without self-interference 153

List of Abbreviations

AD ..... Analog to Digital

AP ..... Access Point

AWGN ..... Additive White Gaussian Noise

AoA/AoD ..... Angle of Arrival/Angle of Departure

AFD ..... Average Fade Duration

BER ..... Bit Error Rate

BPSK ..... Binary Phase Shift Keying

BS ..... Base Station

BSDK ..... Board Software Development Kit

BSS ..... Basic Service Set

BWRC ..... Berkeley Wireless Research Center

CC ..... Convolutional Codes

CLT ..... Central Limit Theorem

CR ..... Cognitive Radio

CRN ..... Cognitive Radio Networks

CSCG ..... Circularly Symmetric Complex Gaussian

CSMA ..... Carrier Sense Multiple Access

CTS/RTS ..... Clear-To-Send/ Request-To-Send

CP ..... Cyclic Prefix

CPE ..... Customer Premises Equipment

CDF ..... Commulative Distribution Function

CVS ..... Contact Verification Signal

D/A ..... Digital to Analog

DAB-T ..... Digital Audio Broadcasting-Terrestrial

DDR3 ..... Double Data Rate Type 3

DFT ..... Discrete Fourier Transform

DS-CDMA ..... Direct Sequence-Code Division Multiple Access

D2D ..... Device-to-Device

DP ..... Data Period

DSA ..... Dynamic Spectrum Access

DoF ..... Degree of Freedom

DVB-T ..... Digital Video Broadcasting-Terrestrial

ECMA ..... European Computer Manufacturers Association

EIRP ..... Equivalent Isotropically Radiated Power

ETSI ..... European Telecommunication Standard Institute

ED ..... Energy Detector

FDC ..... Full-Duplex Communication

FDC-SS ..... Full-Duplex Spectrum Sensing

FER ..... Frame Error Rate

FFT ..... Fast Fourier Transform

FPGA ..... Field Programmable Gate Arrays

FCC ..... Federal Communication Commission

FDD ..... Frequency Division Duplex

FC ..... Fusion Center

GPS ..... Global Positioning System

GSM ..... Global System for Mobile Communication

GDB ..... Geolocation Database

GDD ..... GDB Dependent Station

HDC ..... Half-Duplex Communication

HDC-SS ..... Half-Duplex Spectrum Sensing

HDMI ..... High-Definition Multimedia Interface

HetNets ..... Heterogenous Networks

IFFT ..... Inverse Fast Fourier Transform

ITU ..... International Telecommunication Union

JTAG ..... Joint Test Action Group

JTRS ..... Joint Tactical Radio System

LCR ..... Level Crossing Rate

LDPC ..... Low Density Parity Check

LLRT ..... Log Likelihood Ratio Test

LOS ..... Line-of-Sight

LRT ..... Likelihood Ratio Test

LTE ..... Long Term Evolution

MIMO ..... Multiple Input Multiple Output

ML ..... Maximum Likelihood

MMCX ..... Multimedia Communication Exchange

mmWave ..... Milimeter Wave

MPC ..... Multipath Component

MAC ..... Medium Access Control

NC-OFDM ..... Non-Contiguous OFDM

NLOS ..... Non-Line of Sight

OFCOMM ..... Office Communication

OFDM ..... Orthogonal Frequency Division Multiple Access

OIC ..... Opportunistic Interference Cancellation

OOB ..... Out-of-Band

OSTBC ..... Orthogonal Space-Time Block Codes

PA ..... Power Amplifier

PAPR ..... Peak-to-Average-Power Ratio

PDF ..... Probability Density Function

PDP ..... Power Delay Profile

PHY ..... Physical

PoE ..... Power over Ethernet

P/S ..... Parallel to Serial

PSD ..... Power Spectral Density

PU ..... Primary User

PSD ..... Power Spectral Density

PMSE ..... Programme Making and Special Events

PCS ..... Personal Communication System/Service

QAM ..... Quadrature Amplitude Modulation

QP ..... Quite Period

QPSK ..... Quadrature Phase Shift Keying

QoS ..... Quality of Service

RF ..... Radio Frequency

RHINO ..... Whitespace Reconfigurable Hardware Interface for

..... ComputatioN and RadiO

ROC ..... Receiver Operating Characteristic Curves

RMS ..... Root Mean Square

RTL ..... Register-Transfer Level

SACC ..... Swarm Aware Control Channel

SDR ..... Software-Defined Radio

SINR ..... Signal to Noise plus Interference Ratio

SoC ..... System on Chip

S/P ..... Serial to Parallel

SP ..... Sensing Period

STBC ..... Space-Time Block Code

SU ..... Secondary User

3GPP ..... 3rd Generation Partnership Project

TDMA ..... Time Division Multiple Access

TS ..... Time Slot

TVBD ..... TV Band Devices

TVWS ..... TV White Space

TDD ..... Time Division Duplex

USRP ..... Universal Software Radio Peripheral

UHF/VHF ..... Ultra High Frequency/Very High Frequency

V2V ..... Vehicle to Vehicle Communication

WCDMA ..... Wideband Code Division Multiple Access

WiFi ..... Wireless Fidelity

WiMx ..... Wireless Interoperability for Microwave Access

WLAN ..... Wireless Local Area Network

WPAR ..... Weighted Probability of Area Recovery

WMAN ..... Wireless Metropolitan Area Network

WPAN ..... Wireless Personal Area Network

WSDB ..... White Space Database

WSD ..... White Space Device

WSM ..... White Space MAP

ZACC ..... Zone Aware Control Channel

Contents

1 Introduction **21**
1.1 Introduction 21
1.2 Motivation 22
1.3 Mitola's and Haykin's View of CR 23
1.4 Thesis Outline and Structure 25

2 Background and Literature Review **28**
2.1 Introduction 28
2.2 Multipath Fading 29
2.3 Impulse Response of Multipath Channels 29
2.3.1 Mean Excess Delay 31
2.3.2 Maximum Excess Delay 32
2.4 Doppler Spread Effects 33
2.4.1 Fast Fading 33
2.4.2 Slow Fading 34
2.4.3 Frequency Flat Fading 34
2.4.4 Frequency-Selective Fading 35
2.5 Rayleigh and Rician Fading 36
2.5.1 Level Crossing Rate(LCR) 37
2.5.2 Average Fade Duration(AFD) 38
2.5.3 Gamma Distribution 38
2.5.4 Chi-squared Distribution 39
2.6 Concept of Spectrum Hole 40
2.6.1 Spectrum Underlay 42

2.6.2 Spectrum Overlay . . . 43
2.7 Performance Metrics . . . 43
2.7.1 Receiver Operating Characteristic Curves (ROC) . . . 43
2.7.2 Weighted Probability of Area Recovery (WPAR) . . . 44
2.7.3 Sensitivity . . . 44
2.7.4 Uncertainities . . . 45
2.7.5 Sample Complexity . . . 45
2.7.6 SNR Wall . . . 45
2.7.7 Interference Temperature Limit . . . 47
2.8 Summary . . . 48

3 Pertinent SDR/CR Hardware 50
3.1 Introduction . . . 50
3.2 Hardware Challenges . . . 50
3.3 NUTAQ's PicoSDR . . . 51
3.3.1 FPGA Section . . . 51
3.3.2 OFDM PHY Transceiver Reference Design . . . 52
3.3.3 Nutaq's PicoSDR Teardown . . . 52
3.4 Ettus USRP . . . 56
3.5 BWRC's BEE2 and BEE3 . . . 58
3.6 WARP SDR . . . 60
3.7 WhiteRhino . . . 61
3.8 RTL-SDR . . . 62
3.9 Summary . . . 64

4 TVWS Network Architecture and WSDB Implementation 66
4.1 Introduction . . . 66
4.2 Cognitive Radio Standards in TVWS . . . 66
4.2.1 IEEE 802.11af . . . 67
4.2.2 IEEE 802.22 . . . 67
4.2.3 Vehicle-to-Vehicle (V2V) Communication . . . 69
4.3 Interference Mitigation in Heterogenous CRNs . . . 70
4.3.1 Interference to PU and Interference from PU . . . 70

4.3.2 Interference among CRNs . . . 71
4.4 TVWS Database Implementation . . . 72
4.5 Summary . . . 74

5 Spectrum Sensing and Sensing-Throughput Tradeoff 75
5.1 Introduction . . . 75
5.2 Binary Hypotheses . . . 76
5.2.1 Single Measurement . . . 76
5.2.2 Multiple Measurements . . . 77
5.3 Likelihood Ratio Test (LRT) . . . 80
5.3.1 Performance Analysis . . . 81
5.4 Spectrum Sensing . . . 84
5.5 System Model . . . 84
5.5.1 Cognitive Radio Throughput . . . 85
5.5.2 Probabilities of Detection and False Alarm . . . 87
5.6 Cooperative Spectrum Sensing . . . 91
5.6.1 Decision and Fusion Strategies . . . 94
5.7 Multi-slot Sensing . . . 96
5.7.1 Data Fusion Sensing . . . 97
5.7.2 Decision Fusion Sensing . . . 98
5.7.3 Optimal Rule . . . 99
5.8 Aggregate Interference and Outage Analysis . . . 104
5.8.1 System Model and Parameters . . . 104
5.8.2 Aggregate Interference with Beacon Tx at PU Rx . . . 106
5.9 Interference and Outage with Cooperative Sensing . . . 110
5.10 Summary . . . 112

6 PAPR Reduction and Sensing-throughput Tradeoff in OFDM-based Cognitive Radio 113
6.1 Introduction . . . 113
6.2 OFDM . . . 114
6.2.1 OFDM Transceiver Architecture . . . 114
6.2.2 PAPR Issue in OFDM . . . 117

6.3 NC-OFDM . . . 117
6.4 PAPR in NC-OFDM . . . 120
6.4.1 Baseband PAPR . . . 121
6.4.2 Passband PAPR . . . 122
6.4.3 Bounds on MPSK-OFDM and MQAM-OFDM PAPR . . . 123
6.4.4 Statistical Characteristics . . . 125
6.5 PAPR of NC-OFDM Signal . . . 128
6.5.1 Maximum PAPR Distribution in NC-OFDM Signal . . . 130
6.6 Sensing-throughput tradeoff in OFDM-based Cognitive Radio . . . 131
6.7 Average OFDM Cognitive Radio Throughput . . . 134
6.8 Autocorrelation Based Sensing of CP-OFDM Signals . . . 135
6.8.1 Autocorrelation based spectrum sensing . . . 136
6.9 Effect of Information of CP . . . 144
6.9.1 Detection Performance in Multipaths . . . 145
6.10 Full-Duplex Communication CR . . . 146
6.10.1 System Model . . . 147
6.11 FDC-SS System Model . . . 149
6.12 Summary . . . 156

7 Conclusion and Future Work **158**
7.1 Conclusion . . . 158
7.2 Full-duplex Green Cognitive Radio . . . 159
7.3 Multi-parameter Cognitive Radio . . . 159
7.4 Cognitive Pilot-Channel LTE-CR . . . 160

A A **161**
A.1 Proof of $\rho_2 = \left(\left(\frac{T_c}{T_c+T_d}\right)\left(\frac{\delta\sigma_s^2}{\delta\sigma_s^2+\sigma_w^2}\right)\right)$ . . . 161

B B **164**
B.1 PicoSDR Configuration Steps . . . 164

Chapter 1

Introduction

1.1 Introduction

Electromagnetic spectrum is one of the scarce and costly commodity in the world crowded by numerous wireless communication standards in various bands with different transmission and propagation requirements. Recently, FCC and OFCOM have legalised the usage of spectrum in VHF/UHF part of the spectrum, because this portion of the spectrum remains largely under-utilised which can be used for various other communication applications by using the concept of Cognitive Radio(CR). TVWS that exists in VHF/UHF part of the TV band is defined differently based on space and time. In US non-contiguous TVWSs are located in frequency range of 54–698 MHz [1] and a portion of frequency ranging from 470MHz to 790 MHz exists in Europe [1]. TVWS can be exploited by unlicensed TV White Space Devices(WSDs) on the condition that they shall respect the rights of incumbent or licensed user and shall not introduce harmful interference. TV band is also used by many other licensed users such as terrestrial TV broadcasting and Program Making and Special Events (PMSE) e.g., wireless microphones which has very narrow spectrum of 200 kHz. TVWS is attractive to many wireless communication standards because of the favourable propagation characteristics and its many inherent advantages. TVWS are favourable for non-line-of-sight communication because of the little attenuation penalty. Additionally, TVWS offer increased range at less transmit power when compared to ISM band. A 20MHz channel used in ISM band

at 2.4 GHz gives increased capacity over short-range, but requires more infrastructure for wider coverage area. In contrast, a 6 MHz channel in VHF/UHF band can propagate longer and can provide a reasonable capacity. However, owing to such advantages a recent migration trend of ISM standards in TVWS has been observed, for example WLAN 802.11af,WRAN 802.22, IEEE 802.15.4, LTE-A, and M2M are such standards few of which are well-established standards and few are in inception. In such scenario, an increased range can give rise to serious interference to incumbents or decreased QoS for secondary user.Therefore an effective coordination, scheduling, and interference cancellation algorithms should be investigated to fully leverage the benefits of TVWSs.

1.2 Motivation

Figure 1.1 shows spectrum utilisation in frequency bands in between 30 MHz and 3 GHz average over six different locations. Such relatively low utilisation of the licensed spectrum reflects that the spectrum scarcity is due to inefficient static frequency allocation. Therefore, spectrum regulating agencies permit secondary users to opportunistically utilize unused licenced primary bands.

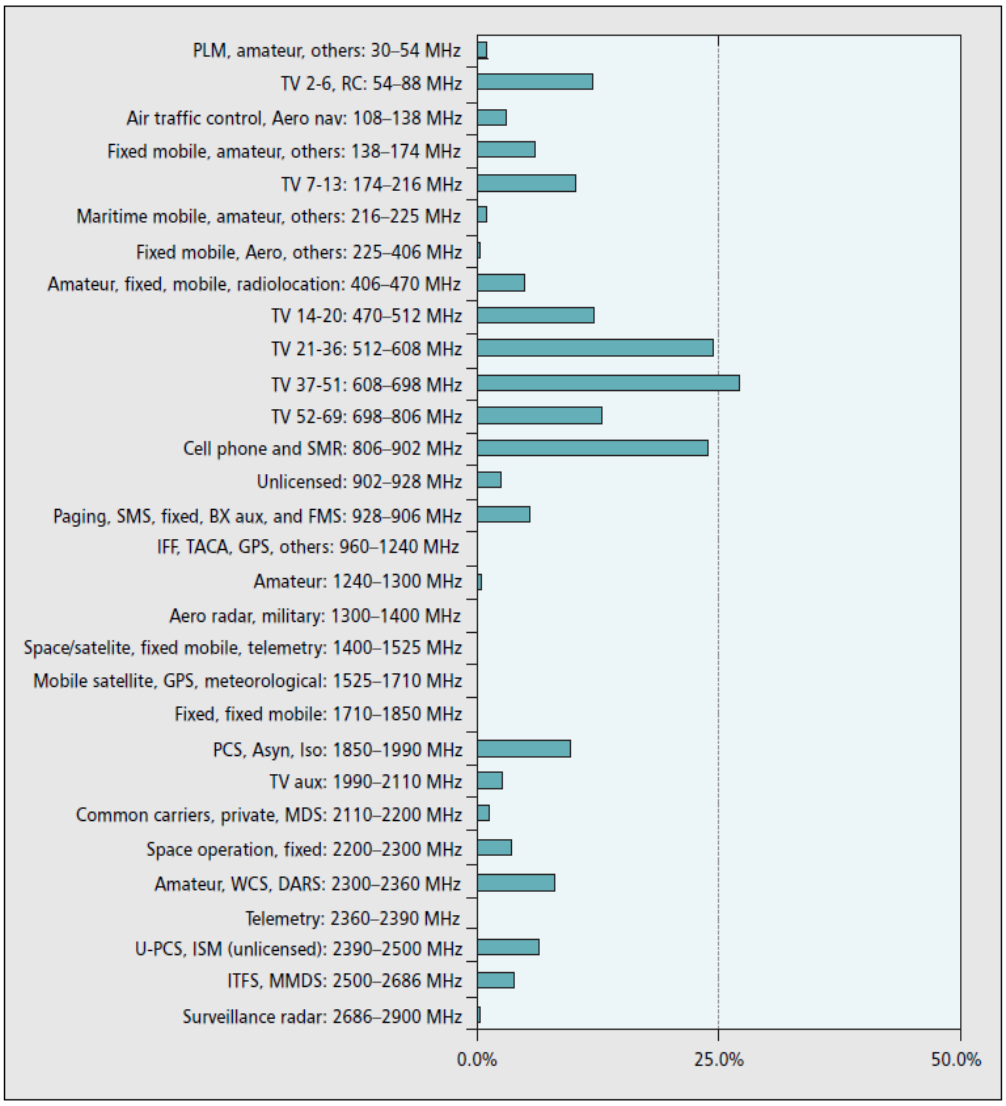


Figure 1.1: Spectrum Usage Measurement over Six Locations[2]

1.3 Mitola's and Haykin's View of CR

The fundamental concepts of cognitive radio was given by Mitola [3][4]which was proposed to target all environment parameters in hole PHY, MAC and application layers as well as the information extracted from the reasoning as shown in Fig. 1.2. Hence, Mitola's concept of CR is referred to as "Full Cognitive Radio". However, due to its difficult implementation FCC and Haykin[5] introduced more

simplified definition focusing on the spectrum sensing aspect of the cognitive radio which is known as "spectrum sensing cognitive radio".Mitola's CR was proposed to be full cognitive radio which could make node intelligent and learn from the atmosphere thereby estimate parameters like transmit power, constellation size, channel coding type and code rate, phase noise introduced in constellation and other user behaviour patterns.

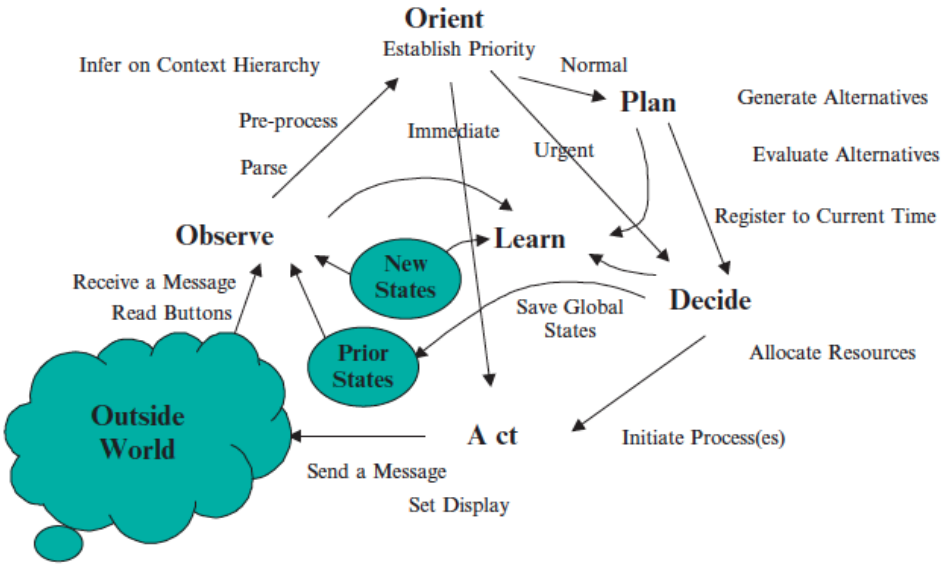


Figure 1.2: Joseph Mitola's view of Cognitive Radio [4]

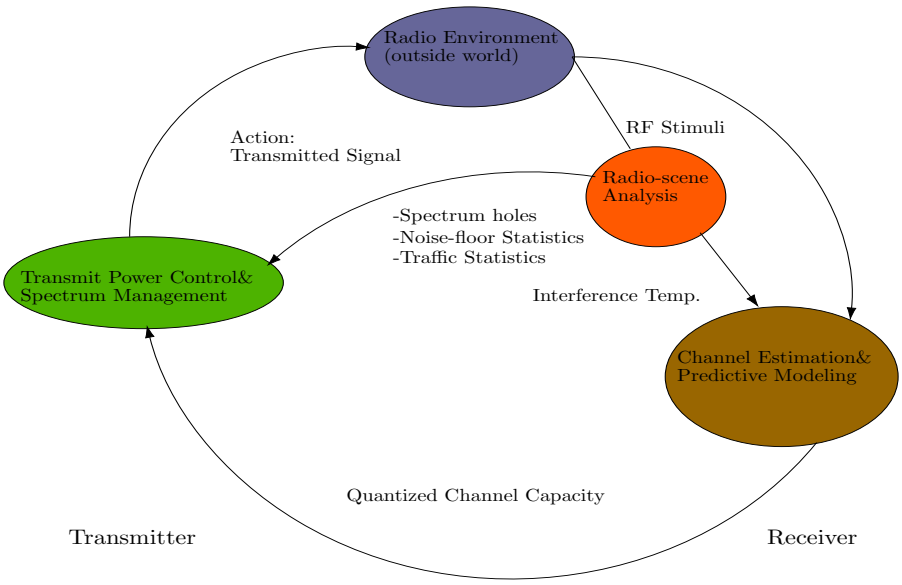


Figure 1.3: Haykin's view of CR[5]

Figure 1.3 shows Haykin's view of Cognitive Radio which focuses on spectrum sensing to find out the spectrum hole based on certain statistical parameters. The CR under discussion in rest of the chapters is based on Haykin's view of cognitive radio that's single parameter CR for spectrum harnessing.

1.4 Thesis Outline and Structure

This thesis is outlined as follows:

Chapter 1: This chapter discusses the motivation beyond the intended work on cognitive radio in TV white space . Two prevalent views regarding the cognitive radio have been discussed of which one is from Joseph Mitolla who gave the concept of multi standard cognitive radio and second by Simon Haykin who gave more pragmatic approach of CR.

Chapter 2: In this chapter fundamentals of wireless communication have been

briefly explained which affect the design of any wireless communication system and cognitive radio is not an exception. For example multipath fading and different statical distribution which model multipath fading channels. Important terms relating to multipaths have been presented for example max. excess delay, delay spread, doppler spread, flat fading and frequency selective fading etc. Additionally important terminology for cognitive radio has also been introduced. For example the concept of spectrum whole nicely conceptualised by UC Berkley's Anant Sahai. Finally, the concept of receiver operating characteristic (ROC) curves, noise uncertainty, sample complexity, SNR wall, noise temperature limit have been introduced.

Chapter 3: This chapter is dedicated to hardware pertinent to SDR/CR where details of different SDR/CR platforms are given along with Nutaq's PicoSDR. Platforms under discussion are Ettus USRP, Rice WARP, BWRC BEE2 and BEE3, RTL-SDR, White RHINO etc. Nutaq's PicoSDR2x2 has been detailed specially the implementation of the OFDM QAM-64 communication system and transmission of video traffic in loopback fashion from host PC to PicoSDR for processing and back to host PC for playback.

Chapter 4: This chapter sheds light on different standards that operate in TV white spaces for example WRAN IEEE 802.22 and WLAN IEEE 802.11af. Additionally white space database implementation strategy has been discussed which is one of the two leading paradigm of CR. Architecture of WSDB and the WSDB accessing strategies have been given to carry out successful transmission and avoid the interference to incumbent PU.

Chapter 5: This chapter thoroughly discusses the spectrum-sensing throughput tradeoff after giving necessary mathematical background i.e. system model in the light of signal only and alternative hypotheses and the factors of sample size, noise variance and SNR which affect the performance of CR given in terms of probability of detection, probability of false alarm and maximum throughput. These performance indicatives terms for cooperative cognitive radio are also under discussion with different raw information and decision fusion strategies at

fusion centre (FC). Different fusion schemes have also been extended to multislot spectrum-sensing throughput with known and unknown channel coefficients. Finally, this chapter is concluded with interference and outage analysis of CR when beacon transmitter is placed at the transmitter or receiver.

Chapter 6: This chapter discusses OFDM-based CR for PU as well as for SU realising the ubiquity of OFDM based communication systems. Moreover, it also treats the NC-OFDM in which subcarriers are nullified on which PU transmission is expected. It also discusses inherent problem PAPR in OFDM-based system.Finally, this chapter has been concluded with FDC-CR-using two antennas for sensing and transmission-whose system model and performance indicative parameters have been discussed with the help of analytical expression and simulation results.

Chapter 7: This chapter contains the conclusion and future avenues of CR in TV white space in the light of recent advances in massive MIMO and device-to-device (D2D) communication, mmWaves, HetNets dense deployment and rising need for energy-efficient communication techniques in which the CR can play a decisive role.

Chapter 2

Background and Literature Review

2.1 Introduction

In this chapter multipath fading is discussed that affects any wireless communication system like cognitive radio. Here brief explanation of the concepts is introduced for example multipath delay spread, mean excess delay spread, maximum excess delay spread and doppler spread. Fundamental receiver operating characteristic curves are introduced which forms the basis of receiver performance used in cognitive radio. Receiver operating characteristic curves is an plot between probability of detection and probability of false alarm for fixed SNR values. In chapter 5 and chapter 6 Cognitive radio performance has been assessed in terms of receiver operating characteristic curves and the probability of detection versus sensing time and SNR.The main aim of this chapter is to discuss the fundamentals of multipath fading and discuss the key parameters used for the design of cognitive radio i.e. types of uncertainties SNR wall for energy detector and matched filter, and interference temperature limit etc.

2.2 Multipath Fading

When a signal emanates from the transmitter it interacts with the objects that comprises the channel. The objects present in the channel vary in their formation,size and other physical properties which play a very important role in signal propagation. Figure 2.1 shows that multiple copies of the transmission signal are received at the receiver with different signal strength, phase and delay. Depending on the location of the receiver MPCs add constructively when the MPCs have same phase and add destructively when MPCs are out of phase, thus the received signal as a function of time constantly varies in its signal strength which is then modelled by different statistical distribution techniques.

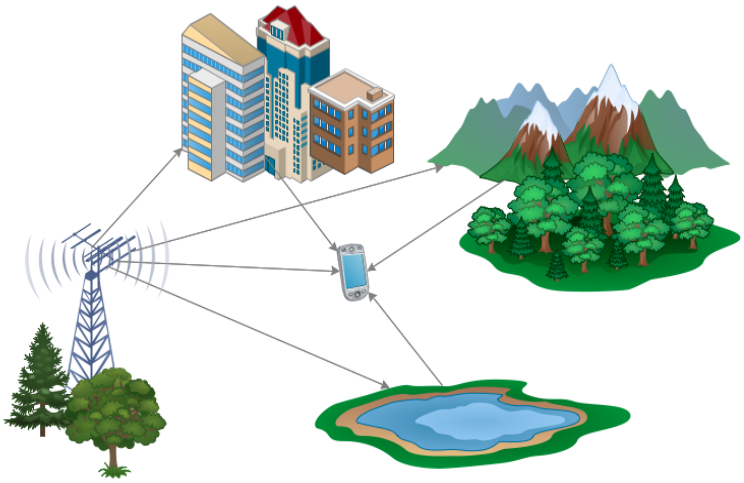


Figure 2.1: A Typical Multipath Fading Scenario

2.3 Impulse Response of Multipath Channels

Mobile radio channel can be modeled as linear filter whose impulse response varies with time. The time variations are caused by receiver motion in space and filtering effect caused by the multipaths. Hence the impulse response of the mobile radio channel is function of space and time $h(d,t)$. For a transmitted signal $x(t)$ and the

channel impulse response $h(d,t)$, the received signal $y(d,t)$ can be given as follows:

$$y(d,t) = x(t) \otimes h(d,t) = \int_{-\infty}^{\infty} x(\tau)h(d,t-\tau) \tag{2.1}$$

Since for a causal system $y(d,t) = \int_{-\infty}^{t} x(\tau)h(d,t-\tau)d\tau$ and position of the receiver $d = vt$ and a receiver moving with constant velocity v the received signal $y(vt,t) = \int_{-\infty}^{t} x(\tau)h(vt,t-\tau)d\tau$ can be expressed as follows:

$$y(t) = \int_{-\infty}^{\infty} x(\tau)h(vt,t-\tau)d\tau \tag{2.2}$$

Where t is time-variation due to motion of the receiver and τ is the channel delay for fixed value of t. Now, the complex basedband impulse response $h_b(t,\tau)$ with discretised multipath delay axis τ see fig.2.2 into equal time-delay segments which are known as *excess delay bins* is as follows:

$$h_b(t,\tau) = \sum_{i=0}^{N-1} a_i(t,\tau)\exp(j\omega_c\tau_i(t) + j\phi(t,\tau))\delta(\tau - \tau_i(t)) \tag{2.3}$$

Where $a_i(t,\tau)$ is amplitude of the ith MPC and $\tau_i(t)$ is excess delay of ith MPC. For time-invariant case above discrete baseband equivalent channel impulse response can be simplified as:

$$h_b(\tau) = \sum_{i=0}^{N-1} a_i\exp(j\theta_i)\delta(\tau - \tau_i) \tag{2.4}$$

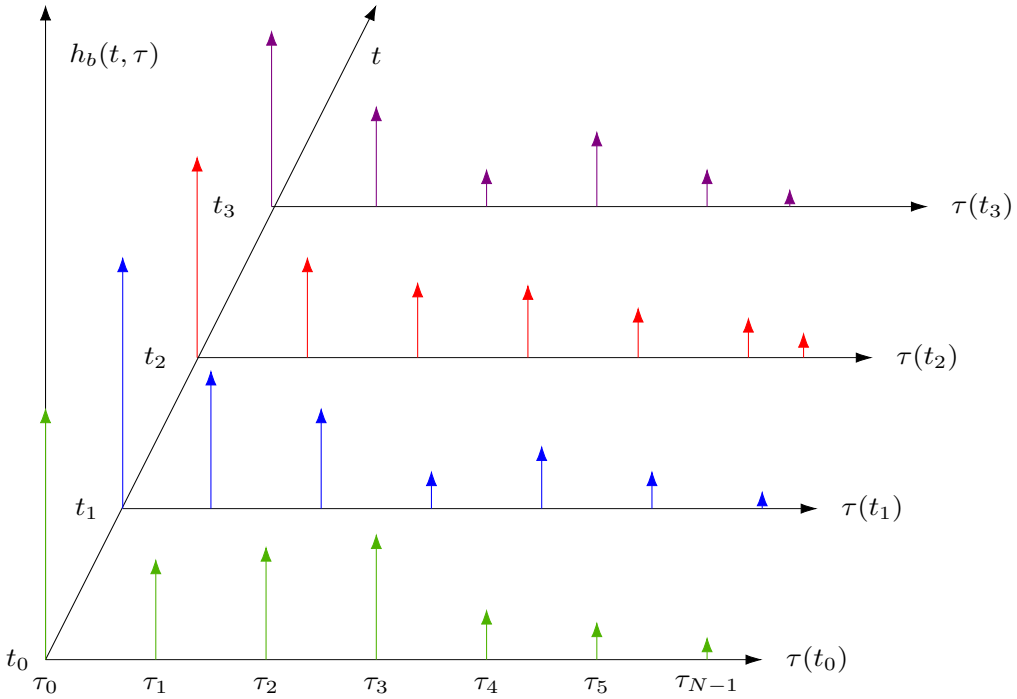


Figure 2.2: Discrete Impulse Response of Mobile Channel

2.3.1 Mean Excess Delay

Mean excess delay can be given by:

$$\bar{\tau} = \frac{\sum_k a_k^2 \tau_k}{\sum_k a_k^2} = \frac{\sum_k P(\tau_k)\tau_k}{\sum_k P(\tau_k)} \tag{2.5}$$

Where as RMS delay spread can be given by following equation:

$$\sigma_\tau = \sqrt{\overline{\tau^2} - (\bar{\tau}^2)} \tag{2.6}$$

Where:

$$\overline{\tau^2} = \frac{\sum_k a_k^2 \tau_k^2}{\sum_k a_k^2} = \frac{\sum_k P(\tau_k)\tau_k^2}{\sum_k P(\tau_k)} \tag{2.7}$$

Typically RMS delay spread is on the order of microseconds for outdoor environment and is on the oder of nanoseconds for indoor environment.

2.3.2 Maximum Excess Delay

Maximum excess delay is the time delay during which the multipaths falls X dB below the maximum. Mathematically, it can be given by:

$$\text{Max. Excess Delay} = \tau_X - \tau_0 \tag{2.8}$$

Where τ_0 is the delay for the first arrival and τ_X maximum delay for which multipath remains below X dB. This can be seen from the Fig.2.3 which shows the example of indoor power delay profile with mean delay spread, RMS delay spread, mean excess delay, and max. excess delay.

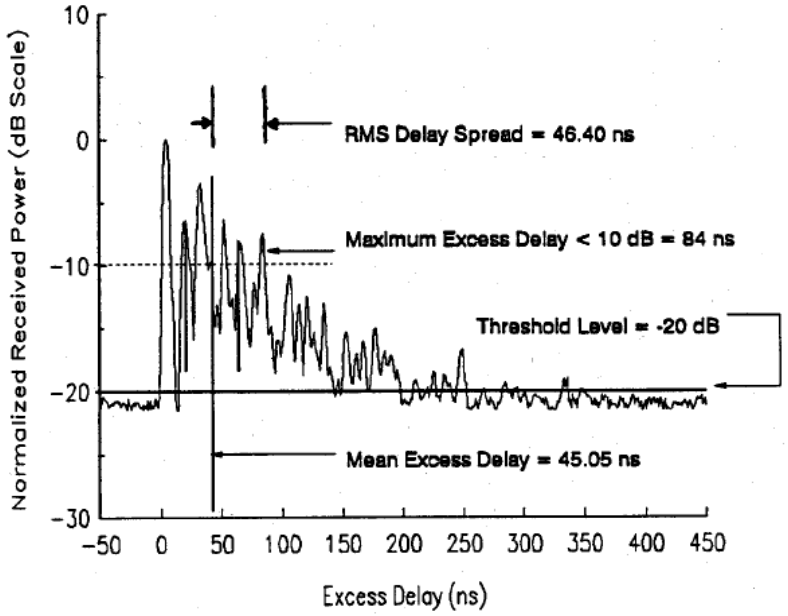


Figure 2.3: Typical Indoor Power Delay Profile [6]

2.4 Doppler Spread Effects

If receiver moves at the constant velocity v along a path with path length difference $\Delta\ell = d\cos\theta = v\Delta t\cos\theta$ and the phase change $\Delta\phi = \frac{2\pi\Delta\ell}{/\lambda} = \frac{2\pi v\Delta t}{\lambda}\cos\theta$ as shown in Fig. 2.4then the Doppler shift can be given as:

$$f_d = \frac{1}{2\pi}.\frac{\Delta\phi}{\Delta t} = \frac{v}{\lambda}\cos\theta \tag{2.9}$$

2.4.1 Fast Fading

This causes the frequency dispersion because of the Doppler shift in the signal which comes with movement of the transceiver or because of the motion of the objects comprising physical channel. Therefore, the channel response $h(t,\tau)$ fluctuates within specified symbol duration T_s which means symbol duration T_s is greater than the channel coherence time T_c i.e. $T_s > T_c$ or $W_s < W_D$ which further

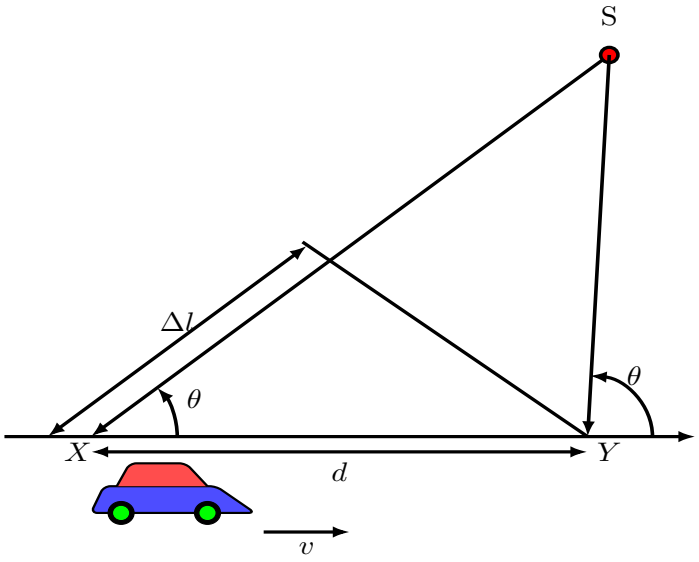


Figure 2.4: Doppler Shift Scenario

means signal bandwidth is less than the amount of Doppler spread.

2.4.2 Slow Fading

This is another effect caused by Doppler spread where the channel impulse response varies much slower than the transmitted signal. It can be said that a signal undergoes slow fading if the symbol duration T_s is less than the coherence time T_c of the channel i.e. $T_s << T_c$. Alternatively, amount of Doppler spread in the channel is much less than the signal bandwidth ($W_s >> W_D$).

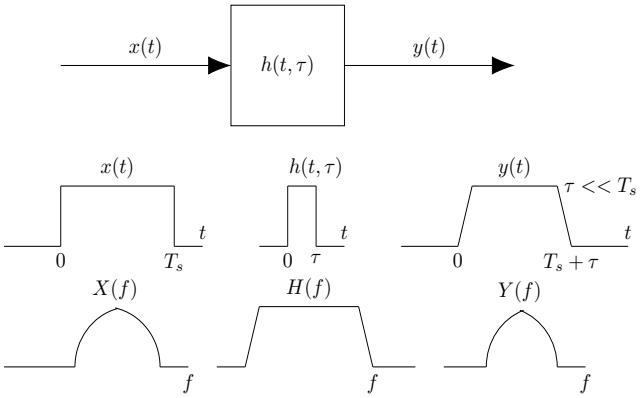
2.4.3 Frequency Flat Fading

If the transmission bandwidth W_s of the signal $s(t)$ is less than the coherence bandwidth W_c of the channel with impulse response $h(t, \tau)$ i.e. $W_s << W_c$ then the signal shall undergo frequency flat fading channel. Equivalently this translates into all the MPCs arriving within symbol duration T_s i.e. $\sigma_\tau << T_s$. This phenomenon can be seen in Fig. 2.5a where the output signal doesn't experience any magnitude

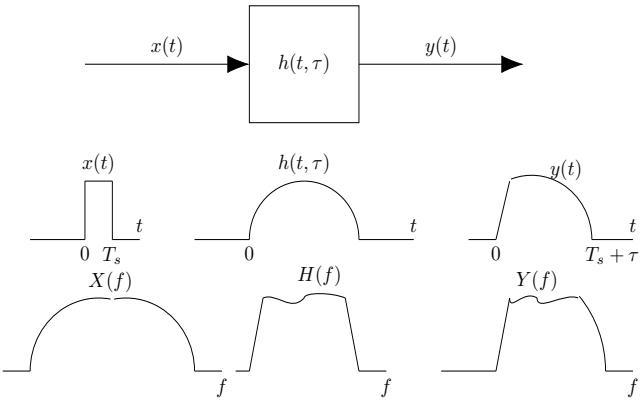
distortion.

2.4.4 Frequency-Selective Fading

If the transmission bandwidth W_s of the signal $s(t)$ is greater than the coherence bandwidth W_c of the channel with impulse response $h(t, \tau)$ i.e. $W_s >> W_c$ then the signal shall undergo frequency-selective fading as shown in Fig. 2.5b. In other words all the MPCs do not arrive within symbol duration $\sigma_\tau >> T_s$. It's clear that the output signal experiences magnitude distortion.



(a) Frequency Flat Fading



(b) Frequency Selective Fading

Figure 2.5: Frequency Flat and Frequency Selective Fading

2.5 Rayleigh and Rician Fading

Rayleigh fading models the outdoor radio propagation channel where there are only multipath components present. The the envelope of the received signals can be modelled with Rayleigh distribution. In contrast, there is another type of fading known as Rician fading and unlike Rayleigh fading it appropriately models the indoor radio propagation environment where the probability of getting line-of-sight (LOS) is higher than the outdoor propagation environment. Rician fading is defined by K factor which is ratio of the LOS component and all the reflected components received at the receiver i.e NLOS components. Mathematically, power through LOS and NLOS respectively is given by:

$$P_{LOS} = \frac{K}{1+K} P_{Total} \tag{2.10}$$

$$P_{NLOS} = \frac{1}{1+K} P_{Total} \tag{2.11}$$

Above equations 2.10 and 2.11 give the relationship between power available in LOS and NLOS component of the signal with total power transmitted. For example for K=2, there shall be 66.66% of total power in the LOS and 43.44% of total power in NLOS signal. Similarly, for a Rician factor K=3 there shall be 75% of the total power in LOS path and rest of the power that is 25% of the total power shall be in NLOS signal. For the sake of comparison and developing general intuition of two fading types Figure 2.6 shows the channel profile of Raleigh and Rician distribution for different values of K-factor and Doppler spread.

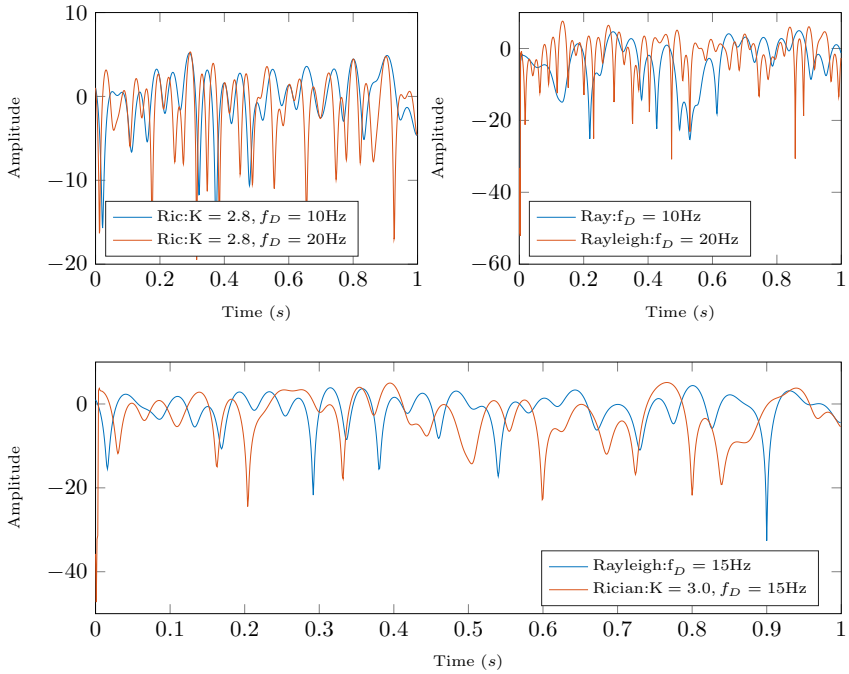


Figure 2.6: Rayleigh and Rician Multipath Fading: No. of Samples=10^3

2.5.1 Level Crossing Rate(LCR)

LCR is defined as expected rate at which the Rayleigh fading signal crosses a specific point in a positive going direction. It's useful to relate the rate of change of the received signal to signal level and velocity of the mobile. The number of level crossing per second is given by:

$$N_R = \int_0^\infty \hat{r} p(R, \hat{r}) d\hat{r} = \sqrt{2\pi} f_m \rho e^{-\rho^2} \tag{2.12}$$

Where $\hat{r}$ is time variation of $r(t)$ and $p(R, \hat{r})$ is joint density function of R and $\hat{r}$ at $r = R$ and $\rho = R/R_{rms}$ is value of specified level normalised to the RMS amplitude of the fading envelope.

2.5.2 Average Fade Duration(AFD)

AFD is defined as the average period of time which the received signal is below a specific point R. Mathematically,

$$\bar{\tau} = \frac{1}{N_R} Pr[r < R] \tag{2.13}$$

Where $Pr[r < R] = \frac{1}{T}\sum_i \tau_i$ and τ_i is duration of the fade and T is the observation interval. For Rayleigh distribution:

$$Pr[r < R] = \int_0^R p(r)dr = 1 - \exp(-\rho^2) \tag{2.14}$$

Hence the average fade duration using above equations can be given by:

$$\bar{\tau} = \frac{e^{\rho^2} - 1}{\rho f_m \sqrt{2\pi}} \tag{2.15}$$

The AFD fading helps determine the number of bits that may be lost during a fade. AFD primarily depends upon the speed of the mobile and decreases as the maximum Doppler frequency f_m becomes large.

2.5.3 Gamma Distribution

Gamma distribution is one of the very important distribution which models the various effects in the wireless channel that takes place. PDF of gamma distribution with scale parameter t and a shape parameterλ can be written as follows:

$$f_X(x;\lambda,t) = \frac{\lambda \exp^{-\lambda x} \left(\lambda x\right)^{t-1}}{\Gamma\left(t\right)} \tag{2.16}$$

Where $\Gamma(t) = \int_0^\infty e^{-y} y^{t-1} dy$. Its expectation and variance are $E(X) = t/\lambda$ and $Var(X) = t/\lambda$. Similarly, its CDF can be given by the following equation:

$$F_X(x;\lambda,t) = \begin{cases} 0 & x \leq 0 \\ \frac{1}{\Gamma(t)} \int_0 \lambda x y^{t-1} e^{-y} dy & x > 0 \end{cases} \tag{2.17}$$

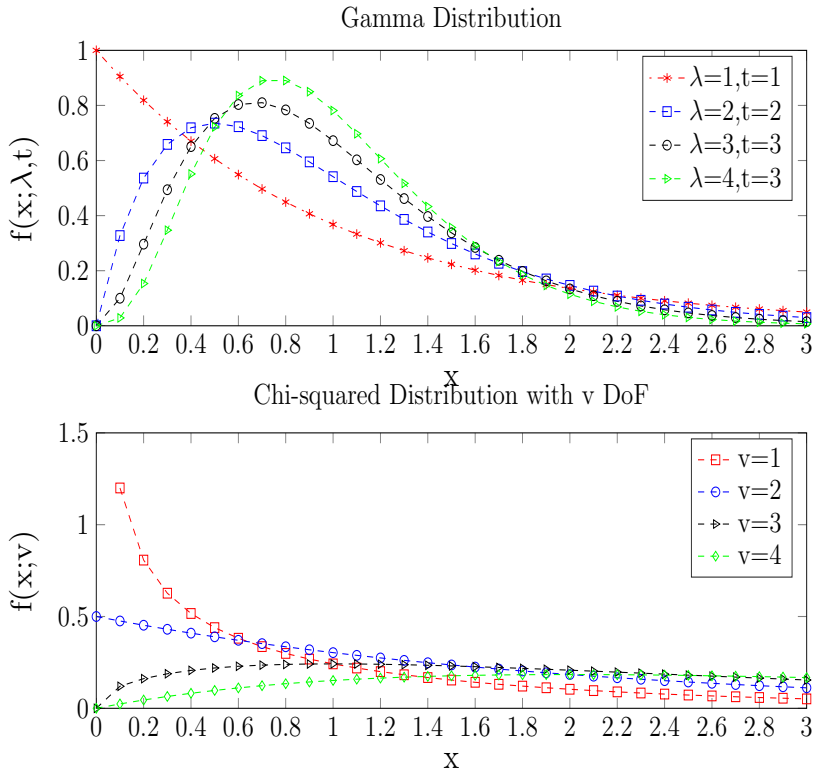


Figure 2.7: Gamma Distribution and Chi-squared Distribution with v Degrees of Freedom (DoF)

2.5.4 Chi-squared Distribution

Chi-squared distribution can be derived from Gamma distribution PDF with scale parameter $\lambda = 0.5$ and shape parameter $t = v/2$ with v degrees of freedom.

$$f_X(x;v) = \frac{1}{\Gamma(v/2)} \left(v/2\right)^{\Gamma/2} x^{v/2-1} e^{-1/2x} \tag{2.18}$$

The mean and variance of Chi-square distribution is $E(X) = v$ and $Var(X) = 2v$.

2.6 Concept of Spectrum Hole

The region of space-time-frequency-code in which SU can perform transmission is called *spectrum hole* [7]. An underused band can accommodate the transmission of SU without harming the incumbent or PU operation. PU transmitters that always communicate to their users in a service area and some of the service area is around PU transmitter can never be used (red area) as shown in Fig. 2.8, where green area further away from PU can be used by CRs. For bands with such PUs recovering spectrum hole in space is major challenge. Let us say system transmits intermittently but serves the entire area of interest. In this case recovering spectrum hole in time is major challenge. Spectrum hole in frequency is defined as frequency band in which secondary can transmit without interfering with PU receivers. SU system performance can naturally be measured using expected throughput. The need to incorporate uncertainties can be seen in time-domain. For example time-domain hole in context of Bluetooth is exploited. The key to exploit such opportunities in the time-domain is SU ability to predict OFF times of PU. TV towers are usually mounted at a height of $500m$ and serve large area with radius of $135\,Km$. Further away from the TV tower signal is very weak and SUs at such locations can transmit without causing interference. Fig. 2.8 shows the two types of serving areas one with radius r_{dec} where the decodablity for PU signal is guaranteed and the other with radius r_p where protection to PU is guaranteed when SU with CR capabilities comes in the green area. Green area represents *sacrificial zone* because PUs between two circles may not be able to get service once the SU is in. This is termed as acceptable loss of PU quality of service (QoS)[7].

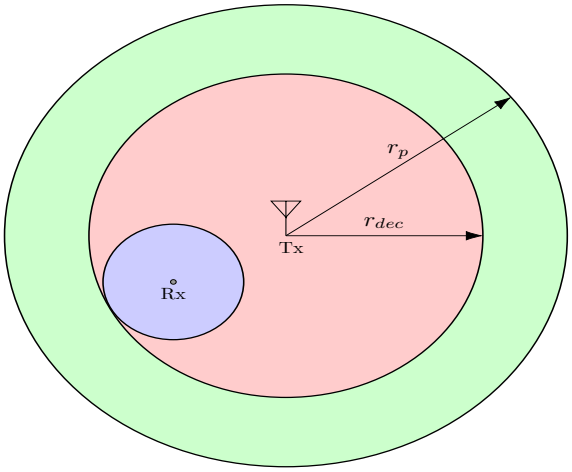


Figure 2.8: Spectrum Hole Concept

The time domain equivalent of $r_{dec} - r_p$ i.e the green area as shown in Fig. 2.9 is short *sacrifical-time* at which beginning of PU transmission during which SUs are permitted to cause interference. Around each protected PU a no-talk region exists as shown in Fig. 2.9 receivers with blue circles where SU can't safely transmit. The over-all no-talk area is union of no-talk zones of all primary receivers and spectrum hole is complement of this area.To recover this area SU must know the location of all PU receivers-since PU receiver may know this information and such complete area recovery is done with the explicit participation of PUs.

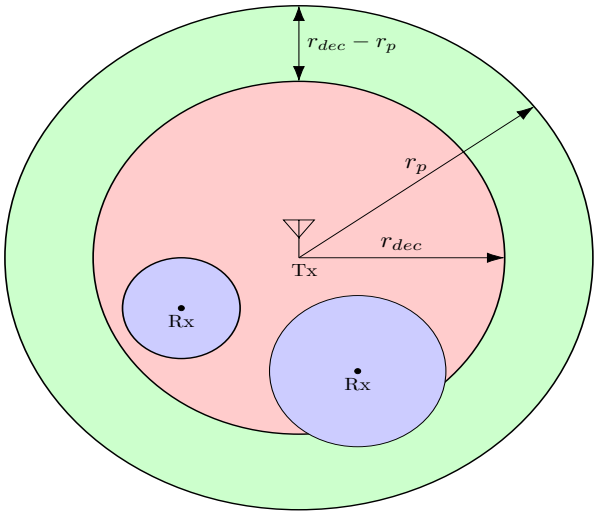


Figure 2.9: Spectrum Hole Concept

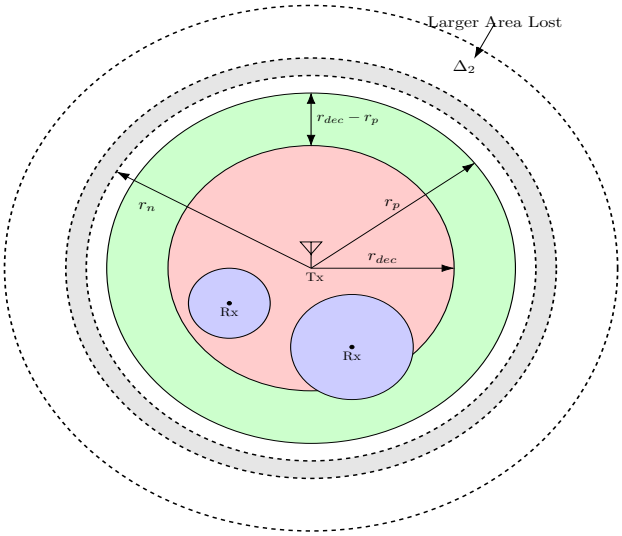


Figure 2.10: Spectrum Hole Concept

2.6.1 Spectrum Underlay

This form of spectrum sharing is constrained on the total power transmitted. CR has to make transmission such that its PSD remains under the noise or PU signal

PSD. UWB transmission and DS-CDMA are the famous examples of spectrum underlay whose PSD remains consistently below noise threshold.

2.6.2 Spectrum Overlay

In this form of spectrum sharing a CR has to be careful while making transmission because its transmission may affect the incumbent who has exclusive rights to use a particular spectrum. CR is constrained when to use and when not to use a particular incumbent's band.

2.7 Performance Metrics

2.7.1 Receiver Operating Characteristic Curves (ROC)

ROC curves of the receiver are the curves that plots the P_D as function of P_{FA} for fixed sensing-time and fixed operational SNR. These curves give us insight about the performance of the detector at the receiver for given signal with certain statistical parameters. Ideally for a CR to have maximum throughput the probability of false alarm should be small and simultaneously the probability of detection should be higher in order to guarantee maximum protection to the PUs. Therefore, the ROC points on ROC curves are the points where excellent combination of the probability of false alarm and probability of detection are acheived.The deflection points on the ROC curves can be considered as the ideal operating points for a given values of P_{FA} and P_D as shown in Fig. 2.11. For a good receiver performance the ROC lines should have angle greater than 45° at which represents the best combination of P_{FA} and P_D [8].

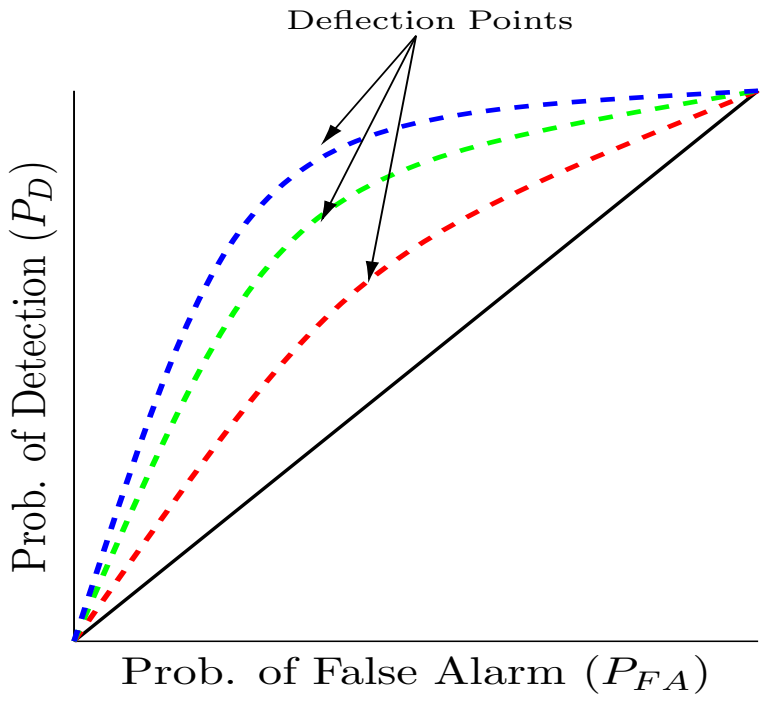


Figure 2.11: Receiver Operating Characteristics (ROC) Curves

2.7.2 Weighted Probability of Area Recovery (WPAR)

It measures the performance of sensing strategy and give good idea of the over-all sensing performance. Mathematically:

$$WPAR = \int_{r_n}^{\infty} P_{FH}(r)w(r)rdr \tag{2.19}$$

Where $w(r)$ is scaling function and $\int_{r_n}^{\infty} w(r)rdr = 1$.

2.7.3 Sensitivity

It's defined as the lowest value of operating SNR for which detector satisfies a given target P_{FA} and P_D. For example the receiver sensitivity for IEEE 802.22

WRAN standard is $-116dB_m$ whereas the receiver sensitivity for IEEE 802.11af is $-92dB_m$.

2.7.4 Uncertainities

There are two classes of uncertainties which are as follows:

- *Device-level uncertainty*: This is caused due to uncertainty in noise power
- *System-level uncertainty*: This is caused by the uncertainties in interference, shadowing and fading distributions. In [9], traditional performance metrics have been suitably modified to characterise the robustness to device-level uncertainties.

2.7.5 Sample Complexity

The performance of detector in terms of overhead is traditionally measured by sensing-time required to achieve target P_{FA} and P_D at a given SNR. The sensitivity and sample complexity are intertwined. Improvement in the sensitivity of the detector shall yield large sample complexity with sensing overheads. In simple words the two quantities are directly proportional to each other with constraint of sensing-time overhead.

2.7.6 SNR Wall

The performance of the detectors is also often times measured in terms of fundamental SNR thresholds called SNR walls below which detection is impossible even if the sensing-time is increased to infinity. Under device-level uncertainty i.e. uncertainty in noise power, both sensitivity and the detector's SNR wall is considered as a measure of performance [9],[10]. There exists a threshold for a given uncertainty of $x\,dB$ below which energy detector can't detect the signal:

$$SNR_{wall} = 10\log_{10}(10^{x/10} - 1) \tag{2.20}$$

SNR wall is SNR threshold at which sample complexity approaches ∞

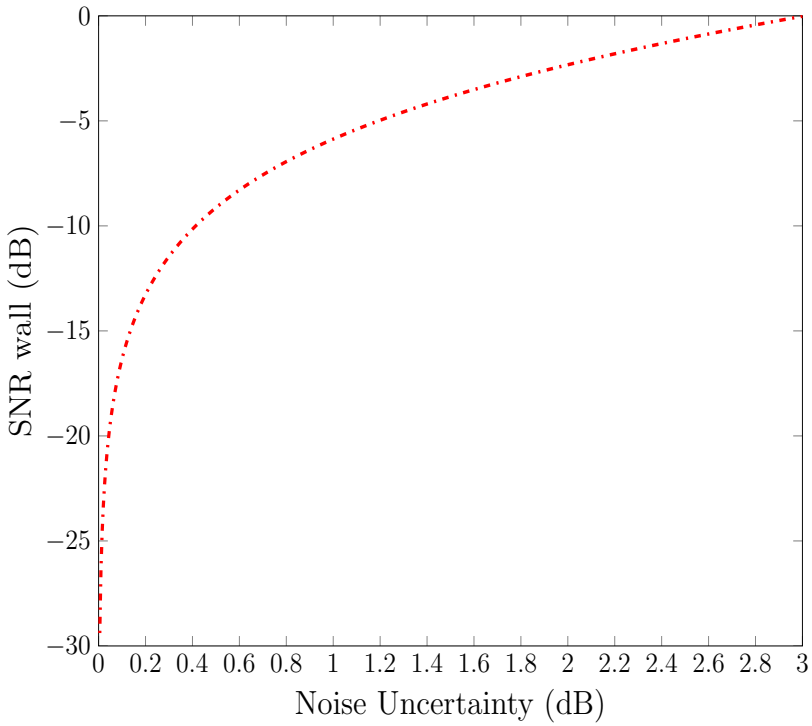


Figure 2.12: SNR Wall versus Noise Uncertainty

Sample complexity is function of SNR, P_{FA}, P_{MD} and noise power uncertainty ρ. Sample complexity of the energy detector and matched filter can be given as follows [9]:

$$N = \frac{2\left[Q^{-1}(P_{FA}) - Q^{-1}(1 - P_{MD}))\right]^2}{\left[SNR - (\frac{\rho^2 - 1}{\rho})\right]^2} \tag{2.21}$$

$$N = \frac{2\left[Q^{-1}(P_{FA}) - Q^{-1}(1 - P_{MD}))\right]^2}{\left[\theta \times N_c \times SNR - \left((\rho^2 - 1)\Big/\rho\right)\right]^2} \tag{2.22}$$

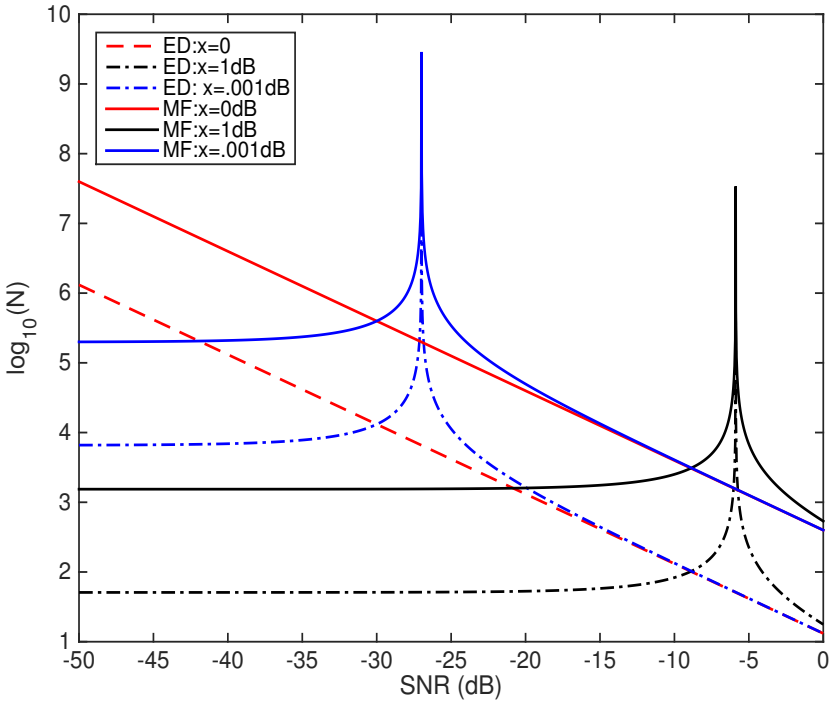


Figure 2.13: Performance Comparison of Energy Detector and Matched Filter

Figure 2.13 compares the performance of energy detector and matched filter for known variance of $1\,dB$ and $0.001\,dB$. There also exist the performance of both type of detectors where there is no noise variance i.e. $x = 0\,dB$. For energy detector (ED) SNR wall occurs at SNR values of $-7\,dB$ and $-27\,dB$ for noise uncertainty values of $1\,dB$ and $.001\,dB$ respectively. Similarly for matched filter, SNR wall is observed at $-7\,dB$ and $-27\,dB$ for noise uncertainty of $1\,dB$ and $0.001\,dB$ respectively, but the sample complexity of matched filter is 0.8 times higher than the sample complexity of the energy detector for given values of noise uncertainty.

2.7.7 Interference Temperature Limit

The concept of interference temperature (ITL) was given by FCC as a way of measuring and managing interference for dynamic allocation of spectrum to cognitive radio. As defined in [11], interference temperature measures the power and

bandwidth occupied by interference. Interference temperature has the following relation with power and the bandwidth:

$$T_I = \frac{P_I(f_c, B)}{kB} \tag{2.23}$$

Where B is bandwidth in Hz, k is Boltzmann's constant, f_c is centre frequency and $P_I(f_c, B)$ is average interference power in Watts. Figure 2.14 gives typical model of the interference temperature limit.

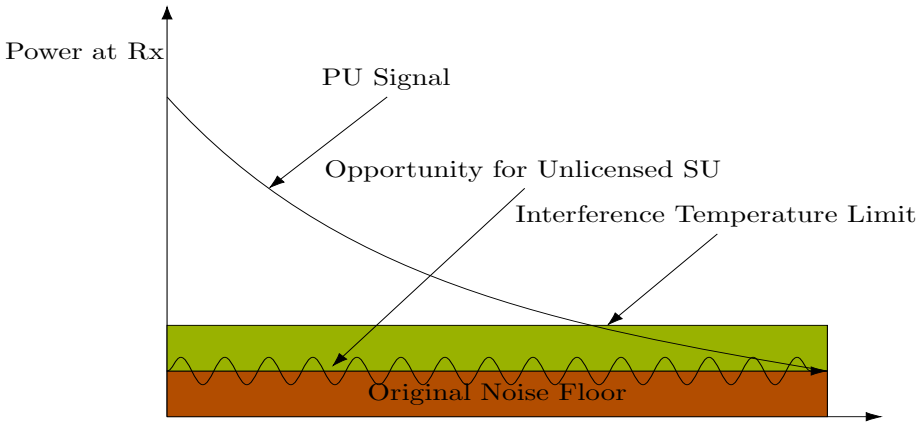


Figure 2.14: Interference Temperature Model[12]

2.8 Summary

Signal transmitted from transmitter interacts objects in the channel and is received at the receiver with constructive or destructive fashion which is known as fading. Mobile radio channel can be modelled as linear filter dependent upon space and time which affects the transmitted signal. There exists various terms used to model the effect of fading for example maximum excess delay is the time delay during which multipath falls some dBs below the minimum. There is another affect that takes place because of the motion of the receiver which is known as Doppler effect. As a result two terms fast fading and slow fading are studied. In fast fading symbol duration is greater than coherence time of the channel. Similarly in slow fading symbol duration is less than the coherence time of the channel. In contrast

to fast fading and slow fading there are other two widely know effects which are frequency flat fading and frequency selective fading. In frequency flat fading signal bandwidth is less than the coherence bandwidth of the channel. Similarly, a signal experiences a frequency selective fading if the signal bandwidth is greater than the coherence bandwidth of the channel. Radio propagation is modelled with two types of statistic al distributions known as Rayleigh fading and Rician fading. In Rayleigh fading no LOS component is received at the receiver and model the outdoor radio propagation channel, whereas in Rician fading NLOS components are accompanied by atleast one LOS components and model the indoor radio propagation channel where the delay is less than the delay spread of the outdoor propagation channel.

Chapter 3

Pertinent SDR/CR Hardware

3.1 Introduction

In this chapter explanation of different hardware platforms is given on which cognitive communication system can be realised. Systematic teardown of different hardware is taken into consideration in the light of various factors for example ADC/DAC resolution, FPGA processing power, its interfacing flexibility, operating frequency range and the individual channel bandwidth etc. Famous SDR/CR platforms has been discussed to name a few are Ettus research USRP, BWRC's BEE2 and BEE3, and Nutaq's PicoSDR. Nutaq's 2x2PicoSDR is used for OFDM QAM-64 system implementation for video transmission between Nutaq's PicoSDR and host PC.

3.2 Hardware Challenges

Ideally an SDR platform should host an antenna very close to ADC/DAC such that antenna should directly transmit and receive from DAC/ADC. But in practice RF front-end can't be ignored and can't be made completely software programmable. Additionally, there are other striking issues which are considered for design and selection of SDR platform for implementation of a CR based digital communication system. Few but important hardware challenges are as follows:

- Large bandwidth and sampling rates

- ADC dynamic range
- Linearity of RF front-end components

3.3 NUTAQ's PicoSDR

Nutaq's 2x2PicoSDR is one of the powerful SDR equipment for multi-mode, multi-standard and cognitive type of radios. Nutaq defines Pico SDR as follows:

"The Nutaq's Pico SDR is a table top SDR solution and incorporates two powerful multimode SDR dual-channel RF transceiver modules, FPGA logic and memory that can be stacked together to form a 2x2 or 4x4 MIMO. The PicoSDR is capable of uplink and downlinking data streams to a remote computer running on Linux or Windows through high-speed GigE interface. Combined with Nutaq's software framework , the PicoSDR can greatly reduce time to market and bring the performance to wide range of applications such as Cognitive Radios in TV White Space and Advanced Telecommunications (LTE and WiFi)". Moreover, PicoSDR from Nutaq can be mainly divided into the following sections:

3.3.1 FPGA Section

Nutaq's PicoSDR host powerful FPGA built around Virtex-6 which offers flexibility and intensive signal processing of wideband waveforms of different standards. It includes:

- 4GB SODIMM DDR3
- QDR2 SRAM
- NOR Flash
- 128 MB DDR3 SRAM
- BSDK's CCE and Microblaze Linux OS
- complete framework for a Virtex-6 interfaces (Nutaq BSDK)
- GigE interface etc.

3.3.2 OFDM PHY Transceiver Reference Design

A model-based OFDM QAM-64 PHY layer is available for simulink users. Through this a real-time HD wireless video transmission can be made between transceivers through 2x2 RF interface.

3.3.3 Nutaq's PicoSDR Teardown

An inside view of the Nutaq's PicoSDR is shown in the following Fig. 3.1.

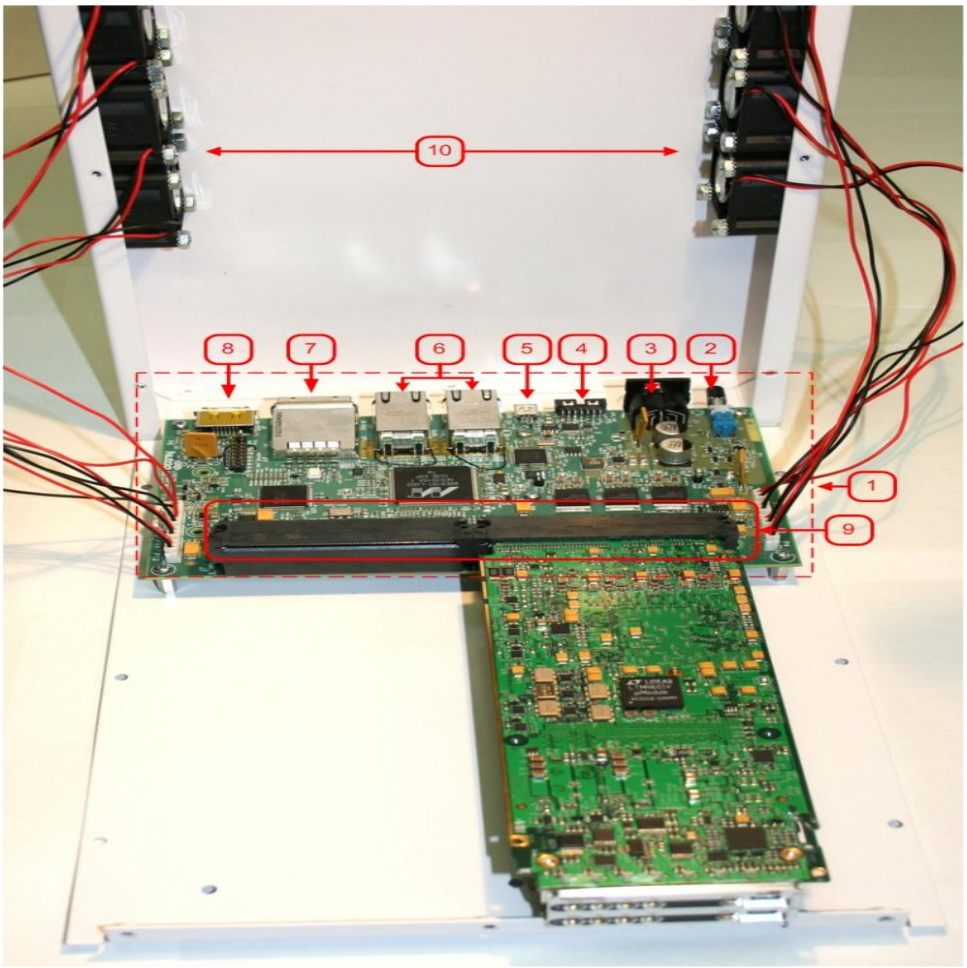


Figure 3.1: Nutaq's PicoSDR Teardown

The back plane board (1) handles the power supply for the whole enclosure as well as the control and data streaming connections with the external world. The

following interfaces are available:

- The reset button (2)
- The power connector (3) (12V DC)
- The FPGA JTAG. (4) connector which allows access to the Perseus FPGA
- A mini-USB connector which is connected to the Perseus serial port (5). The user can access the Perseus emdedded Linux serial console.
- Two RJ-45 Ethernet connectors (6) connected to a Gigabit Ethernet switch for control and data streaming
- A PCIe 4x connector (7) (optional) for control and data streaming.
- A SATA connector (8) (optional) to interface an external Hard Disk Drive to the embedded CPU in the PicoSDR2x2-E. The HDD allows prolonged recording and playback.
- 2 AMC connectors (9). In the PicoSDR2x2 case, only the right connector is used to power and control a Perseus601x. The connector also routes the Gigabit Ethernet and PCIe links between the backplane and the Perseus601x.

In the PicoSDR2x2, the Perseus601x carrier (1) is equipped with Virtex6 FPGA (LX240, LX550, SX315 and SX475 models are available), a 4 GB DDR3 SODIMM and a Radio420M FMC stack (2) consisting of two Radio420 daughter cards. The Radio420M is powered and controlled through the Perseus High Pin Count FMC connector (3).

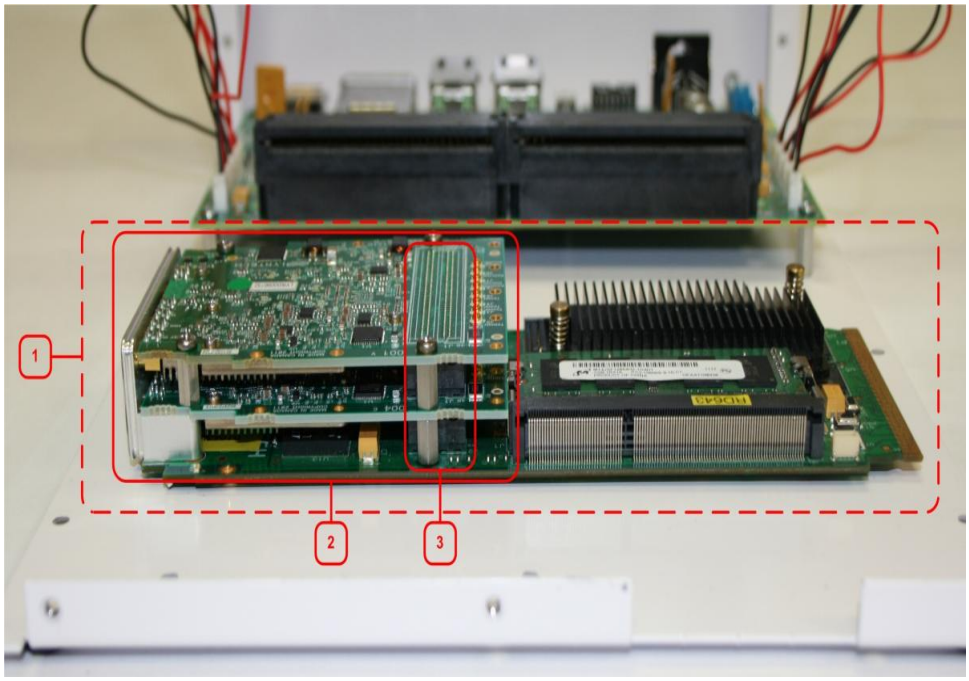


Figure 3.2: PicoSDR Side View

The PicoSDR2x2 front panel gives access to the following connectors for each Radio420:

- 1 TX connector (MMCX antenna connector)
- 1 RX connector (MMCX antenna connector)
- 1 Reference clock in connector. (MMCX).
- 1 Reference clock out connector (MMCX). With the reference clock in connector, allows frequency synchronisation between two Radio420 boards.
- 1 PPS in connector (MMCX). Allows the Radio420 to synchronize its clock to a GPS Pulse-per-second signal.
- 1 custom IO connector (microHDMI). Allows MIMO synchronisation between Radio420m stacks for 4x4 or 8x8 MIMO.

Figure 3.3 shows the BER performance of M-QAM and M-PSK with diversity order of two. It is shown the 64-QAM in terms of BER outperforms other constellation sizes i.e.128-QAM and 256-QAM etc. This is because the large constellation

size becomes prone to phase noise error and small noise vector magnitude might result in decision boundary of the adjacent vector on vector space. Similarly 4-PSK is better than 8-PSK and 16-PSK in terms of BER performance.

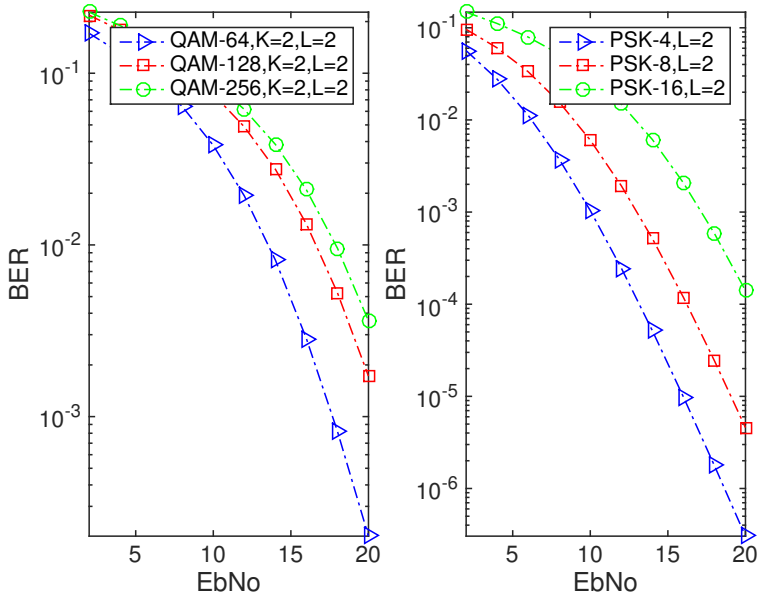


Figure 3.3: BER performance of M-QAM and M-PSK in Rician fading with diversity order of $L = 2$

Figure 3.4 shows the PSD of OSTBC-QPSK modulated signal over 4x4 MIMO channel with $2Hz$ maximum Doppler shift. MATLAB object function known as `comm.MIMOChannel` has been used to generate OSTBC-QPSK modulated signal for transmission over 3-tap and 2-tap fading channel with channel path gains $[0, -5, -7], [0, -3]$and path delays of $[0, 2e^{-3}, e^{-3}], [0, 2e^{-3}]$ respectively.

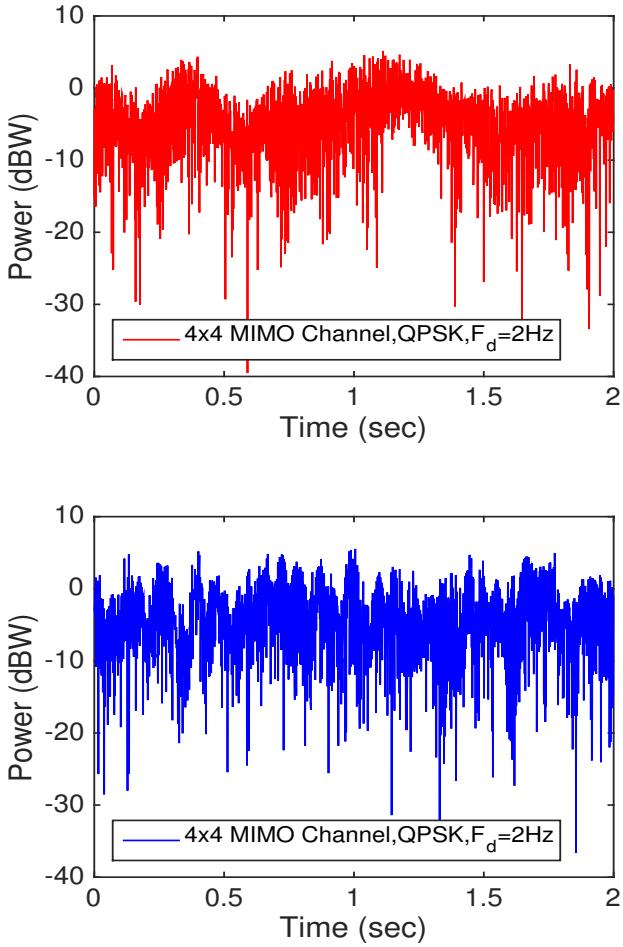


Figure 3.4: PSD of OSTBC-QPSK Signal over 4x4 MIMO Channel 2-tap and 3-tap fading channel Respectively

3.4 Ettus USRP

There are various RF front ends and USRP devices by ettus research which are given as follows:

B200 and B210

- frequency range: 70MHz to 6GHz

- resolution: 12 bit ADC/DAC
- dynamic range: 78 dBc (Spurious Free Dynamic Range)
- Tx/RX Duplexing: full duplex
- USB 3.0, where B200 is bus powered and B210 requires external power for both channels
- it costs around $675 to $1100

N200 and N210

- frequency range: 0 MHz to 46GHz
- dynamic range: daughter card dependent
- instantaneous bandwidth: 25MHz
- external power required
- TX/RX duplexing: full duplex
- Gigabit ethernet and cost around $1515-$1717

X300 and X310

- frequency range: 0 to $6GHz$
- resolution: depends on daughterboard
- instantaneous bandwidth: $120MHz$
- TX/RX duplexing: full duplex
- PCIe x4, ExpressCard or 10 GigE with external power supply
- it costs around $3900 to $4800

E100 and E110

- frequency range: 0 to 6GHz
- resolution: 12-bit ADC, 14-bit DAC
- instantaneous bandwidth: 8MHz
- TX/RX dupling: full duplexing
- external power is required and costs around $1313 to$1515

E300

- frequency range: 70MHz to 6GHz
- resolution: 12-bit ADC/DAC
- dynamic range: 78 dBc
- TX/RX duplexing: full duplex
- Embedded Xilin Zynq-700
- battery powered and has form factor of bulky cell phone

3.5 BWRC's BEE2 and BEE3

Berkeley Emulation Engine 2 (BEE2) is an scalable FPGA based computing platform that targets many applications for high performance signal processing such as cognitive radio, real-time telescope signal processing, bioinformatics and sequence matching etc. BEE2 is general purpose module and have five Xilinx FPGAs, 20GB high-speed DDR2 DRAM memory, and high-speed serial and parallel links to connect FPGAs. BEE3 is extended version of BEE2 with high amount of memory and its PCB can host variants of Xilinx FPGA Virtex 5. Figure 3.5 shows actual BEE2 board and Fig. 3.6 shows the schematic layout of BEE2 board.

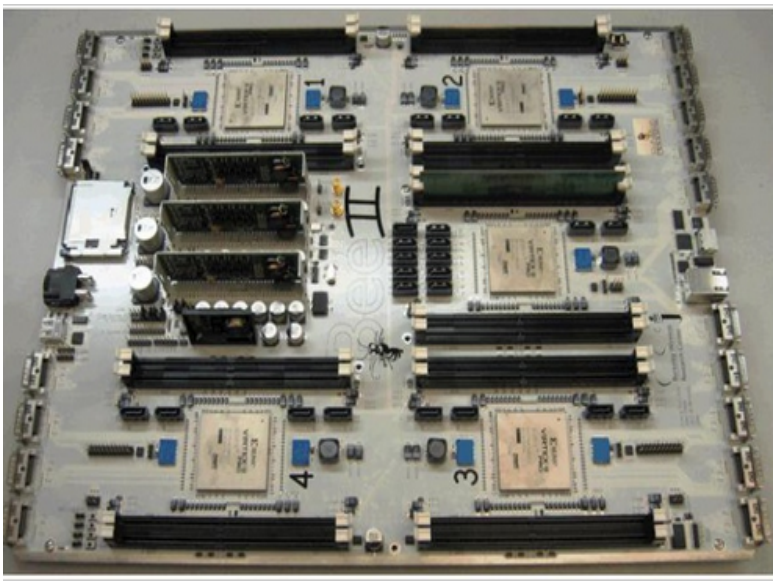


Figure 3.5: BWRC's Berkeley Emulation Engine

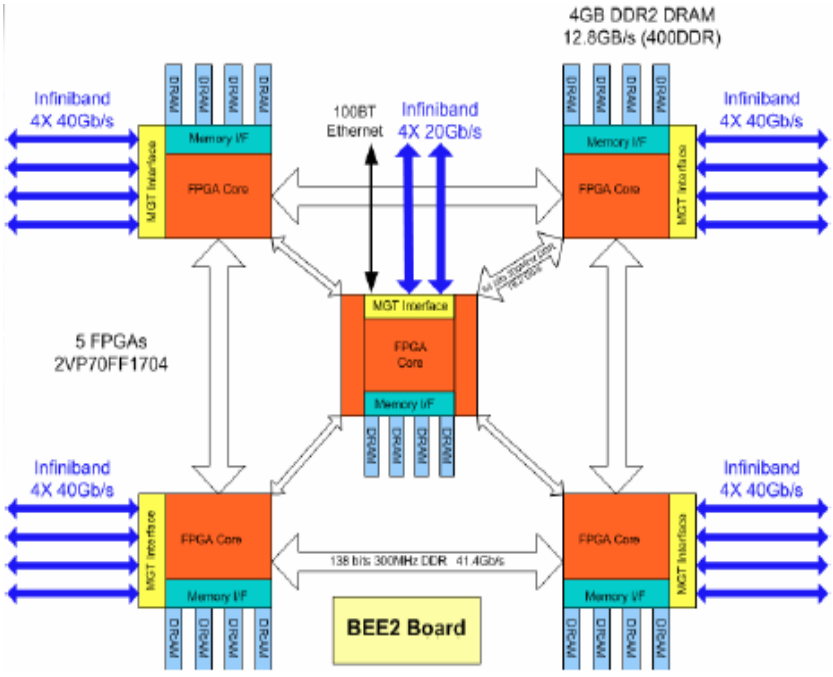


Figure 3.6: BEE2 Board Layout

3.6 WARP SDR

WARP SDR is developed by Rice University and is an open source platform and can be bought from third party vendor. It allows users to incorporate their own daughter cards to extend the functionalities for example RF computing. Rice WARP board has a Xilinx Virtex-II pro FPGA as shown in Fig. 3.7 and contains the following:

- PowerPC core
- three Gigabit ethernet to support fast I/O
- four additional daughtercard interfaces

the interface include

- *analog interface card*: it further contains 14-bit 65 MSPS ADC and a dual 16-bit 125 MSPS DAC
- *RF interface*: it allows transmit and receive at 2400-2500MHz and 4900-5875MHz

A more recent Rice WARP board uses Virtex-4 FPGA offering more slices, support for upto 2GB of memory and a higher clock rate. Finally, Rice WARP allows free implementation of OFDM on FPGA for Virtex-II pro FPGA in addition to CSMA MAC protocol.

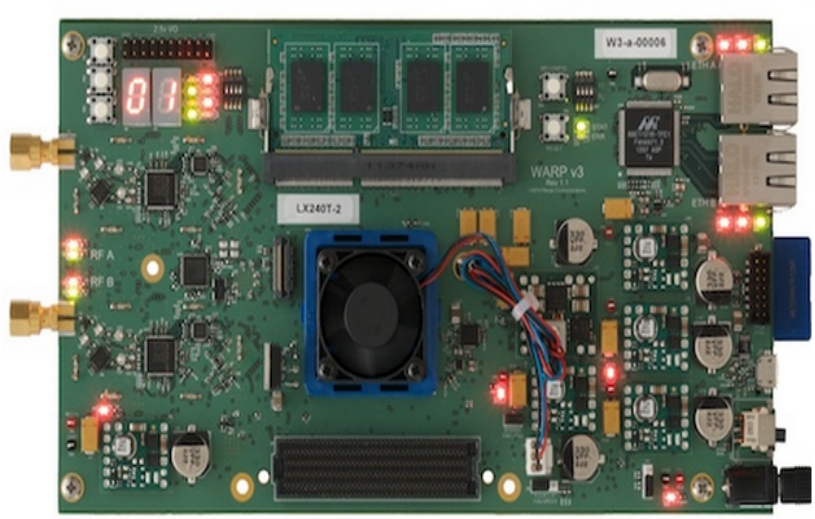


Figure 3.7: Rice University's WARP Prototype

3.7 WhiteRhino

Whitespace Reconfiurable Hardware Interface for ComputatioN and RadiO (Whitespace RHINO)[13] is an SDR platform for Radar. It contains Xilinx Zynq7000 and Lim Micro LMS6002D primary system on chip (SoCs) and has the processing architecture similar to Digilent Zed-board. The board hosts two 1000 base-T Ethernet connections, 12v battery and Power over Ethernet (PoE). White Rhino is able to perform:

- Detect surface based or airborne targets
- implement WRAN IEEE 802.22 standard

Figure 3.8 shows the White RHINO board on which various hardware ports and communications networking ports are visible.

Table 3.1: Computational requirements of White RHINO[13]

S.No.	Requirements	Description
1	Programmable Logic	FPGA Zynq7000
2	Processing	Dual-Core ARM Cortex A-9 processors
3	Memory	512 MB DDR3 SDRAM
4	TX Power	30dBm or 1W
5	Operational BW	512MHz-698MHz
6	Ports	2X 1000 Ethernet
7	Power Consumption	less than 25W

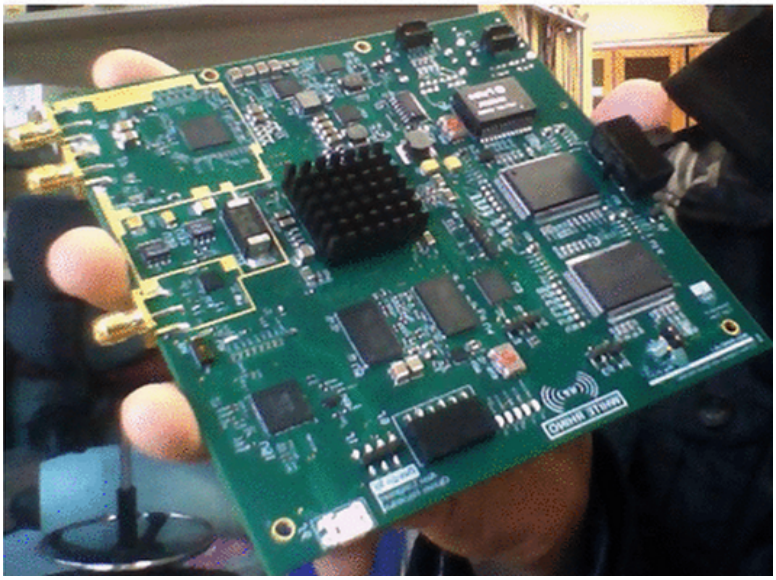


Figure 3.8: White RHINO board[13]

3.8 RTL-SDR

Specifications of RTL-SDR varies, but the typical specifications are:

- frequency range: 25MHz to 2100MHz
- resolution: 8 bits

- dynamic range: not great
- instantaneous BW: 2.4MHz
- TX/RX duplexing: receiver only
- USB 2.0 and is bus powered
- costs between $15-$30

Figure 3.9 shows internal circuitry of DVT-T, DAB+FM USB dongle.



Figure 3.9: RTL-SDR DVB-T, DAB+FM teardown

Figure 3.10 shows the time variation of the received signal and the corresponding waterfall graph of the received signal. There received signal is colour coded where dark red shows the signal activity on a yellow and light blue background which means noise only.

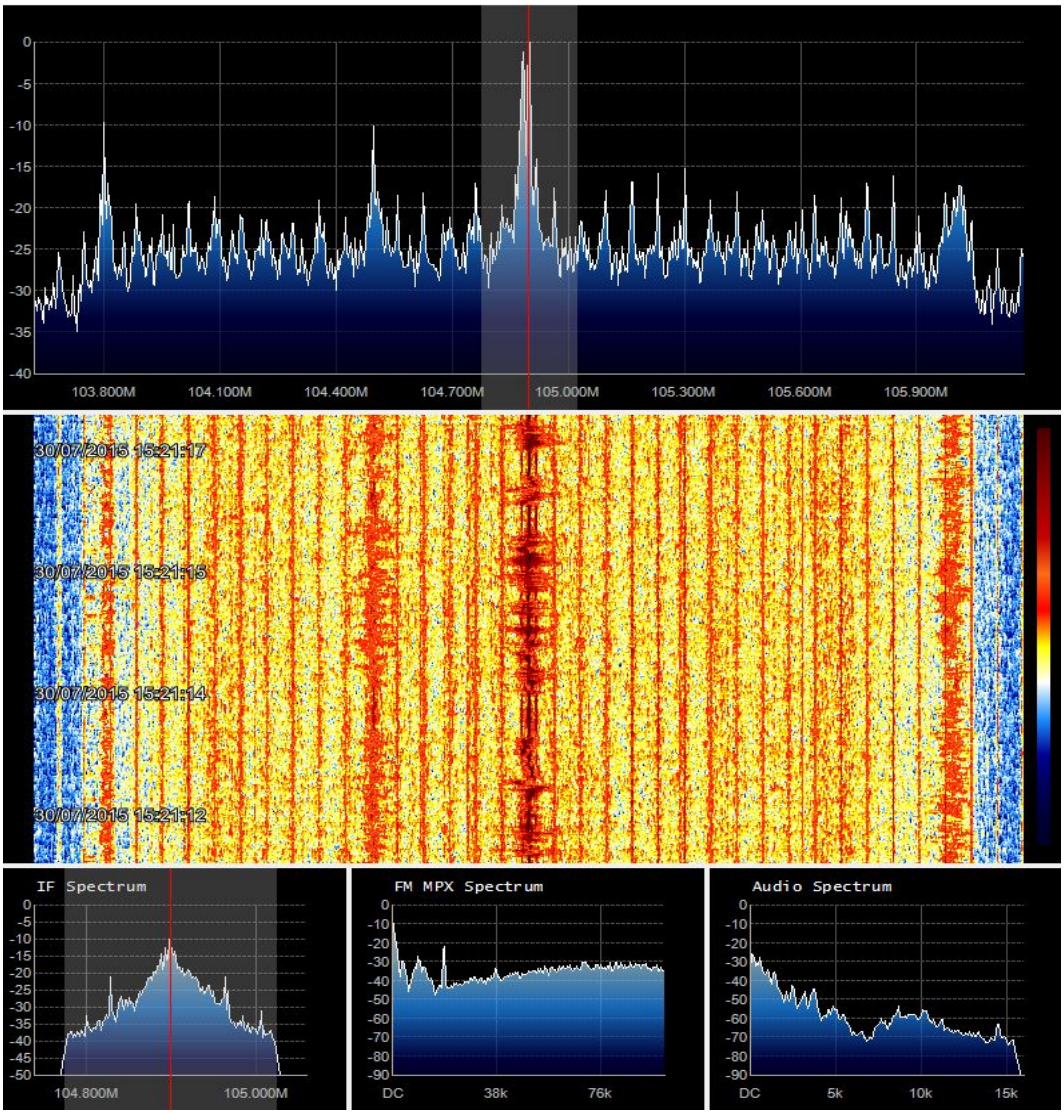


Figure 3.10: BBC Leicester FM 104.9 signal, waterfall graph,IF spectrum, MPx spectrum, and audio spectrum as received on DAB-T USB dongle at High Frequency Measurement and Characterization Lab,GGIEMR, The University of Nottingham,UK

3.9 Summary

Different hardware platforms are used to realise a software defined radio or cognitive radio communication system, hardware platforms targeted for SDR/CR are

often designed to meet the specification of SDR/CR systems. Therefore, almost all of the SDR platforms are reconfigurable and multi-standard with high-performance FPGA on it. There are different hardware challenges in order to realise a fast and efficient cognitive radio. Few to mention are ADC/DAC resolution, programmability and linearity of RF front-ends, large bandwidths and sampling rates. Famous SDR platforms include USRP from Ettus research, picoSDR from Nutaq, WARP SDR from Rice University, BEE2 and BEE3 from Berkeley wireless research centre, and other cheap receive only platforms like RTL-SDR USB dongle. picoSDR from Nutaq's is multi-mode and multi-standard table top SDR solution that incorporates two powerful multimode SDR dual-channel RF transceiver modules. PicoSDR can uplink and downlink data stream to remote computer with linux or windows. PicoSDR can be configured in 2x2 or 4x4 MIMO fashion. PicoSDR2x2 is equipped with Virtex6 FPGA, Radio420M FMC stack, two radio420 daughter cards. Similarly, Ettus research supplies URRP and different RF front ends few are B200, N200, X300 and E300 with different frequency ranges, ADC/DAC resolution, dynamic range and FPGA types. Other notable SDR platforms are BWRC BEE2/BEE3, Rice's WARP and White Rhino. Cheap and handy RTL-SDR is used to decode FM and DAB-T signals which can be visualised using SDR# on windows-based PC.

Chapter 4

TVWS Network Architecture and WSDB Implementation

4.1 Introduction

In chapter focuses on another widely known paradigm of CR which is obtaining under-utilised channels through white space database (WSDB). Different methods of accessing WSDB and channel assignment strategies are discussed for example how AP in IEEE 802.11af standard assigns available channels to its Mode I devices. Briefly explanation of the standards is given and compared the architecture of two famous TVWS standards WRAN IEEE 802.22 and WLAN IEEE 802.11af. Parameters like bandwidth, type of modulation, code rate, TX power and Rx sensitivity have been shown in tabular form for comparison. Considering the effect of interference with the help of comprehensive coexisting TVWS standards diagram. Special interference possibilities are the interference from SU to PU or interference between existing and co-locating CRNs. Finally, this chapter has been concluded with accessing strategies of WSDB by white space devices (WSD).

4.2 Cognitive Radio Standards in TVWS

This section briefly defines various standards which are designed truly on cognitive principles in addition to foreseeable wireless standards that shall migrate to

TVWS. Therefore it's essential to know about their network architecture, spectrum requirements and interference limitations. Because of this wireless standards that operate in TVWS are focused.

4.2.1 IEEE 802.11af

IEEE 802.11af is OFDM based WLAN standard which is specially targeted for TVWS. It's also known as super WiFi or White WiFi and uses CSMA like MAC protocol. Its network architecture according to FCC specifications consists of a fixed device Mode II known as Access Point(AP) and portable or Mode I mobile device, OFCOM stipulates it as master and slave architecture. It uses a fix bandwidth of 5 MHZ or 10 MHz, 20 MHz using bonding of multiple non-contiguous subbands. IEEE 802.11af is characterised with lower transmission power of 100mW and sensing threshold of -64 dBm.

- *GDB enabling Station* This entity in IEEE 802.11af is directly connected with GDB and get access to White Space Map(WSM) which contains the permissible frequencies in particular area within Basic Service Set (BSS). This device has the capability to update and enable the Mode I or slave devices based on the geolocation information sent by them. It also maintains the WSM through intermittent signal sent.

- *GDB dependent Station*: GDD dependent station is Mode I device always connected and operates under the instructions of the GDD enabling station which get the WSM from GDB based on the coordinates transmitted by it. WSM which contains the empty frequency bands suitable for GDD dependent station transmission. GDD sends contact verification signal (CVS) to verify the validity of WSM.

4.2.2 IEEE 802.22

IEEE 802.22 is an point-to-multipoint architecture for internet access at remote locations and rural areas. It consists of fixed device known as Base Station (BS) and a portable device known as customer premises equipment(CPE). It uses TDMA like MAC protocol and serves a cell range of 10 km–100 km. Transmission power

of 802.22 is 4 W(36 dBm), reception sensitivity of -97 dBm and transmission bandwidth of 6 MHz. Fixed devices are not permitted in VHF band, they are allowed to transmit in UHF channels except 14-20 channels and channel 37 which is reserved for radio astronomy related measurements. There is additional requirement for fixed devices that is its antenna should be mounted outdoors at least 10m above ground.

It can be seen that the sensing threshold of IEEE 802.11af is much greater than sensing threshold of IEEE 802.22 i.e. -64dBm>>-97dBm. In contrast, transmission power of IEEE 802.22 is 80% greater than the transmission power of IEEE 802.11af AP i.e. 4W(36dBm)>>100 mW(20 dBm). These transmission power caps are valid when CR is transmitting in TVWS non-adjacent to incumbent-occupied or primary user band. Transmission power for adjacent TVWS drops to 1 W(30 dBm) for IEEE 802.22 and 40 mW(16 dBm) for IEEE 802.11af. This is because of the low cost digital filters can spill over in the adjacent bands and interfere–aptly known as out-of-band(OOB) interference. It can be seen from Tab. 1 that IEEE 802.22 uses Low Density Parity Check (LDPC) codes as a Forward Error Correction (FEC) techniques which guarantees near-Shannon limit performance for larger block lengths and ensure decodability at lower SNRs. LDPC when combined with diversity techniques like Space-Time Block Code (STBC) can deliver higher data rates. IEEE 802.11af delivers high throughput comparatively at shorter distances that depends on the choice of modulation schemes and hence the gradient data rates.

Table 4.1: OFDM based cognitive wireless standards in TVWS

Parameter	IEEE 802.22	IEEE 802.11af
Bandwidth	6,7,8 [MHz]	5,10,20 [MHz]
FFT size	2048	64,128,256,512,1024
Modulation	OFDM/ QPSK, 16QAM, 64QAM	OFDM/BPSK, QPSK, 16QAM, 64QAM
Data Subcarrier	1440	48
Symbol Duration	317.39μs	4 μs
Maximum Data Rate	22.69Mbps	12 Mbps
FEC	CC, STBC, LDPC	CC
Coding Rate	5/6	3/4
MA Scheme	OFDMA	CSMA/CA, TDMA
Tx Power [dBm]	20dBm	20 and 16dBm
Rx Sen. [dBm]	-97dBm	-64dBm
Frame Length[Octets]	4096	2048

4.2.3 Vehicle-to-Vehicle (V2V) Communication

Apart from earlier discussed standards cognitive radio can be used for vehicle-to-vehicle communication. In[14], it has been experimentally shown the communication between three vehicles or nodes in TVWS using Zone Aware Control Channel (ZACC) and Swarm Aware Control Channel(SACC) for real-time image or break information transmission. Additionally, Ettus Research USRP equipment has been used for reconfigurability, the dual polarization antenna for interference avoidance and wideband energy detection for sensing with the concept of Quite Period (QP) and Data Period (DP). It has been experimentally shown that the probability of missed detection is less than 10^{-5} for 10^5 sensing samples.

4.3 Interference Mitigation in Heterogenous CRNs

The issue of interference is of high importance that is likely when many of the wireless networks may migrate to operate in TVWS. There will be interference between low-power devices in IEEE 802.11af, ECMA 392 and IEEE 802.22 high-powered BS. Interference may also increase because of the favourable propagation in VHF/UHF which tends to increased distance in contrast to WLAN standards where spatial reuse is used for capacity enhancement. Interference in TVWS can be divided into the following three categories:

4.3.1 Interference to PU and Interference from PU

TV stations transmitting as high as 1000 KW may contribute to interference to secondary cognitive networks and prevent secondary user to detect the incumbent or PU. Such interferences are usually subject to locations, frequency, time and transmission powers. Interference minimisation techniques can be categorised into three groups which are as follows:

- *Interference Avoidance*: Both primary and secondary networks use TDMA or FDMA to assess the their respective spectrum in order to avoid interference to primary users. The main idea is detection and sharing of the gaps in TVWS.

- *Interference Control*: In this technique PU and SU can coexist on the same spectrum provided they don't introduce harmful interference to each other and can be judged by QoS parameters. Concept of MIMO-smart antenna is proposed in which cognitive user direct their signals at the null of PU. In [15], throughput of cognitive radios under various interference limits is well investigated.

- *Interference Mitigation*: It has similar mechanism as interference control, but here additional information is needed about the primary users messages or codebooks. It is also known as Opportunistic Interference Cancellation (OIC) where secondary users have information about the primary users codebook with partial or full transmission messages.

4.3.2 Interference among CRNs

Multiple CRNs may select the same channel because of the limited channel availability or additional constraints which force them to operate co-channel. Co-channel operation or less information about each other's transmission may result in packet drop and can degrade the performance of entire CRN cluster. Interference contribution to TVWS can be assessed by the following factors:

- *Channel Bandwidth*: WRAN IEEE 802.22 operate over channel bandwidth of 6 MHz and IEEE 802.11af operate on channel bandwidth of 5 MHz or 10 MHz and 20 MHz by bonding two or more available TV channels etc.

- *Insufficient Signal-to-Interference plus Noise Ratio*: SINR is generally considered as direct replacement of Frame Error Rate (FER), but this may differ for heterogenous networks case where the interference is treated as non-Gaussian noise. In [16], FER and BER in Gaussian noise are mathematically related as follows:

$$FER = 1 - (1 - BER)^{L_{frame}} \tag{4.1}$$

  Where L_{frame} is the length of the frame.

- *Variation in Power levels*: CRNs consist of mix of devices with variable power levels and classified as Master and Slave by OFCOM and Mode I and Mode II devices as mentioned earlier in architecture of IEEE 802..22 and IEEE 802.11af. For example fixed device in IEEE 802.22 may transmit a power of 4 W EIRP and Mode II or portable may transmit to a maximum of 100 mW. Any device with very small power levels can easily be masked out by the louder users i.e. user closer to the BS or with high SNRs.

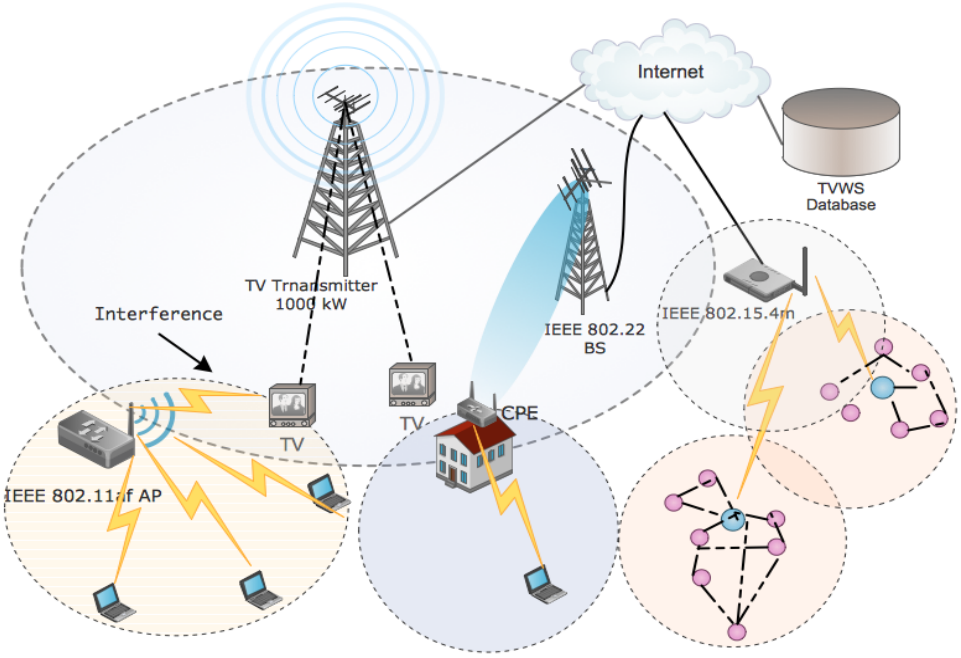


Figure 4.1: Coexistence and Interference scenario of CRNs in TVWS

4.4 TVWS Database Implementation

Geolocation database can receive inputs from multiple entities for example from public users, white space devices, licensed PUs, other WSDs, and regulators etc. It may held bidirectional session with data sources, WSDs, and other GDBs as shown in 4.2.

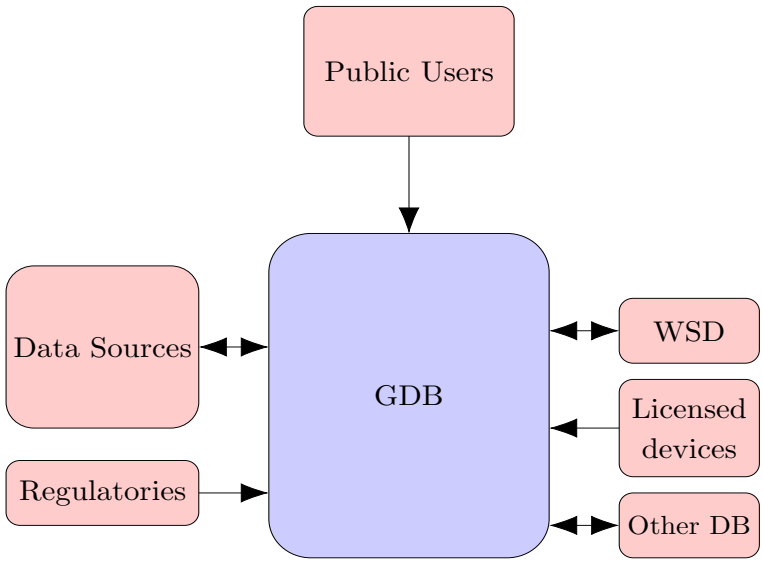


Figure 4.2: Database Architecture

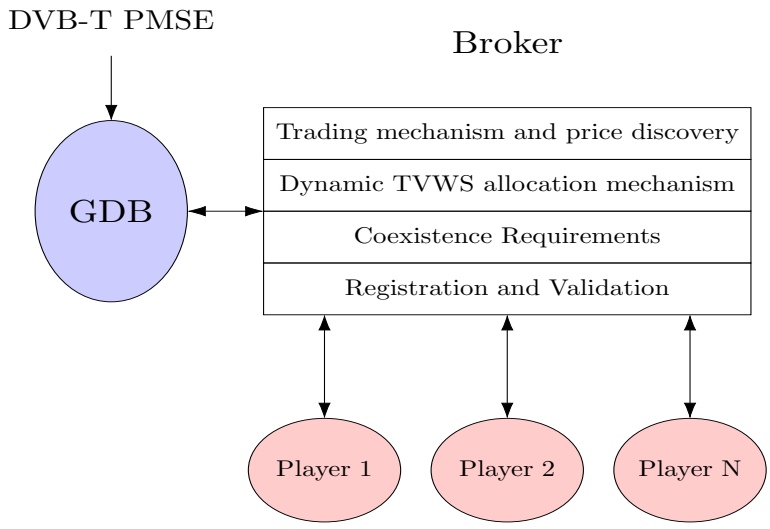


Figure 4.3: Cognitive Radio ETSI Database Implementation

4.5 Summary

There are two types of CR paradigms which are obtaining the information about under-utilised bands using WSDB or through performing sensing at each independent CR. These techniques are central to broadband standards targeted for WRAN, WLAN and WPAN type of networks for example IEEE 802.22, IEEE 802.11af and IEEE 802.15.4m etc. There can be host of other standards migrating to TV band which results in interference and state-of-the-art self-location techniques. IEEE 802.11af uses OFDM in its PHY layer and uses fixed bandwidth of 5MHz or 10MHz or 20 MHZ. Its architecture consists of Mode I devices and Mode II devices. IEEE 802.11af is characterised with lower transmission power of 100 mW and sensing threshold of -64 dBm. Additionally, it has GDB enabling station and GDB dependent station in its architecture. Similarly, IEEE 802.22 is used for point-to-multipoint architecture for broadband internet access in rural areas and covers the range of 10 km to 100 km. Similar to IEEE 802.11af it also uses transmission power cap which is 4 W or 36 dBm and uses frequency bandwidth of 6 MHz and reception sensitivity of -97 dBm. Both of the TV white space standards use OFDM in PHY layer with BPSK, QPSK and M-QAM modulation schemes with some form of coding for example convolutional codes and LDPC codes. Therefore, BER and FER performance of different modulation as standardised in IEEE 802.22 and IEEE 802.11af is essential. In order to meet the same BER and FER performance certain power penalty is experienced in fading than AWGN channel for all type of modulation techniques.

Chapter 5

Spectrum Sensing and Sensing-Throughput Tradeoff

5.1 Introduction

In this chapter heart of pragmatic Cognitive Radio i.e. spectrum sensing and decision making for single CR and the cooperative CR is discussed. In the very beginning single-sample measurement and multiple sample measurement are taken into consideration which form the basis for further discussion. The aim of this chapter is to derive the analytical expressions for probability of detection and probability of false alarm for single CR and multiple CR which operate in cooperative fashion using different information and decision fusion strategies, for example AND, OR and ML rule. In cooperative cognitive radio the maximisation of throughput of the SU for a given target probability of detection and target probability of false alarm is stressed. The concept of single slot sensing to multislot sensing is extended under the condition that the fading coefficients are known and unknown with different decision fusion strategies. Thereafter, unique solution of beacon placement at the PU receiver to avoid interference is discussed and probability of beacon missed detection and probability of outage for such setup has been emphasised in Rayleigh and Rician fading channel.

5.2 Binary Hypotheses

Binary hypothesis decision theory for single sample measurements and multiple sample measurements for noise only or null-hypothesis and signal plus noise or alternative hypothesis is used to detect the presence or absence of PU.

5.2.1 Single Measurement

Let us say $\mathcal{H}_0$ is null hypothesis means when no signal is present. Similarly, $\mathcal{H}_1$ is defined as the alternative hypothesis means signal is present along with noise. For a single sample measurement two types of hypothesis are:

$$X = \begin{cases} w & \mathcal{H}_0 \\ \\ A + w & \mathcal{H}_1 \end{cases} \tag{5.1}$$

Where w is AWGN with zero mean and variance σ^2 i.e. $w \sim \mathcal{N}(0, \sigma^2)$ and has the PDF:

$$p_W(w) = \frac{1}{\sqrt{2\pi}\sigma} \exp\left(\frac{-1}{2}\Big(\frac{w - \mu_w}{\sigma}\Big)^2\right) = \frac{1}{\sqrt{2\pi}\sigma} \exp\left(\frac{-1}{2}\Big(\frac{w}{\sigma}\Big)^2\right) \tag{5.2}$$

and

$$\begin{aligned} \text{Under} \quad \mathcal{H}_0 \ &: p(x|\mathcal{H}_0) \sim \mathcal{N}\Big(0, \sigma^2\Big) \\ \text{Under} \quad \mathcal{H}_1 \ &: p(x|\mathcal{H}_1) \sim \mathcal{N}\Big(A, \sigma^2\Big) \end{aligned} \tag{5.3}$$

Where $p(x|\mathcal{H}_0)$ and $p(x|\mathcal{H}_1)$ are the conditional PDFs for null-hypothesis and alternative hypothesis.

5.2.2 Multiple Measurements

Single measurement analytical expressions can be extended for multiple measurement case for N samples or readings at the output of the energy detector.

$$x(n) = \begin{cases} w(n) & \mathcal{H}_0 \quad n = 1, 2, 3, ..., N-1 \\ A + w(n) & \mathcal{H}_1 \end{cases} \tag{5.4}$$

Now the average of data points also known as *test statistics* can be written as:

$$T = \frac{1}{N} \sum_{n=0}^{N-1} x(n) \tag{5.5}$$

and the test statistics T can be compared with threshold γ to select noise only case or signal plus noise as follows:

$$T = \frac{1}{N} \sum_{n=0}^{N-1} x(n) \underset{\mathcal{H}_0}{\overset{\mathcal{H}_1}{\gtrless}} \gamma \tag{5.6}$$

Test statistics T is sum of Gaussians and has the mean for null-hypothesis and alternative hypothesis as follows:

$$\begin{aligned} \mathbb{E}\big(T|\mathcal{H}_0\big) &= \mathbb{E}\Big(\frac{1}{N} w(n)\Big) = 0 \\ \mathbb{E}\big(T|\mathcal{H}_1\big) &= \mathbb{E}\left(\frac{1}{N}\Big(A + w(n)\Big)\right) = \frac{NA}{N} = A \end{aligned} \tag{5.7}$$

and its variance for the two hypotheses as:

$$\begin{aligned} Var(T|\mathcal{H}_0) &= Var\Big(\frac{1}{N} \sum w(n)\Big) = \frac{1}{N^2} \sum Var(w(n)) \\ &= \frac{1}{N^2} N\sigma^2 = \frac{\sigma^2}{N} \end{aligned} \tag{5.8}$$

$$Var(T|\mathcal{H}_1) = \frac{\sigma^2}{N} \tag{5.9}$$

In nutshell the test statistics under two hypotheses is as under:

$$\begin{aligned} \mathcal{H}_0: \quad & T \sim \mathcal{N}\Big(0, \frac{\sigma^2}{N}\Big) \\ \mathcal{H}_1: \quad & T \sim \Big(A, \frac{\sigma^2}{N}\Big) \end{aligned} \tag{5.10}$$

Now performance metric SNR as ratio of powerA^2 in signal to noise power$\frac{\sigma^2}{N}$ which is given as:

$$SNR = \frac{A^2}{\sigma^2/N} = \frac{A^2}{\sigma^2}N \tag{5.11}$$

From above expression it can be seen that detection performance of the system improves if:

$$SNR^{\uparrow} \Rightarrow A^{\uparrow}, N^{\uparrow}, {\sigma^2}_{\downarrow} \tag{5.12}$$

Figure 5.1 shows the histogram of null-hypothesis and alternative hypothesis and show how these performance parameters may affect the detection performance of the receiver.

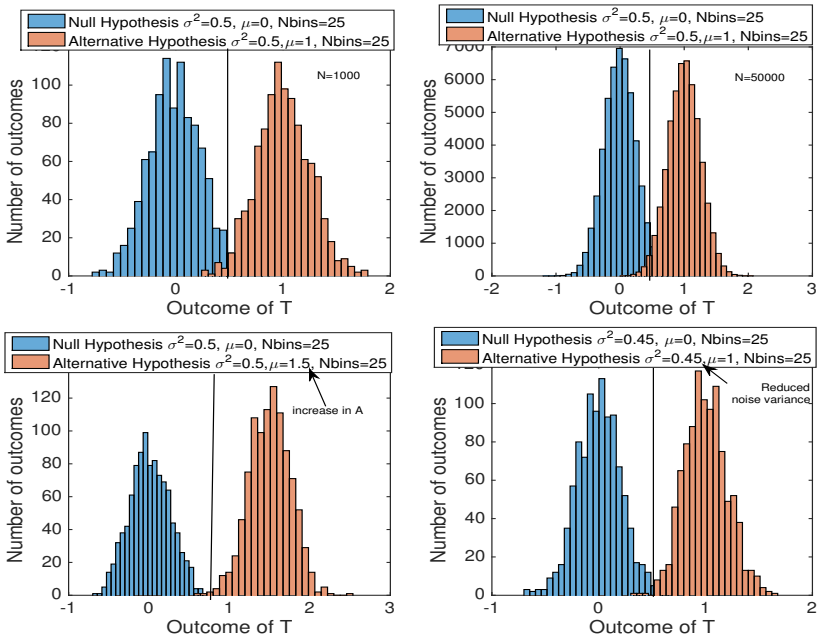


Figure 5.1: Null hypothesis and alternative hypothesis with increase in signal mean A, increase in sample size N and decrease in variance σ^2

Figure 5.2 shows the sinusoid and noise signal on time-frequency graphs and their corresponding PSD estimates in dB/Hz using Welch method are also shown.

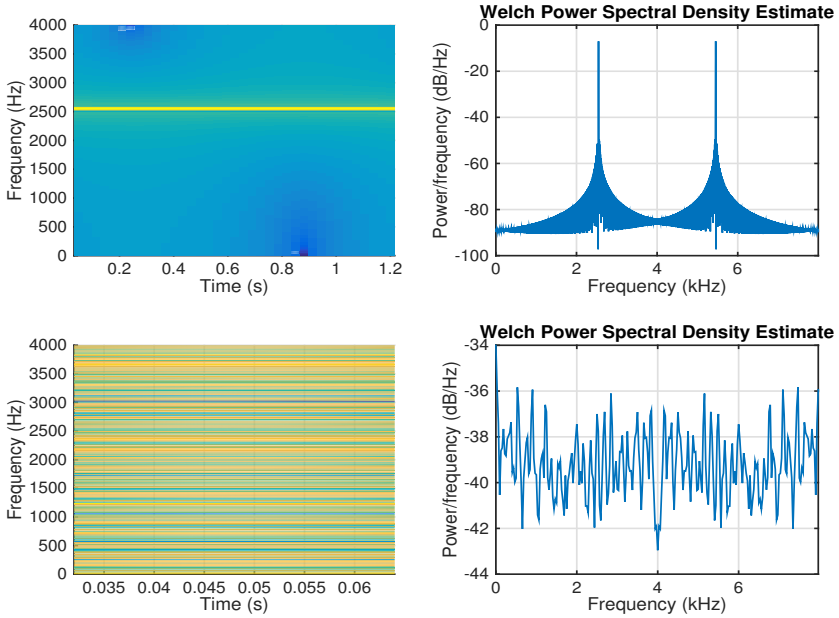


Figure 5.2: Spectrogram and PSD of a sinusoid and AWGN noise with $\mu = 0$ and $\sigma = 1$

5.3 Likelihood Ratio Test (LRT)

Here detailed investigation of the performance analysis of likelihood ratio test is done and analytical expression are developed for probability of detection P_D in terms of probability of false alarm P_{FA}, sample size N and noise variance σ^2. Therefore, system model for binary hypotheses can be written as:

$$x(n) = \begin{cases} w(n) & \mathcal{H}_0 \quad n = 1, 2, 3, ..., N-1 \\ A + w(n) & \mathcal{H}_1 \end{cases} \tag{5.13}$$

Above expressions for system model can be rewritten as:

$$\begin{aligned} \mathcal{H}_0 : \quad & \mathbf{x} = \mathbf{w} \\ \mathcal{H}_1 : \quad & \mathbf{x} = A.\mathbf{I} + \mathbf{w} \end{aligned} \tag{5.14}$$

Where $\mathbf{x} = [x_1, x_2, ..., x_N]^T$,$\mathbf{w} = [w_1, w_2, ..., w_N]^T$ and $\mathbf{I} = [1, 1, ..., 1]^T$ are the signal vector, noise vector and vector of ones. Now ratio of the two likelihoods which is also known as likelihood ratio test (LRT):

$$\frac{p(\mathbf{x}|\mathcal{H}_1)}{p(\mathbf{x}\mathcal{H}_0)} \gtrless \xi \tag{5.15}$$

$$\begin{aligned} p(\mathbf{x}|\mathcal{H}_1) &= \frac{1}{\left(2\pi\sigma^2\right)^{N/2}} \exp\left(\frac{-1}{2}\Big(\mathbf{x} - A\mathbf{I}\Big)^T \mathbf{c}^{-1}\Big(\mathbf{x} - A\mathbf{I}\Big)\right) \\ p(\mathbf{x}|\mathcal{H}_0) &= \frac{1}{\left(2\pi\sigma^2\right)^{N/2}} \exp\left(\frac{-1}{2}\mathbf{x}^T\mathbf{c}^{-1}\mathbf{x}\right) \end{aligned} \tag{5.16}$$

$\therefore$

$$L(\mathbf{x}) = \frac{\exp\left(\frac{-1}{2\sigma^2}\sum\Big(x(n) - A\Big)^2\right)}{\exp\left(\frac{-1}{2\sigma^2}\sum x^2(n)\right)} \underset{\mathcal{H}_0}{\overset{\mathcal{H}_1}{\gtrless}} \xi \tag{5.17}$$

Taking log on bothside

$$\frac{-1}{2\sigma^2}\sum\big(x(n) - A\big)^2 + \frac{1}{2\sigma^2}\sum x^(n) \underset{\mathcal{H}_0}{\overset{\mathcal{H}_1}{\gtrless}} = \ln\xi \tag{5.18}$$

$$\frac{-1}{2\sigma^2}\Big(-2A\sum x(n) + NA^2\Big) \underset{\mathcal{H}_0}{\overset{\mathcal{H}_1}{\gtrless}} \ln\xi \tag{5.19}$$

$$\underbrace{T(x) = \frac{1}{N}\sum_{n=0}^{N-1} x(n)}_{\text{Sufficient statistic}} \underset{\mathcal{H}_0}{\overset{\mathcal{H}_1}{\gtrless}} \underbrace{\frac{\sigma^2}{NA}\ln\xi + A/2}_{\xi'} \tag{5.20}$$

Where noise variance σ^2 and signal amplitude A are unknown.

5.3.1 Performance Analysis

Considering test statistics $T(x) = 1/N\sum_{n=0}^{N-1} x(n)$ as random variable such that

$$\begin{aligned}\mathbb{E}\Big(T(x)|\mathcal{H}_0\Big) &= \mathbb{E}\bigg(\frac{1}{N}\sum w(n)\bigg) = 0 \\ \mathbb{E}\Big(T(x)|\mathcal{H}_1\Big) &= A\end{aligned} \tag{5.21}$$

$$\begin{aligned}Var\Big(T(x)|\mathcal{H}_0\Big) &= Var\left(\frac{1}{N}\sum w(n)\right) \\ &= \frac{1}{N^2}N\sigma^2 = \frac{\sigma^2}{N} \\ &= Var\Big(T(x)|\mathcal{H}_1\Big)\end{aligned} \tag{5.22}$$

$\because$

$$\begin{aligned}\mathcal{H}_0: &\quad T(x) \sim \mathcal{N}\Big(0, \sigma^2/N\Big) \\ \mathcal{H}_1: &\quad T(x) \sim \mathcal{N}\Big(A, \sigma^2/N\Big)\end{aligned} \tag{5.23}$$

Now the probability of false alarm $P_{FA} = Pr.\Big(T(x) > \gamma|\mathcal{H}_0\Big)$ can be given as follows:

$$\begin{aligned}P_F = Pr.\Big(T(x) > \xi|\mathcal{H}_0\Big) &= \int_{\xi'}^{\infty} \frac{1}{\sqrt{2\pi\sigma^2/N}} \exp\left(\frac{t^2}{2\sigma^2/N}\right)dt \\ = Q\bigg(\frac{\xi'}{\sqrt{\sigma^2/N}}\bigg) = \alpha \Rightarrow \xi' &= \sqrt{\frac{\sigma^2}{N}}Q^{-1}\Big(P_{FA}\Big)\end{aligned} \tag{5.24}$$

Similarly, the probability of detection $P_D = Pr.\Big(T(x) > \xi\mathcal{H}_1\Big)$ can be given as

follows:

$$\begin{aligned} P_D &= \int_{\xi'}^{\infty} \frac{1}{\sqrt{2\pi\sigma^2/N}} \exp\left(\frac{-\left(t-A\right)^2}{2\sigma^2/N}\right) dt \\ &= Q\left(\frac{\xi' - A}{\sqrt{\sigma^2/N}}\right) \\ &= Q\left(\frac{\sqrt{\sigma^2/N}Q^{-1}\left(P_F\right) - A}{\sqrt{\frac{\sigma^2}{N}}}\right) \\ &= Q\left(Q^{-1}\left(P_F\right) - \sqrt{\frac{NA^2}{\sigma^2}}\right) \end{aligned} \tag{5.25}$$

and the probability of missed detection $P_{md} = Pr.\left(x < \xi | \mathcal{H}_1\right)$

$$\begin{aligned} P_{MD} &= 1 - P_D \\ &= 1 - Q\left(Q^{-1}\left(P_F\right) - \sqrt{\frac{NA^2}{\sigma^2}}\right) \end{aligned} \tag{5.26}$$

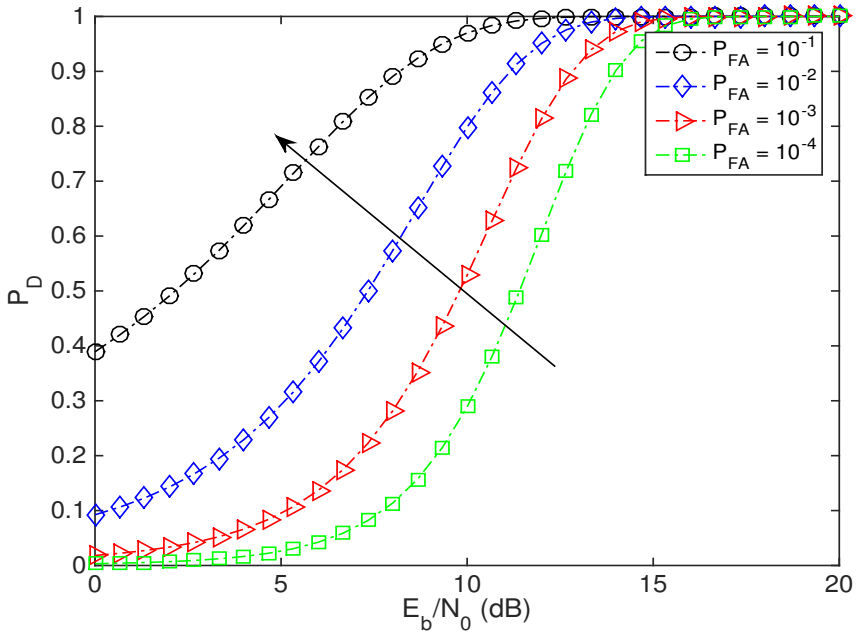


Figure 5.3: Probability of detection for various values of probability of false alarm

Figure 5.6 shows the probability of detection versus $E_b/N_0$for various values of probability of false alarms. It can see that the P_D increases with the increase in P_{Fa}.

5.4 Spectrum Sensing

Cognitive Radio performs spectrum sensing in order to harness the spectrum opportunity without introducing the harmful interference to incumbent. CR frame structure is shown in the following Fig. 5.4 where it can be seen that the total frame time is divided into sensing time, sensing decision reporting time and data transmission time. Increase in sensing time may yield increased probability of detection hence better protection for PU, but at the cost of low data transmission period which means less throughput for SU.



Figure 5.4: Frame Structure used in Cognitive Radio

5.5 System Model

Spectrum sensing involves the decision regarding presence of PU from the observations of a signal received at the receiver. Therefore, sampled received signal at ℓth CR node:

$$\begin{aligned} y_\ell(n) &= s_\ell(n) + w_\ell(n) \\ n &= 0, 1, 2, \ldots, N-1 \\ \ell &= 1, 2, \ldots, M \end{aligned} \tag{5.27}$$

Where $s_\ell(n)$ is the signal from primary user received at ℓth CR and is modelled as iid Gaussian process with mean zero and variance $E[|s_\ell(n)|^2] = \sigma_s^2$ i.e. $s_\ell(n) \sim \mathcal{N}(0, \sigma_s^2)$and $w_\ell(n)$ is the sampled signal at ℓth CR and is also iid Gaussian process

with zero mean and variance of $E[|w_\ell(n)|^2] = \sigma_w^2$ i.e. $w_\ell(n) \sim \mathcal{N}(0, \sigma_w^2)$.Moreover, the two processes are independent such that $E[s_\ell(n)w_\ell(n)] = 0$ Now, under the hypotheses $\mathcal{H}_0$ and $\mathcal{H}_1$ respectively it can be written:

$$\mathcal{H}_0 : y_\ell(n) = w_\ell(n) \tag{5.28}$$

$$\mathcal{H}_1 : y_\ell(n) = h_\ell(n)s(n) + w_\ell(n) \tag{5.29}$$

where $h_\ell(n)$ is a flat-fading channel gain between PUs and the SUs such that one-tap equalizer shall be required at the CR. Now, average PU SNR at each CR can be given as follows:

$$\begin{aligned} \gamma &= E[|h_\ell(n)|^2]E[|s_\ell(n)|^2] \Big/ E[|w_\ell(n)|^2] \\ &= \sigma_h^2\sigma_s^2/\sigma_w^2 \end{aligned} \tag{5.30}$$

5.5.1 Cognitive Radio Throughput

Let C_0 and C_M represents the throughout for CR when PUs are absent and present respectively which can be mathematically defined as follows:

$$C_0 = \log_2\left(1 + \frac{P_s}{N_0}\right) = \log_2\left(1 + SNR_s\right) \tag{5.31}$$

and

$$\begin{aligned} C_M &= \log_2\left(1 + \frac{P_s}{\sum_{i=1}^{N} P_i + N_0}\right) \\ &= \log_2\left(1 + \frac{P_s/N_0}{1 + \sum_{i=1}^{N} P_i/N_0}\right) \end{aligned} \tag{5.32}$$

Our interest lies in underutilised frequency band where probability of absence of PU is $P(\mathcal{H}_0) \geq 0.5$. Obviously, $C_0 > C_M$ because CR experiences interference from PUs in second scenario. When PUs are absent the achievable throughput of the SU link is:

$$\left(1 - \frac{\tau}{T}\right) C_0 \tag{5.33}$$

and in presence of PUs the achievable throughput of CR is

$$\left(1-\frac{\tau}{T}\right)C_M \tag{5.34}$$

The probabilities with which two equations are guaranteed are $(1-P_{FA}(\tau,\xi)P(\mathcal{H}_0)$ and $(1-P_D(\tau,\xi))P(\mathcal{H}_1)$ where $P(\mathcal{H}_1)$ is probability of presence of PUs. Therefore, the throughput at CR in absence of PU is

$$R_0(\tau,\xi)=\left(1-\frac{\tau}{T}\right)C_0(1-P_{FA}(\tau,\xi))P(\mathcal{H}_0) \tag{5.35}$$

and the throughput at CR in presence of PUs is

$$R_M(\tau,\xi)=\left(1-\frac{\tau}{T}\right)C_M(1-P_D(\tau,\xi))P(\mathcal{H}_1) \tag{5.36}$$

Hence the total throughput is summation of the throughput of the CR in absence and presence of PUs.

$$R(\tau,\xi)=R_0(\tau,\xi)+R_M(\tau,\xi) \tag{5.37}$$

This is an optimisation problem where for a fixed threshold ξ and the sensing time τ_s can be maximised such that:

$$\begin{aligned}\max_{\tau}\ & R(\tau)=R_0(\tau,\xi)+R_M(\tau,\xi)\\ \text{s.t:}\ & P_D(\tau,\xi)\geq\bar{P}_D\end{aligned} \tag{5.38}$$

Where $\bar{P}_D$ is target probability of detection. It's clear that the first term in previous equation dominates the second term, therefore the total achievable throughput can be given as follows:

$$\begin{aligned}\max_{\tau}\ & R(\tau)=R_0(\tau,\xi)\\ \text{s.t.:}\ & P_D(\tau,\xi)\geq\bar{P}_D\end{aligned} \tag{5.39}$$

For a given sensing time τ_s, let us choose a flexible detection threshold ξ_0 s.t.

$$P_D(\tau,\xi_0)=\bar{P}_D \tag{5.40}$$

Let us choose another threshold ξ_1 and call it conservative threshold s.t. $\xi_1 < \xi_0$ and

$$P_D(\tau, \xi_1) > \bar{P}_D \tag{5.41}$$

Obviously, $P_{FA}(\tau, \xi_1) > P_{FA}(\tau, \xi_0)$ which leads to $R_0(\tau, \xi_1) < R_0(\tau, \xi_0)$ and $R_M(\tau, \xi_1) < R_M(\tau, \xi_0)$. Hence the total throughput can be given as:

$$R_0(\tau, \xi_1) + R_M(\tau, \xi_1) < R_0(\tau, \xi_0) + R_M(\tau, \xi_1) \tag{5.42}$$

5.5.2 Probabilities of Detection and False Alarm

Considering each CR uses energy detection as spectrum sensing scheme and collects N sample values. The test statistics $T_\ell(n)$ for energy detection scheme can be given as:

$$T_\ell = (1/N) \sum_{n=1}^{N} |y_\ell(n)|^2 \tag{5.43}$$

Now the probability of false alarm for a threshold ξ as derived in [17] can be given by:

$$P_{FA}(\tau, \xi) = Pr(T_\ell > \xi | \mathcal{H}_0) = \int_{\xi}^{\infty} p_0(x) dx \tag{5.44}$$

and similarly the probability of detection

$$P_D(\tau, \xi) = Pr(T_\ell > \xi | \mathcal{H}_1) = \int_{\xi}^{\infty} p_1(x) dx \tag{5.45}$$

Where $p_0(x)$ and $p_1(x)$ are the PDFs of signals forming null hypothesis and alternative hypothesis or noise only and signal plus noise only hypothesis respectively. The two PDFs follow Chi-squared distribution with $2N$ degrees of freedom for complex values and N degrees of freedom for real values.

When PU signal is complex-valued PSK modulated, then the probability of detection and false alarm respectively at ℓth CR with the assumption that each CR uses the same threshold ξ as given in [17] can be rewritten as follows:

$$P_D(\tau,\xi) = \mathcal{Q}\left(\left(\frac{\xi_\ell}{\sigma_w^2(\gamma+1)} - 1\right)\sqrt{\tau f_s}\right) \tag{5.46}$$

$$P_{FA}(\tau,\xi) = \mathcal{Q}\left(\left(\frac{\xi_\ell}{\sigma_w^2} - 1\right)\sqrt{\tau f_s}\right) \tag{5.47}$$

Where $\mathcal{Q}(t) = \frac{1}{2\pi}\int_t^\infty e^{-t^2}dt$ is known as Q-function and measures the right-tail probability of Gaussian distribution. Minimum number of samples required can be given by following expression:

$$N_{min} = \left[Q^{-1}(P_{FA}) - Q^{-1}(P_D) + \sqrt{2\gamma+1}\right]^2 \Big/ \gamma^2 \tag{5.48}$$

It can be seen from Fig. 5.5 that probability of false alarm decreases with the increase in sensing time for a fixed sample size. It is also shown that the it decreases with the increase in SNR from $2dB$ to $8dB$. Similarly, Fig. 5.6 says the probability of detection increases with the increase in sensing time and it also increases with the increase in SNR from $2dB$ to $8dB$.

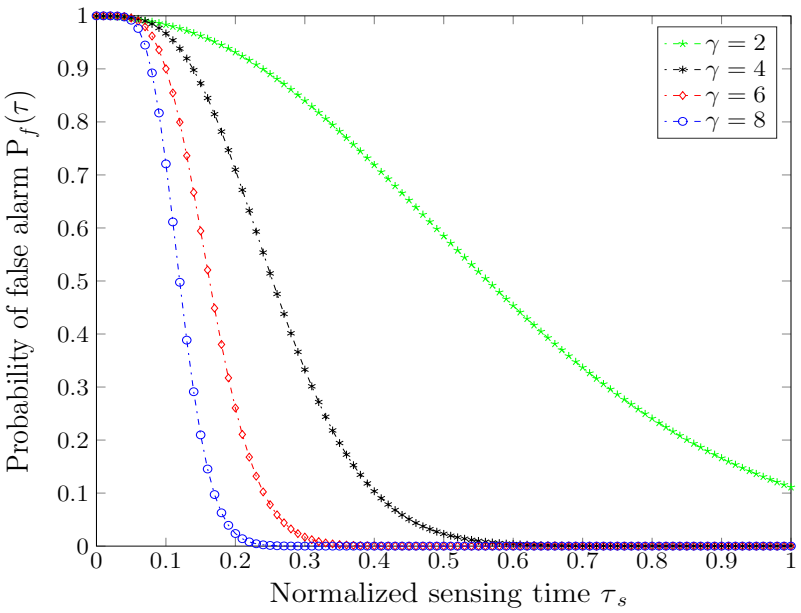


Figure 5.5: Probability of false alarm versus sensing time

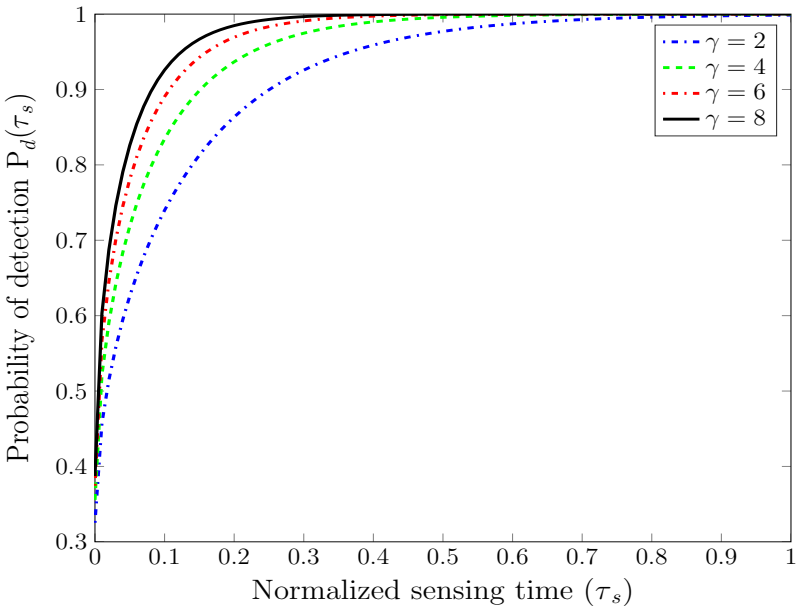


Figure 5.6: Probability of detection versus sensing time

In Fig.5.7 it is shown that probability of detection increases with the increase in probability of false alarm. It also increases with the increase in SNR values. It can also be seen from Fig. 5.8 that minimum number of samples required decreases as the probability of false alarm increases. Additionally, for a fixed probability of false alarm minimum number of samples required also decreases with the increase in SNR.

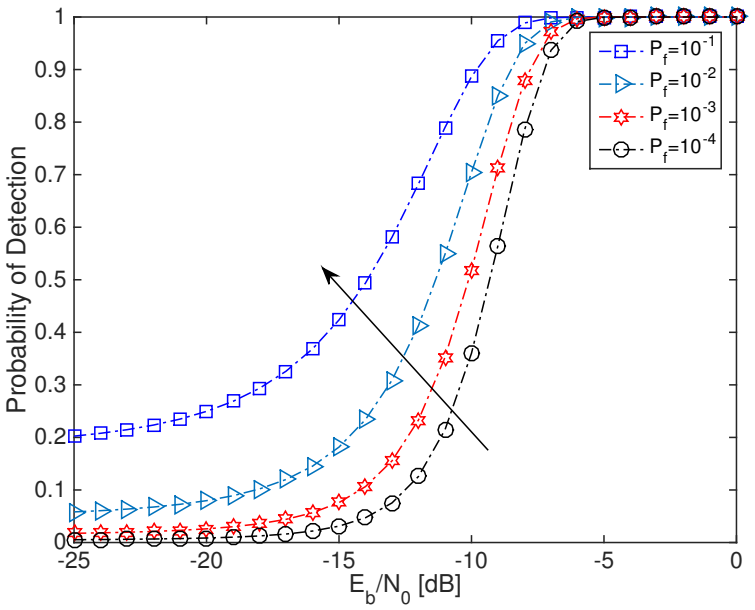


Figure 5.7: Probability of detection versus SNR

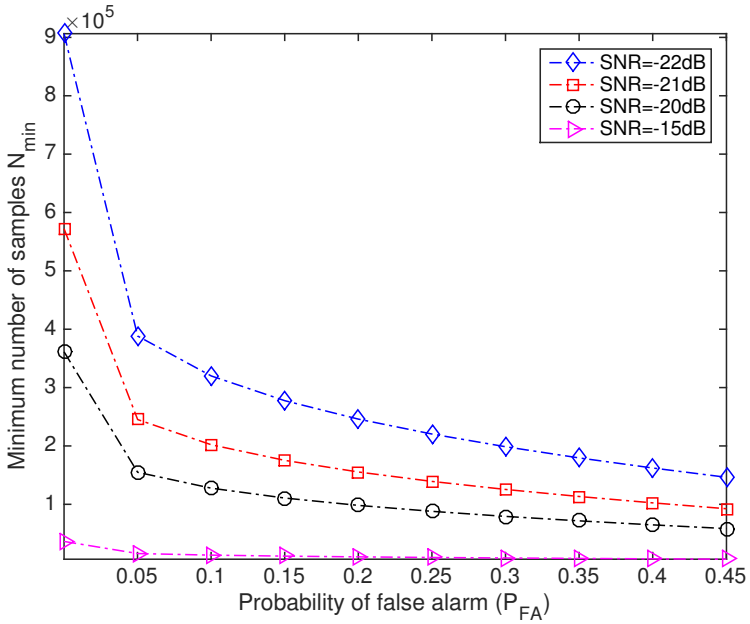


Figure 5.8: Minimum number of samples required versus probability of false alarm

5.6 Cooperative Spectrum Sensing

Let us consider that the M CRs are performing independent sensing of particular band and cooperatively transmit their decision to base station (BS) or fusion centre (FC) which combines the decision information with its own decision about particular band. After receiving spectrum decision from all the CRs it declares the global decision whether a particular band is empty or not. This information is included in white space map (WSM) and considering IEEE 802.11af this is then transmitted to all the Mode II or portable devices through contact verification signal (CVS). Hence the global probability of detection and false alarm respectively for a sensing threshold Ξ at FC can mathematically be represented as:

$$\mathbb{P}_D(\tau, k, \Xi) = \sum_{\ell=k}^{M} \binom{M}{\ell} P_D(\tau, \xi)^{\ell} (1 - P_D(\tau, \xi))^{M-\ell} \tag{5.49}$$

$$\mathbb{P}_{FA}(\tau, k, \Xi) = \sum_{\ell=k}^{M} \binom{M}{\ell} P_{FA}(\tau, \xi)^{\ell} (1 - P_{FA}(\tau, \xi))^{M-\ell} \tag{5.50}$$

The decision $D_\ell = 1$ represents that PU is detected and the decision $D_0 = 0$ represents PU is not detected. Every CR performs its decision and later sends it to the FC. It's assumed that signal experiences flat-fading between PU and the ℓth CR and between ℓth CR and FC

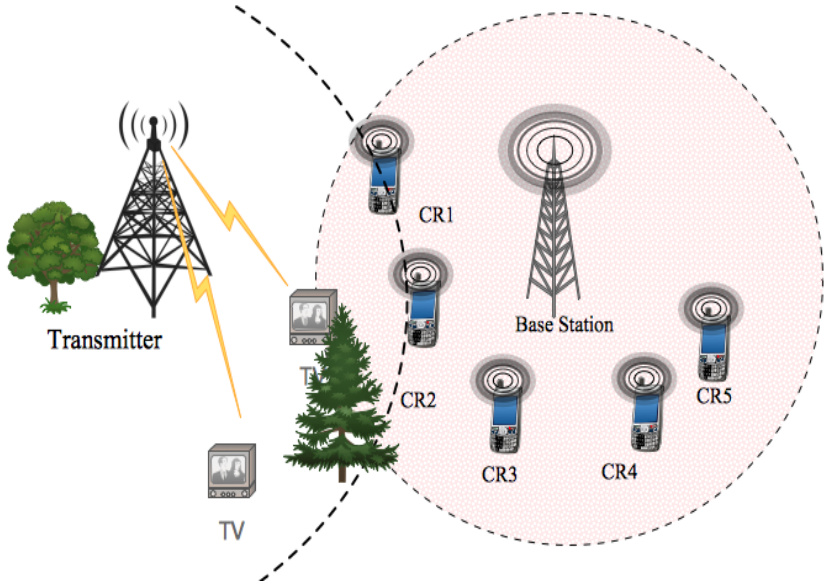


Figure 5.9: Cooperative Cognitive Radio network coexisting with PU TV network

$$\sum_{\ell=1}^{M} T_\ell = (1/N) \sum_{n=1}^{N} |y_\ell(n)|^2 \underset{D_0}{\overset{D_1}{\gtrless}} \xi_\ell \tag{5.51}$$

Let us say C_0 and C_M are the throughputs of SU if it's allowed to continuously operate in absence and presence of PUs. Figure 5.4 shows the cognitive radio frame structure where entire frame duration is divided into sensing time τ_s, spectrum reporting time τ_r and data transmission time. Since a length of τ_s period out of the total frame time T that is used for sensing is $\tau_s = T - \tau_r - \{T - (\tau_r + \tau_s)\}$ and length of period τ_r is used for spectrum reporting to decision time is $\tau_r = T - \tau_s - \{T - (\tau s + \tau_r\})$. Since $\tau_s >> \tau_r$ therefore the achievable normalised throughputs of the SUs under these scenarios are:

$$R_0(\tau, k, \Xi) = C_0 P(\mathcal{H}_0) \left(1 - \frac{\tau}{T}\right) (1 - \mathbb{P}_{FA}(\tau, k, \xi)) \tag{5.52}$$

$$R_M(\tau, k, \Xi) = C_M P(\mathcal{H}_1) \left(1 - \frac{\tau}{T}\right) (1 - \mathbb{P}_D(\tau, k, \xi)) \tag{5.53}$$

Where $P(\mathcal{H}_0)$ and $P(\mathcal{H}_1)$ are the probabilities of the PU being absent and present in the channel respectively. Average achievable throughput of SU is given as:

$$R(\tau, k, \Xi) = R_0(\tau, k, \xi) + R_M(\tau, k, \xi) \tag{5.54}$$

Similar to equation (5.37) this is an optimisation problem where can optimise τ and k number of CRs participating in decision::

$$\begin{aligned} \max_{\tau,k,\Xi} \quad & R(\tau, k, \Xi) \\ \text{s.t.} \quad & \mathbb{P}_D(\tau, k, \Xi) \geq \bar{\mathbb{P}}_D \\ & 0 \leq \tau \leq T \\ & 1 \leq k \leq M \end{aligned} \tag{5.55}$$

Where $\bar{\mathbb{P}}_D$ is target probability of detection at FC to protect PU. Optimum value of τ,k and Ξ can be obtained by fixing one parameter and optimising the remaining parameters. Let us say $\mathbb{P}_D(\tau, k, \Xi) = \bar{\mathbb{P}}_D$ for a given τ and k two thresholds $\Xi = \Xi_0$ and $\Xi = \Xi_1$ are defined such that $\Xi_1 < \Xi_0$. Then similar to equation (5.40) and (5.41):

$$\begin{aligned} \mathbb{P}_D(\tau, k, \Xi_1) > \mathbb{P}_D(\tau, k, \Xi_0) \\ \mathbb{P}_{FA}(\tau, k, \Xi_1) > \mathbb{P}_{FA}(\tau, k, \Xi_0) \end{aligned} \tag{5.56}$$

which leads to the conclusion

$$\begin{aligned} R_1(\tau, k, \Xi_1) < R_0(\tau, k, \Xi_0) \\ R_0(\tau, k, \Xi_1) < R_0(\tau, k, \Xi 1) \end{aligned} \tag{5.57}$$

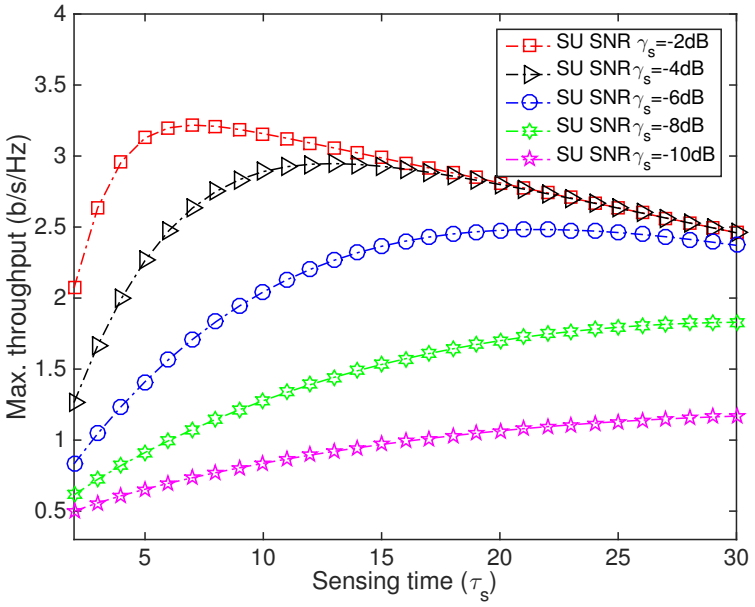


Figure 5.10: Secondary user maximum throughput versus sensing time

Figure 5.10 shows that the maximum normalised throughput increases with the increase in sensing time and attains maximum value and then settles down. This behaviour is kick-started by increase in sensing time which results in decrease in data transmission time. Throughput also increases with the increase in SNR value at SU from $-10dB$ to $-2dB$.

5.6.1 Decision and Fusion Strategies

OR Rule

If one of the SU declares that there is PU, then the final decision at FC is declared that there is PU. For all the independent decisions, the probability of detection and probability of false alarm at FC are:

$$\mathbb{P}_D(\tau, k, \Xi) = 1 - \prod_{\ell=1}^{M} (1 - P_{Di}(\tau, k, \xi)) \tag{5.58}$$

$$\mathbb{P}_D(\tau, k, \Xi) = 1 - \prod_{\ell=1}^{M} (1 - P_{FAi}(\tau, k, \xi)) \tag{5.59}$$

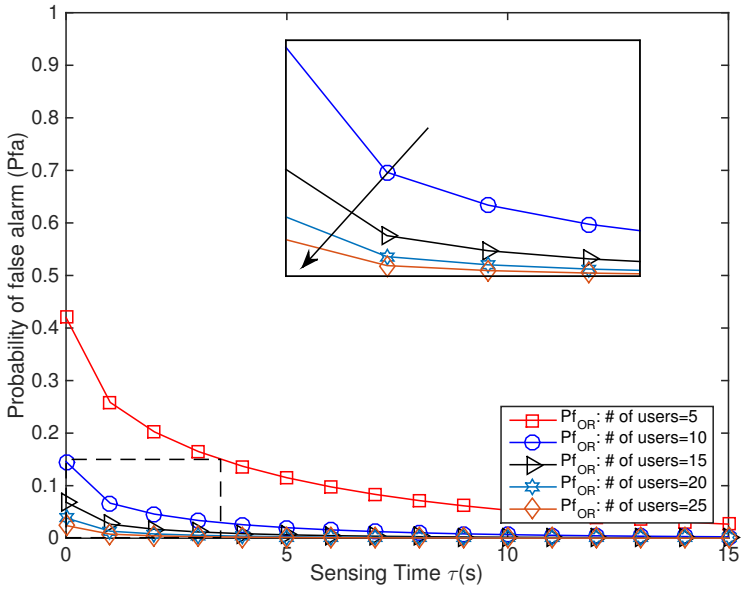


Figure 5.11: Probability of false alarm as a function of number of cooperative users OR fusion strategies

The performance of OR fusion strategy is shown in Fig. 5.11 where is it is obvious that as the number of users increases the probability of false alarm declaring the presence of PU decreases.

AND Rule

If all the SUs says that there is PU, then the final decision at FC is declared that there is PU. For all the independent decisions, the probability of detection and probability of false alarm at FC are:

$$\mathbb{P}_D(\tau, k, \Xi) = \prod_{\ell=1}^{M} P_D(\tau, k, \Xi) \tag{5.60}$$

$$\mathbb{P}_{FA}(\tau, k, \Xi) = \prod_{\ell=1}^{M} P_{FA}(\tau, k, \Xi) \tag{5.61}$$

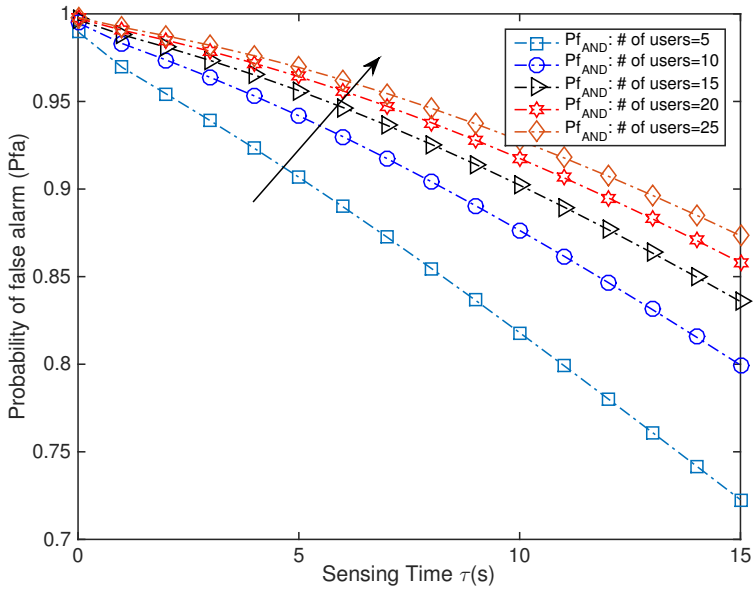


Figure 5.12: Probability of false alarm as a function of number of cooperative users AND fusion strategies

Figure 5.12 shows the probability of false alarm increases with the increase in number of SUs participating in decision. This is because if one of the user detects the PU and other false alarms then the collective decision shall be presence of PU. This is highly likely for AND when the number of users increase.

k-out-of-M Rule

If half or more CRs decide in favour of the presence of the PU then the final decision at FC is presence of PU.

5.7 Multi-slot Sensing

Here in this scheme each frame is divided into multiple minislots which are discontinuous. Let M represents the number of minislots, τ_1 sensing time for each

minislot such that $\tau = M\tau_1$ and $N_1 = N/M$ are the total number of samples for each minislots then the hypotheses for each ith minislots are:

$$\begin{aligned} \mathcal{H}_0 : &\quad y_i(n) = w_i(n) \\ \mathcal{H}_1 : &\quad y_i(n) = h_i s_i(n) + w_i(n) \end{aligned} \tag{5.62}$$

where $h_i \sim \mathcal{N}(0,1)$ and noise is i.i.d for each of the M minislots and $\mathbb{E}\big(|s_i(n)|^2\big) = \sigma_s^2$ and $\mathbb{E}\big(|w_i(n)|^2\big) = \sigma_u^2 \forall i$. The decision about the presence and absence of PU can be divided into two categories ad follows:

Data Fusion

All the sample measurements from M minislots are processed jointly at FC and a final decision is declared.

Decision Fusion

Each measurement from Mminilot is processed separately. Final decision is declared after fusing the decisions of M minislots

5.7.1 Data Fusion Sensing

In this scheme test statistics of the ith minislot is

$$T_i(y) = \frac{1}{N_1} \sum_{n=0}^{N_1-1} |y_i(n)|^2 \tag{5.63}$$

Now using data fusion the test statistics used for final decision is then represented as

$$T(y) = \sum_{i=0}^{M-1} g_i T_i(y) \tag{5.64}$$

Where $g_i \geq 0$ is scaling factor of ith minislot. From [17] if low SNR regime is region of our interest then for target $\bar{P}_{FA}$ and when the channel coefficients are unknown then P_{FA} and P_D are as follows:

$$P_{FA} = Q\left(\beta_2 Q^{-1}\big(P_D\big) + \gamma\sqrt{\frac{N_1}{M}}\sum_{i=0}^{M-1}|h_i|^2\right) \tag{5.65}$$

and

$$P_D = Q\left(\frac{1}{\beta_2}Q^{-1}\big(P_{FA}\big) - \gamma\sqrt{\frac{N_1}{M}}\sum_{i=0}^{M-1}\right) \tag{5.66}$$

Where $\beta_2 = \sqrt{1 + \frac{2\gamma}{M}\sum_{i=0}^{M-1}|h_i|^2}$. Now for a static channel $|h_i| = 1$ and $g_i = \frac{1}{\sqrt{M}}$, the division of sensing time into Mminislots doesn't give additional performance gain and the P_{FA} and P_D can be given as follows:

$$P_{FA} = Q\left(\sqrt{2\gamma+1}Q^{-1}\big(\bar{P}_D\big) + \gamma\sqrt{MN_1}\right) \tag{5.67}$$

$$P_D = Q\left(\frac{1}{\sqrt{2\gamma+1}}Q^{-1}\big(P_{FA}\big) - \gamma\sqrt{MN_1}\right) \tag{5.68}$$

Normalized throughput for average probability of false alarm $\tilde{P}_{FA}$ for all frames is:

$$B(\tau) = \frac{T-\tau}{T}\left(1 - \tilde{P}_{FA}\right) \tag{5.69}$$

5.7.2 Decision Fusion Sensing

Let P_D^i and P_{FA}^i denote the probability of detection and probability of false alarm for the ith minislot respectively; then for a given threshold ξ_0 P_D^i and P_{FA}^i for ith minislots are

$$P_D^i = Q\left(\left(\frac{\xi_0}{\sigma_w} - \gamma|h_i|^2 - 1\right)\sqrt{\frac{N_1}{2\gamma|h_i|^2+1}}\right) \tag{5.70}$$

$$P_{FA}^i = Q\left(\left(\frac{\xi_0}{\sigma_w} - 1\right)\sqrt{N_1}\right) \tag{5.71}$$

5.7.3 Optimal Rule

Let D_i represents the binary decision of ith minislot where $D_i \in \{0,1\}\, \forall i = 0, 1, \ldots, M-1$, the optimal rules is Chair-Varshney rule [18]:

$$\Lambda = \sum_{i=0}^{M-1} \left[D_i \log \frac{P_D^i}{P_{FA}^i} + \big(1 - D_i\big) \log \frac{1 - P_D^i}{1 - P_{FA}^i} \right] + \log \frac{P(\mathcal{H}_1)}{P(\mathcal{H}_0)} \tag{5.72}$$

If $\Lambda \geq 0$ then presence of PU is declared.

OR Rule

In this scheme if one of the participating SU declares the presence of PU then final decision is declared as presence of PU. Mathematically:

$$\Lambda = \sum_{i=1}^{M-1} D_i \tag{5.73}$$

If $\Lambda \geq 1$ then PU is present. For all independent decisions , the P_D and P_{FA} for final decisions are:

$$\begin{aligned} P_D &= 1 - \prod_{i=0}^{M-1} \left(1 - P_D^i\right) \\ P_{FA} &= 1 - \prod_{i=0}^{M-1} \left(1 - P_{FA}^i\right) \end{aligned} \tag{5.74}$$

AND Rule

Here presence of PU is declared if all the participating SU declare in favour of PU. Mathematically:

$$\Lambda = \prod_{i=0}^{M-1} D_i \tag{5.75}$$

If $\Lambda = 1$ then PU is declared present otherwise there is no PU.

$$\begin{aligned} P_D &= \prod_{i=0}^{M-1} P_D^i \\ P_{FA} &= \prod_{i=0}^{M-1} P_{FA}^i \end{aligned} \tag{5.76}$$

k-out-of-N Rule or Majority Rule

If half of the decisions favour presence of PU then the final decision is declared as presence of PU otherwise absence of PU is declared. Mathematically:

$$\Lambda = \sum_{i=0}^{M-1} D_i \quad \Lambda \geq \left\lceil \frac{M}{2} \right\rceil \tag{5.77}$$

Assuming all decisions are independent and $P_D^0, P_D^1, \ldots, P_D^{M-1} = P_{D,0}$ and $P_{FA}^0, P_{FA}^1, \ldots, P_{FA}^{M-1} = P_{FA,0}$then P_D and P_{FA} for final decisions are:

$$\begin{aligned} P_D &= \sum_{j=0}^{M-\left\lceil M/2 \right\rceil} \binom{M}{\left\lceil M/2 \right\rceil + j} \left(1 - P_{D,0}\right)^{M-\left\lceil M/2 \right\rceil - j} P_{D,0}^{\left\lceil M/2 \right\rceil + j} \\ P_{FA} &= \sum_{j=0}^{M-\left\lceil M/2 \right\rceil} \binom{M}{\left\lceil M/2 \right\rceil + j} \left(1 - P_{FA,0}\right)^{M-\left\lceil M/2 \right\rceil - j} P_{FA,0}^{\left\lceil M/2 \right\rceil + j} \end{aligned} \tag{5.78}$$

It can be seen from Fig.5.13 that the average detection probability with known channel coefficients increases with the increase in number of multi-slots for a fixed PU SNR of $-15dB$. The performance gap is significant between single sensing slot and the mutlislot sensing which thereafter decreases as the number of multislot increases. Second trend shows that the average probability of detection increases with the increase in sensing time of the CR. Similarly, as shown in Fig. 5.14 the average probability of missed detection with known channel coefficients increases with the increase in number of multislots with the performance gap larger between single slot sensing and the multislot sensing which thereafter saturates. Second

trend shows the probability of missed detection decreases as the sensing time increases.

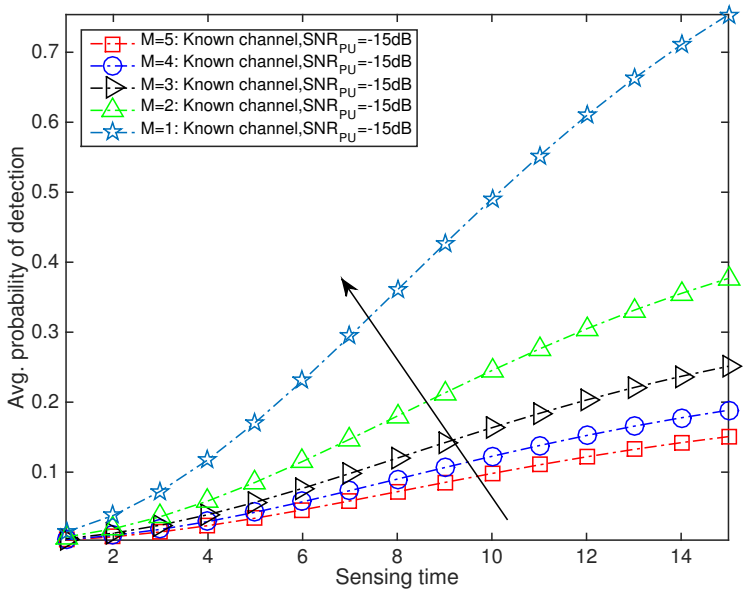


Figure 5.13: Average probability of detection as a function of sensing time in multi-slot sensing

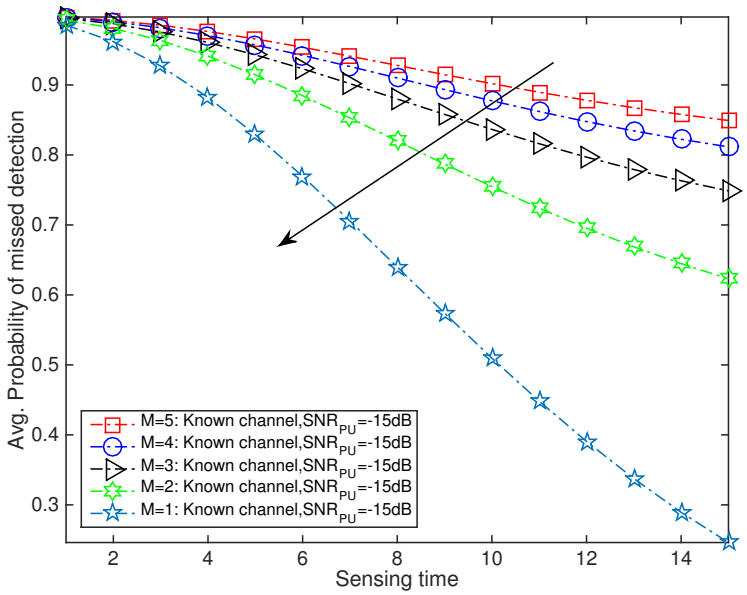


Figure 5.14: Average probability of missed detection as a function of sensing time in multi-slot spectrum sensing

Figure 5.15 shows that the average probability of false alarm decreases as the sensing time increases for known channel coefficients. The average probability of false alarm also decreases with the increase in multi-slots, however, the performance gap shrinks with the increase in number of multi-slots. It can also be shown in Fig.5.16 that the probability of false alarm decreases as the sensing time increases. Secondly, the probability of false alarm decreases when number of sensing slots is increased from one to five. However, the performance gaps shrinks at the sensing time of $8ms$ with the increase in multislots.

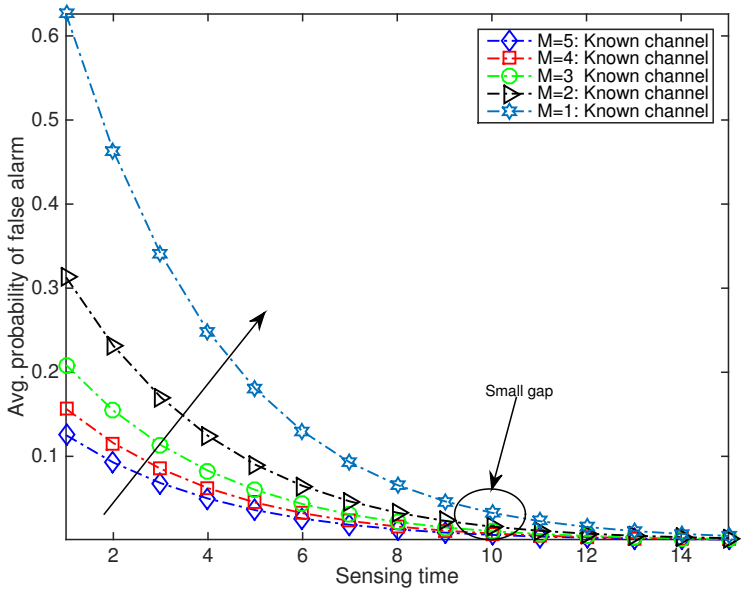


Figure 5.15: Average probability of false alarm as a function of sensing time with known channel coefficients

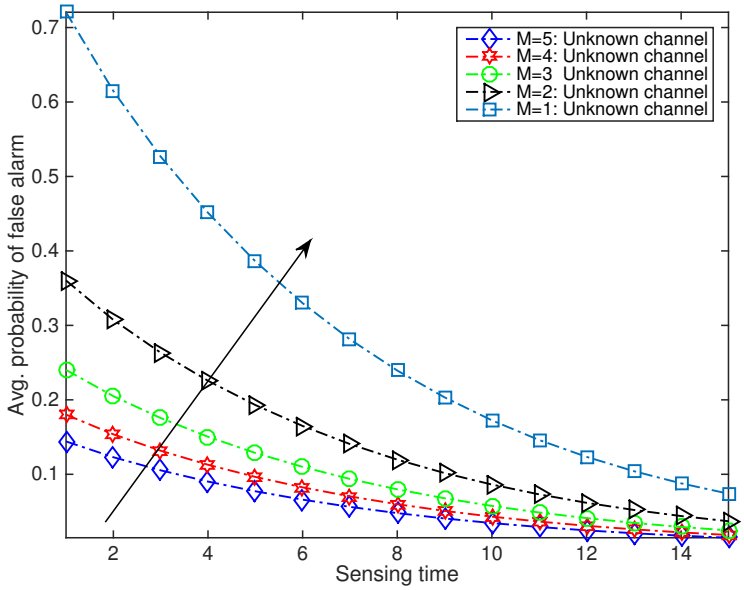


Figure 5.16: Average probability of false alarm as a function of sensing time with unknown channel coefficients

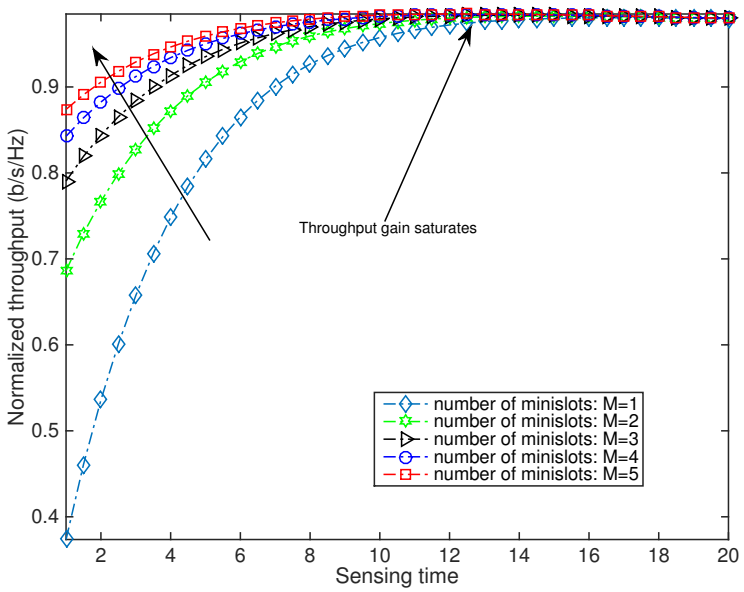


Figure 5.17: Normalized throughput as a function of sensing time in multislot scenario

Figure 5.17 shows the plots between sensing time and the normalised throughput in $bit/sec/Hz$. It is shown that the normalised throughput increases with the increase in sensing time. It can also be shown that the throughput increases with the increase in multislots, however the performance gap shrinks at sensing of $8ms$ as the number of multislots increases.

5.8 Aggregate Interference and Outage Analysis

5.8.1 System Model and Parameters

Received beacon signal at the ith SU transceiver can be given as:

$$y_{bi}(n) = \tilde{g}_i d_{bi}^{-\alpha/2} s_b(n) + w_b(n) \tag{5.79}$$

Where $s_b(n)$ is the transmitted beacon signal with power P_b and $w_b(n) \sim \mathcal{N}(0, \sigma_w^2)$. Received SNR of the beacon signal at SU Tx is written as:

$$\gamma_i = P_b \mid \tilde{g}_i \mid^2 d_{bi}^{-\alpha} \Big/ \sigma_w^2 \tag{5.80}$$

In reference [19]. exact probability of detection of an energy detector is given by:

$$P_D(\gamma_i) = Q\left(\left(Q^{-1}(P_{FA}) - \sqrt{\nu}\gamma_i \right) \Big/ \sqrt{1 + 2\gamma_i} \right) \tag{5.81}$$

The detection probability for a small value of P_{FA} can be approximated as [20]:

$$P_D(\gamma_i) = \begin{cases} 0, & \text{if } \gamma_i < \gamma_0 \\ 1, & \text{if } \gamma_i \geq \gamma_0 \end{cases} \tag{5.82}$$

Where $\gamma_0 = Q^{-1}\Big(P_{FA}\Big) \Big/ \sqrt{\nu}$. Now the average beacon probability of miss at ith SU be approximated as $P_{mi} \simeq Pr.(\gamma_i < \gamma_0)$ and assuming $\gamma = \sigma_w^2 \gamma_0 / P_b$, then

$$\begin{aligned} P_{mi} &\simeq Pr\Big(\mid g_i \mid^2 < \frac{\sigma_w^2 \gamma_0}{P_b} d_{bi}^{\alpha} \Big) \\ &\simeq Pr\big(\mid g_i \mid^2 < \gamma d_{bi}^{\alpha} \big) \end{aligned} \tag{5.83}$$

Now, the received signal at PU Rx can be written as:

$$y_0 = h_0 s_0 + \sum_{i=1}^{M} F_i h_i s_i + n_0 \tag{5.84}$$

Where s_0 is transmitted signal from PU with power P_0 and s_i is transmitted signal from ith SU with power P and F_i is ith SU's transmission coincident with PU transmission if it misdetects the beacon signal and has Bernoulli distribution.

$$F_i = \begin{cases} 1, & P_{mi}\beta \\ 0, & \big(1 - P_{mi}\beta\big) \end{cases} \tag{5.85}$$

Aggregate interference produced by SUs is as follows:

$$I_0 = \sum_{i=1}^{M} I_i = P_{mi} L_i = P_{mi} \beta P \mid \tilde{h_i} \mid^2 r_i^{-\alpha} \tag{5.86}$$

Where $L_i = P_{mi} \beta P \mid \tilde{h_i} \mid^2 r_i^{-\alpha}$ is the level of interference introduced by ith SU to PU Rx if it misdetects the beacon signal.

Table 5.1: System Model Parameters

Parameters	Description
R_0	PU communication link distance
M	number of SU users
r_i	distance between ith SU Tx and PU Rx where $\epsilon \leq r_i \leq R$
λ	Density of SUs per unit area
α	Path Loss
β	Pr. with which SU transmits
h_0	Channel impulse response of the PU-SU Tx link
h_i	Channel response from ith SU Tx to PU Rx
d_{Bi}	Distance between beacon Tx and ith SU Tx
γ_i	Received SNR of the beacon signal at SU Tx

5.8.2 Aggregate Interference with Beacon Tx at PU Rx

In this section mathematical expressions of the aggregate interference in Rayleigh and Nakagami fading are developed.

Rayleigh Fading

Aggregate interference when the signal experiences Rayleigh fading the power content in the channel is exponential distributed with parameter 1 is considered. Beacon misdetection probability is given as:

$$P_{mi} \simeq 1 - e^{-\gamma d_{bi}^{\alpha}} \tag{5.87}$$

Generally, P_{mi} is kept low for good operation. Therefore above expression for probability of misdetection can be approximated as:

$$P_{mi} \simeq 1 - \left(1 - \gamma d_{bi}^{\alpha}\right) = \gamma d_{bi}^{\alpha} \tag{5.88}$$

When beacon TX is located at PU Rx then $d_{bi} = r_i$. Therefore, mathematically interference can be written as:

$$\begin{aligned} I_i = P_{mi} L_i &= P_{mi} \beta P \mid \tilde{h_i} \mid^2 r_i^{-\alpha} \\ &= \gamma r_i^{\alpha} \beta P \mid \tilde{h_i} \mid^2 r_i^{-\alpha} \\ &= P \beta \gamma \mid \tilde{h_i} \mid^2 \end{aligned} \tag{5.89}$$

Since $\mid \tilde{h_i} \mid^2$ is exponentially distribution with parameter 1, therefore $I_i s$ are iid random variables and are exponentially distribution with parameter $1/P\beta\gamma$. As a consequence, aggregate interference $I_0 = \sum_{i=1}^{M} I_i$ has Gamma distribution with shape parameter $P\beta\gamma$ and $E[I_0] = MP\beta\gamma$.

$$f_{I_0}\left(i_o; M, P\beta\gamma\right) = \frac{i_0^{M-1} e^{-i_0/P\beta\gamma}}{\left((P\beta\gamma)^M \Gamma(M)\right)}, \quad i_0 > 0 \tag{5.90}$$

Figure 5.18 shows the CDF and PDF of the aggregate interference.

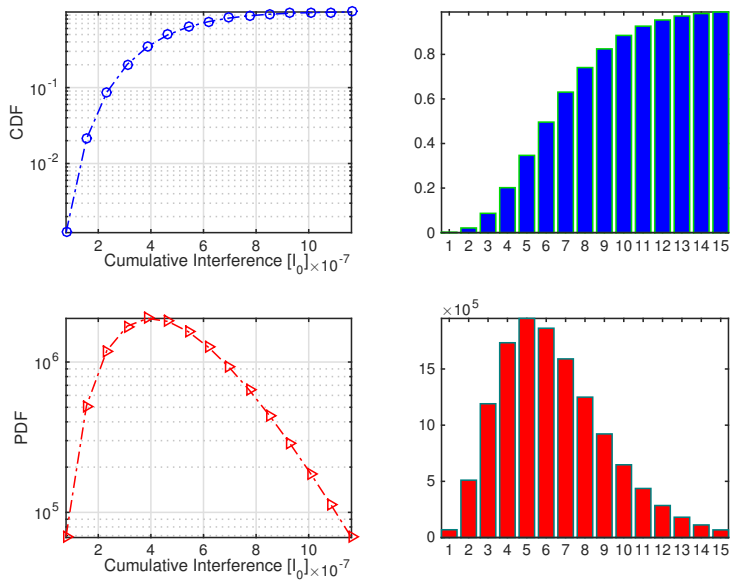


Figure 5.18: CDF and PDF of cumulative interference in Rayleigh fading

Nakagami Fading

Nakagami fading channel is characterised by average received power P_{avg} and the fading parameter m, the channel power $|\tilde{h_i}|^2$,$|\tilde{g_i}|^2$ has Gamma distribution with $k = m$ and $\theta = 1/m$. Considering the P_{mi} is Gamma distributed and has the following CDF:

$$\begin{aligned} P_{mi} = Pr\big[\,|\tilde{g_i}|^2 < \gamma r_i^{\alpha}\big] &= \frac{\Gamma\Big(k, \gamma r_i/\theta\Big)}{\Gamma(k)} \\ &= \frac{\Gamma\Big(m, m\gamma r_i^{\alpha}\Big)}{\Gamma(m)} \end{aligned} \tag{5.91}$$

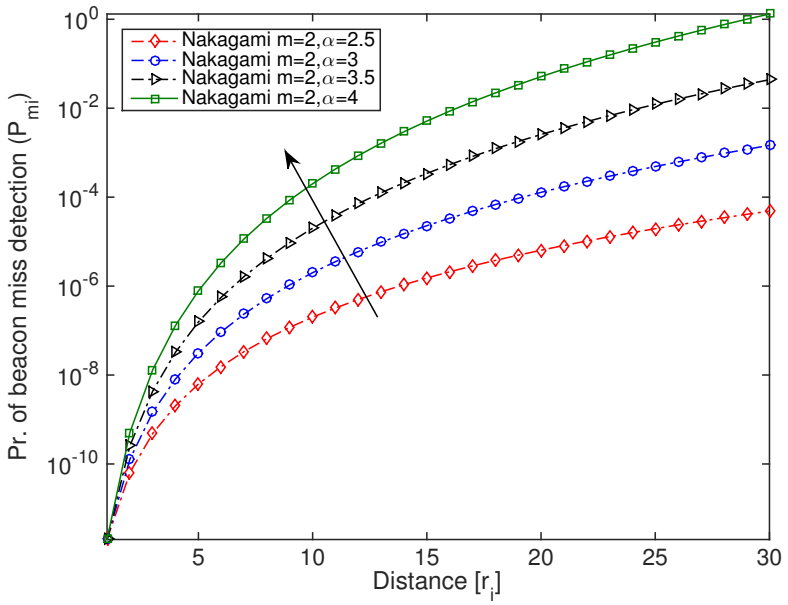


Figure 5.19: Probability of beacon miss detection (Pmi) versus the distance r_i over Nakagami fading channel with different values of pathloss: $\beta = 0.001$,$\lambda = 0.01$,$\gamma = 10^{-6}$,$m = 2$,$M = 5$

In Fig. 5.19 it's shown that the probability of beacon miss detection increases with the increase in distance and it also increases with the increase in pathloss. Therefore, higher the pathloss higher shall be the probability of beacon miss detection in this case SU can make transmission and hence introduce interference to PU. Where $\Gamma(s) = \int_0^\infty r^{s-1}e^{-t}dt$ is gamma function and $\Gamma(s,x) = \int_0^x t^{s-1}e^{-t}dt$ is lower incomplete Gamma function. These two function can be computed with the readily available MATLAB functions: `gamma(x)` and `gammainc(x,y)`. For $\gamma << 1$,$\Gamma\left(m, m\gamma r_i^\alpha\right) \approx \left(m\gamma r_i^\alpha\right)^m / m$. Therefore the aggregate interference is

$$
\begin{aligned}
I_0 &= \sum_{i=1}^{M} I_i, \\
I_i = P_{mi}L_i &= \frac{\left(m\gamma r_i^\alpha\right)^m}{m\Gamma(m)}\beta P \mid \tilde{g}_i \mid^2 r_i^{-\alpha} \\
&= P\beta\frac{\left(m\gamma\right)^m}{m\Gamma(m)} \mid \tilde{g}_i \mid^2 r_i^{\alpha(m-1)}
\end{aligned}
\tag{5.92}
$$

Interference I_0 is statistically modelled with the mean and variance which are calculated as following this. It's given that $f_{r_i}(r_i) = 2r_i\Big(R^2 - \epsilon^2\Big)^{-1}$ $\epsilon \leq r_i \leq R$. For $\epsilon << R$:

$$\mathbb{E}\Big[r_i^{\alpha(m-1)}\Big] = \frac{2R^{\alpha(m-1)}}{\Big(\alpha(m-1)+2\Big)} \tag{5.93}$$

Therefore, the mean and variance of the aggregate interference becomes:

$$\mathbb{E}\big[I_0\big] \simeq MP\beta\frac{\big(m\gamma\big)^m}{m\Gamma(m)}\frac{2R^{\alpha(m-1)}}{\alpha(m-1)+2} \tag{5.94}$$

$$\begin{aligned}\mathrm{Var}\Big[\mid \tilde{h_i} \mid^2 r_i^{\alpha\left(m-1\right)}\Big] &\simeq \Big(R^{2\alpha\left(m-1\right)}\Big/m\Big) \\ &\times \left[\frac{\Big(2-\alpha\big(m-1\big)^2\Big)}{\Big(\alpha\big(m-1\big)+1\Big)\Big(\alpha\big(m-1\big)+2\Big)}\right]\end{aligned} \tag{5.95}$$

$\mathbb{E}\Big(\mid \tilde{h_i} \mid^2\Big) = 1$

$$\begin{aligned}\mathrm{Var}\big[I_0\big] &\simeq M\left(P\beta\frac{\big(m\gamma\big)^m}{m\Gamma(m)}\right)^2\frac{R^{2\alpha\left(m-1\right)}}{m} \\ &\times \left[\frac{2-\alpha(m-1)^2}{\big(\alpha(m-1)+1\big)\big(\alpha(m-1)+2\big)}\right]\end{aligned} \tag{5.96}$$

5.9 Interference and Outage with Cooperative Sensing

In Fig. 5.20 two distinct trends are observed that are as the distance between beacon transmitter and SU increases the probability of beacon miss detection increases.Similarly, as the cooperative distance increases the probability of beacon miss detection decreases.

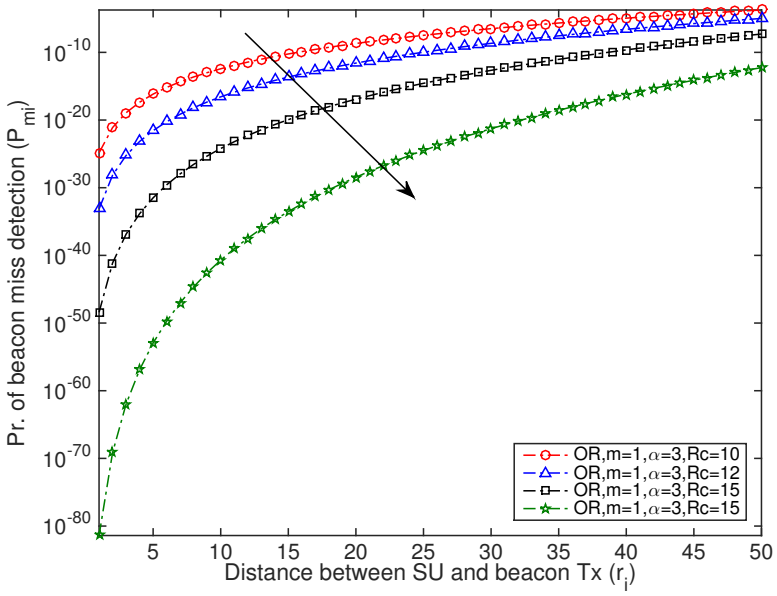


Figure 5.20: Probability of beacon miss detection versus distance between beacon Tx and SU

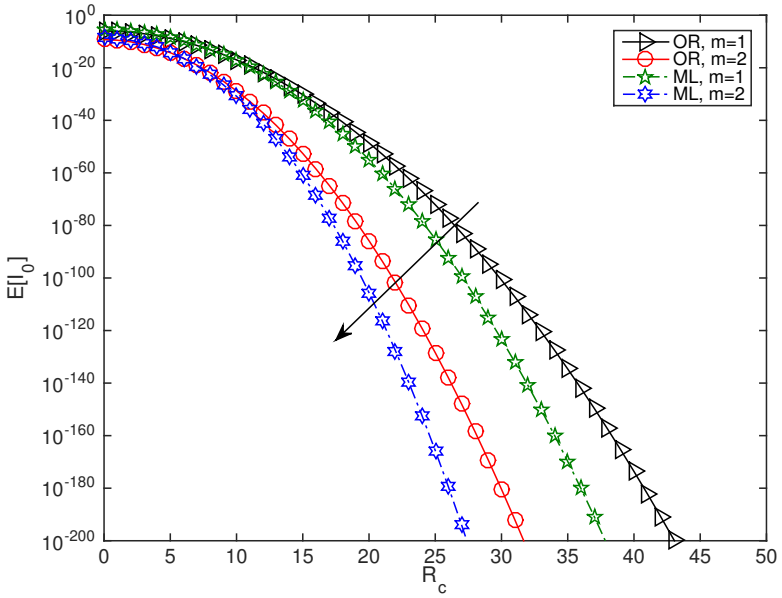


Figure 5.21: Mean of the cumulative interference versus cooperation distance with ML detection and OR sensing strategy

Figure 5.21 shows the plots between mean interference and cooperative distance for OR and ML rule. It can be seen that the ML rule outperforms OR rule i..e for a fixed cooperative distance ML experiences less mean interference than the OR rule. Generally, the means interference for OR and ML rule decreases as the parameter increases from $m = 1$ to $m = 2$.

5.10 Summary

Spectrum sensing is one of the important characteristic of cognitive radio used to find out the under-utilised band. Additionally, spectrum sensing-throughput tradeoff is performed in order to protect the primary user and increased the throughput for secondary user with sensing time. Sensing-throughput tradeoff depends upon the type of receiver used in cognitive radio. Energy detector is considered for carrying out the comprehensive analysis. For null-hypothesis and signal only hypothesis performance of receiver depends on the signal amplitude, sample size and noise variance. It means receiver performance can be increased by increasing the amplitude , increasing sample size and decreasing noise variance. Receiver operating characteristic curve involves probability of detection and probability of false alarm at given SNR values. The two probabilities for single CR and at the FC play vital role for determinning the possible spectrum opportunity. The two probabilities are for single CR and multiple CR sending their raw data or decision information to FC. In additional to SNR values and the P_D and P_{FA} values choice of selection of threshold is also important in determining the presence and absence of primary user. Various fusion strategies are used to asses the performance of cooperative half-duplex communication cognitive radio for example AND, OR and k-out-of-N rule. Multislot is also beneficial to further optimise the throughput in known and known channel environment. It's also worthwhile to assess the performance of CR in terms of aggregate interference and outage analysis.This is done by placing beacons at the PU Rx in Rayleigh, Rician and Nakagami fading environments. Finally, interference and outage analysis has been carried out for cooperative sensing using OR and ML rule.

Chapter 6

PAPR Reduction and Sensing-throughput Tradeoff in OFDM-based Cognitive Radio

6.1 Introduction

In this chapter deals with introduction of OFDM and OFDM-centric CR because of ubiquitous nature of OFDM in communication standards it's highly likely that PU signals are OFDM signals. Therefore, starting with OFDM transmitter and receiver structure at the corresponding signal model. The aim of this chapter is to deal with the problem of PAPR which is prevalent in OFDM based systems. In CRNs our fundamental objective is to protect the PU or incumbent and increase the throughput for SU. In order to increase the throughput it's preferred to dynamically access larger chunks of bandwidth which is uncommon for CR-based SU specially in TV bands. This leads to the OFDM based technique where preference is given to aggregation of non-contiguous spectrum with the help NC-OFDM. The concept beyond NC-OFDM is CR nulls the carriers at which PU is expected to be present and performs it transmission where there is no SU. After discussing NC-OFDM and the corresponding PAPR reduction techniques special focus placed on maximisation of the sensing-throughput of the CR. Finally, Full-Duplex Communication(FDC) Cognitive Radio is discussed and performance of FDC-CR and

Half-Duplex Communication (HDC) CR with FDC-SS and HDC-SS sensing strategies is compared. It's seen that the FDC-CR which uses two different antennas for sensing and data transmission at the same time yields higher throughput than the HDC-CR which uses same antenna for sensing and data transmission purpose.

6.2 OFDM

6.2.1 OFDM Transceiver Architecture

Figure 6.1 and Fig. 6.2 shows the basic OFDM transmitter and receiver architecture. In OFDM high data stream generated by source is divided into N parallel low data stream and these streams are modulated by M-PSK or M-QAM. The M-QAM modulated streams are transmitted on orthogonal subcarrier using serial-to-parallel block and finally are summed up to form an OFDM signal. The orthogonal subcarriers in time-domains and frequency domain are given in Fig.6.3 and Fig.6.4. OFDM signal can be written mathematically as follows:

$$x_m(t) = \frac{1}{N}\sum_{k=0}^{N-1} X_{m,k} \exp\left(j2\pi\frac{k}{T}(t-t_s)\right) \quad t_s \leq t \leq t_s + T \tag{6.1}$$

Where $X_{m,k}, \quad = 0, 1, \ldots, N-1$ are the complex input signals of kth subcarrier at mth time instant. Similarly, discretised OFDM signal is:

$$x_m(t) = \frac{1}{N}\sum_{k=0}^{N-1} X_{m,k} \exp\left(j2\pi\frac{kn}{N}\right) \quad n = 0, 1, \ldots, N-1 \tag{6.2}$$

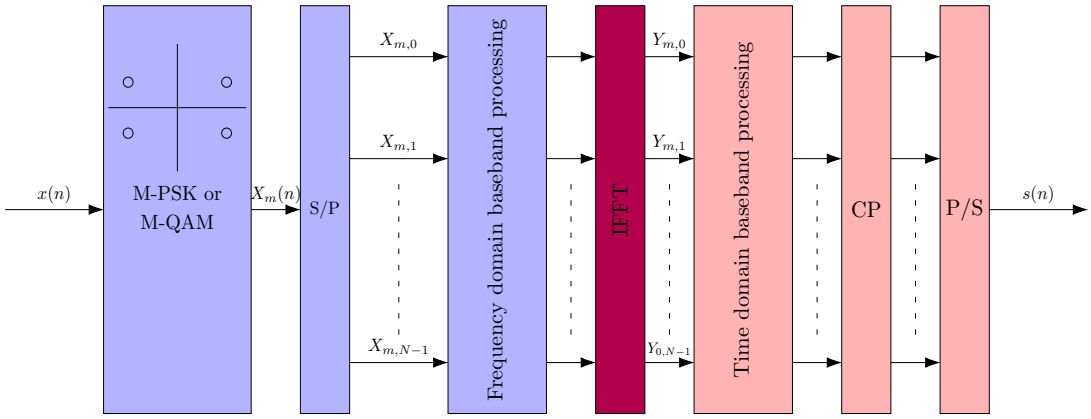


Figure 6.1: OFDM Transmitter Architecture[21]

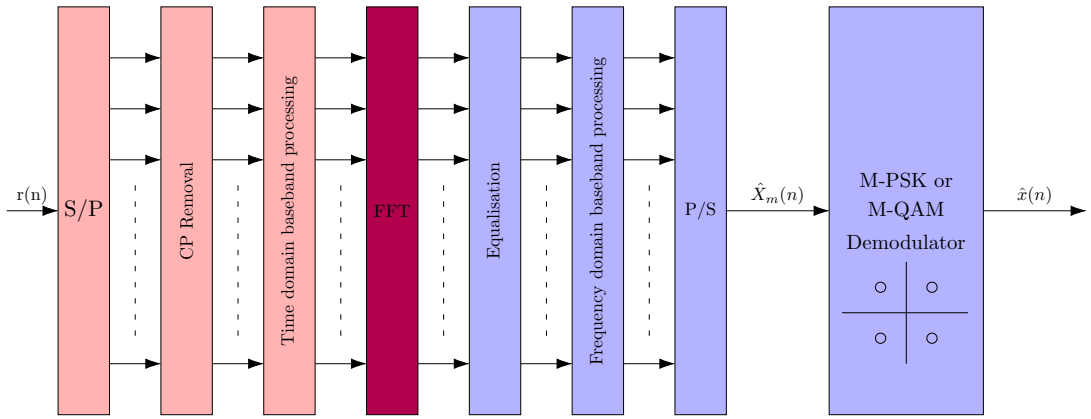


Figure 6.2: OFDM Receiver Architecture[21]

Guard interval in each OFDM symbol is used whose duration is greater than the maximum delay spread of the channel such that MPC don't arrive into multiple symbols and hence avoid interference. After performing P/S conversion the baseband OFDM signal is up sampled and passed through D/A converter. Finally, it's bandpass filtered, upconverted and passed through PA for amplification and then transmitted through antenna over the wireless channel.

At OFDM receiver reverse operation is performed to that of OFDM transmitter i.e. RF to baseband conversion, lowpass filter, pass through A/D converter and

the serial stream is converted into parallel stream and cyclic prefix is discarded. In order to convert time-domain signal into frequency domain at the receiver DFT is used which is as follows:

$$\hat{X}_{m,k} = \sum_{n=0}^{N-1} r_{m,n} \exp\left(j2\pi \frac{kn}{N}\right) \quad n = 0, 1, \ldots, N-1 \tag{6.3}$$

Where $r_{m,n}$ is the composite received signal. After DFT parallel stream is multiplexed into serial stream. OFDM signals are highly suscebtible to phase and frequency offset. Therefore, in order to recover correct OFDM symbol frequency and timing synchronisation is assured. It may also require channel estimation and equalisation based on the BER and system requirements.

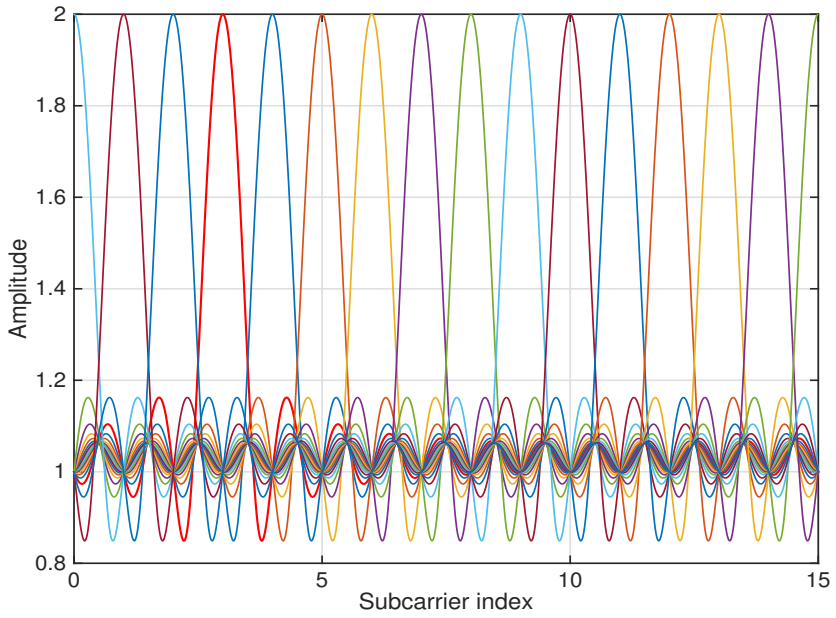


Figure 6.3: Consecutive OFDM subcarriers in time domain

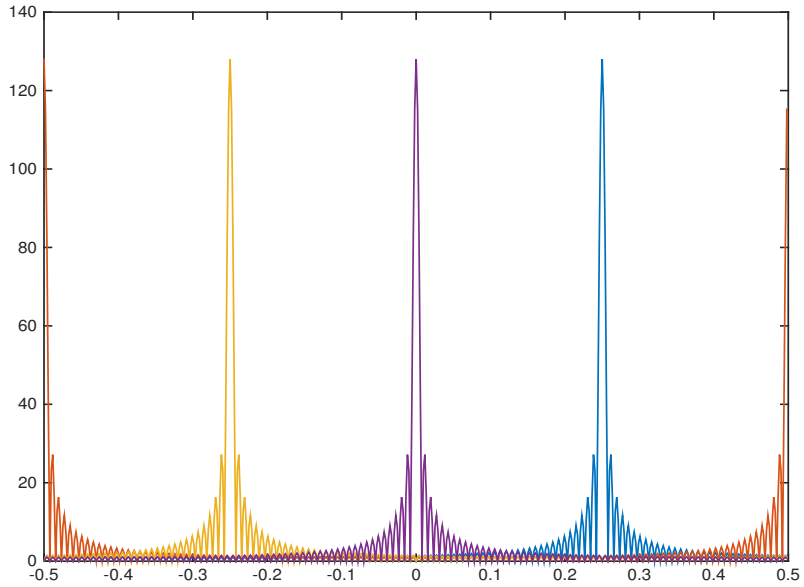


Figure 6.4: OFDM subcarrier spectrum

6.2.2 PAPR Issue in OFDM

At the OFDM transmitter orthogonal subcarriers are summed together which results on composite time-domain signal exhibit large PAPR. In order to deal with high PAPR the D/A converter with high dynamic range is used and PA with highly linear characteristics. Both of the requirements make the receiver more complex and costly. Therefore, it's imperative to reduce PAPR of the OFDM signal. OOB is reduced in order to accommodate and coexist CR users. There are several methods to suppress side lobe levels to reduce OOB for example border carrier deactivation[22],windowing [23],subcarrier weighting[24]and insertion of cancellation carriers[25].

6.3 NC-OFDM

An OFDM architecture can be transformed into NC-OFDM by nulling some carrier on which PU is expected. In this way high data rates for SU can be acheived by

aggregating non-contiguous smaller chunks of spectrum which is under-utilised by PU. Figure 6.5 and Fig.6.6 shows the transmitter architecture of the NC-OFDM respectively. Similar to legacy OFDM, M-PSK/M-QAM modulated high data stream is divided into N lower data streams using S/P converter block. Contrary to OFDM transmission all the subcarriers are not need to be activated in NC-OFDM. Active subcarriers are allowed only in unoccupied band which is predicated based on spectrum sensing. What makes NC-OFDM unique is the subcarrier nulling block which periodically obtains information about the spectrum status which is obtained from spectrum sensing. The subcarriers which corresponds to incumbent PU are nullified at the transmitter for avoiding any interference. After converting a high data stream into N lower data stream IFFT is used to these lower streams to modulate on different subcarriers. Mathematically, the complex baseband NC-OFDM signal is:

$$x_m(t) = \frac{1}{N} \sum_{k=0}^{N-1} X_{m,k} \exp^{j2\pi kt/T} \tag{6.4}$$

Where Xm, k is symbol of the kth subcarrier, $X_{m,k} \in \{1, -1\}$ for BPSK and $X_{m,k} \in \{\pm 1, \pm j\}$ for QPSK signalling and T is symbol duration. $X_{m,k} = 0$ for kth deactivated subcarrier. The discretised version of NC-OFDM signal can be rewritten as:

$$x_(n) = \frac{1}{N} \sum_{k=0}^{N-1} X_{m,k} \exp^{j2\pi kn/N} \quad n = 0, 1, \ldots, N-1 \tag{6.5}$$

Cyclic prefix in each NC-OFDM symbol whose length is greater than the channel delay spread. This is done in order to avoid the detrimental effect of ISI. Moreover, baseband NC-OFDM signal $x(n)$ is passed through RF chain and unconvered to intended center frequency.

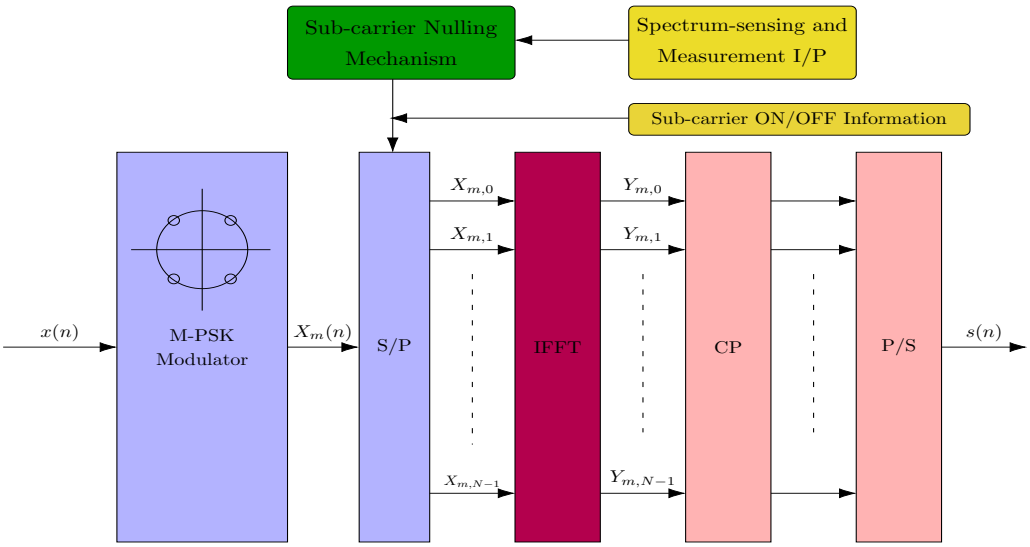


Figure 6.5: Transmitter Architecture of NC-OFDM

As shown in Fig. 6.6, the NC-OFDM receiver performs inverse operation to that of NC-OFDM transmitter. Received NC-OFDM RF signal is downconverter for baseband processing, then the signal is passed through P/S block for parallel to serial conversion, CP is removed and FFT is applied to converted time-domain signal to frequency-domain. After channel estimation and equalisation to compensate the effect of fading, active NC-OFDM subcarriers are passed through P/S converter and hence original high stream date is reconstructed.

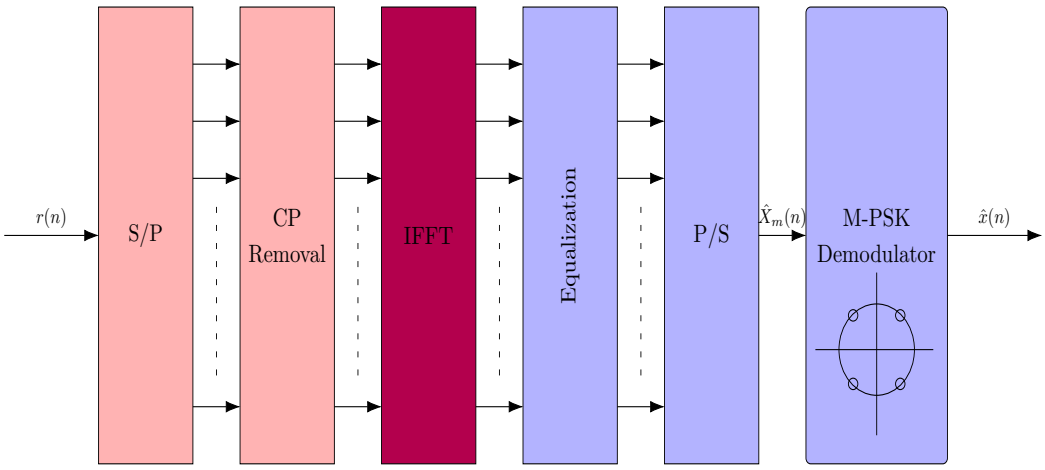


Figure 6.6: Receiver Architecture of NC-OFDM

NC-OFDM is advantageous for SU maximising its throughput by aggregating the non-contiguous chunks of underutilised PU band. In addition to its advantage, it has the same disadvantage of PAPR as it's for the legacy OFDM. When subcarriers are added coherently, the NC-OFDM signal exhibits large PAPR. In order to run the system at high PAPR DAC with higher resolution is used and PA with high linearity in order to avoid amplitude clipping. This may lead complex and costly receiver.

6.4 PAPR in NC-OFDM

NC-OFDM exhibits large PAPR similar to OFDM because of the summation of the subcarriers at the transmitter side. In order to counter act the negative effect of PAPR there are various techniques proposed in literature. For example filtering[26][27][28], error control coding [29][30][31], constellation shaping techniques[32][33][34] and power adjustment techniques[35][36][35].

PAPR Definition

PAPR is defined as*PPAPR is ratio of the peak power present in subcarriers to the average power.* The highest PAPR is exhibited by the NC-OFDM signal when the

subcarriers are added coherently.

6.4.1 Baseband PAPR

In the following subsection continuous time version and discrete time version definition of the baseband PAPR is discussed.

Continuous Time PAPR

It's known that baseband OFDM signal consisting of N continuous subcarriers can be given as follows:

$$x(t) = \frac{1}{N} \sum_{k=0}^{N-1} X_k e^{j2\pi kt/T} \tag{6.6}$$

Where X_k is the kth carrier symbol and T is OFDM symbol duration. Now for such OFDM signal the PAPR is defined as:

$$PAPR = \frac{\underset{0 \le t \le T}{max} |x(t)|^2}{\mathbb{E}\Big[|x(t)|^2\Big]} \tag{6.7}$$

Discrete Time PAPR

Continuous Time PAPR is uncommon therefore discrete PAPR is taken into consideration. The discretised version of the above equation with some oversampling factor L is given by:

$$x(n) = \frac{1}{N} \sum_{k=0}^{N-1} A_k e^{j2\pi kn/LN} \quad n = 0, 1, \ldots, LN-1 \tag{6.8}$$

Mathematicall, discrete PAPR of baseband OFDM signal is given by:

$$PAPR = \frac{\underset{0 \le n \le LN-1}{max} |x(n)|^2}{\mathbb{E}\Big[|x(n)|^2\Big]} \tag{6.9}$$

6.4.2 Passband PAPR

Real signal of passband OFDM signal can be given as follows:

$$\begin{aligned} x_{PB} &= \Re\{x(t)e^{2\pi f_c t}\} \\ &= \Re\{x(t)\cos(2\pi f_c t) - \Im\{x(t)\sin(2\pi f_c t)\}\} \\ &= \{x_I(t)\cos(2\pi f_c t) - \{x_Q(t)\sin(2\pi f_c t)\}\} \end{aligned} \tag{6.10}$$

Oftentimes carrier frequency is much higher than the signal bandwidth, therefore the maximum of modulated signal is $max|s_{BP}(t)| \approx max|s(t)|$. Now the average power of the passband signal:

$$\begin{aligned} \mathbb{E}|x_{PB}(t)|^2 &= \mathbb{E}\Big[|\Re\{x(t)e^{2\pi f_c t}\}|^2\Big] \\ &= \mathbb{E}\Big[|x_I(t)\cos(2\pi f_c t) - \{x_Q(t)\sin(2\pi f_c t)\}|^2\Big] \\ &= \frac{1}{2}\mathbb{E}\Big[\{x_I(t)\}^2 + \{x_Q(t)^2\}\Big] \\ &= \frac{1}{2}\mathbb{E}\Big[|x(t)|^2\Big] \end{aligned} \tag{6.11}$$

Hence the passband PAPR can be given as:

$$\begin{aligned} PAPR\{x_{PB}\} &= \frac{max|x_{PB}(t)|}{\mathbb{E}\Big[|x_{PB}(t)|^2\Big]} \\ &\approx \frac{max|x(t)|}{\frac{1}{2}\mathbb{E}\Big[|x(t)|^2\Big]} \\ &\approx 2PAPR\{x(t)\} \end{aligned} \tag{6.12}$$

Above equation shows that the passband PAPR is approximately twice the banseband PAPR.

6.4.3 Bounds on MPSK-OFDM and MQAM-OFDM PAPR

MPSK and MQAM are frequently used modulation techniques with OFDM transceivers, therefore it's essential know upper and lower bounds of PAPR.

MPSK-OFDM

All the subcarriers in MPSK modulated OFDM system amplitude level of the signals in constellation is constant. Therefore, all the subcarriers have constant power. Let us say that the input data sequence is MPSK modulated and power across subcarriers is constant. Then the PAPR of OFDM signal[37]:

$$\underset{0\leq n\leq LN-1}{max}|x(n)|^2 = \underset{0\leq n\leq LN-1}{max}\left|\frac{1}{N}\sum_{k=0}^{N-1}X_k e^{j2\pi kn/LN}\right|^2 \tag{6.13}$$

All the subcarriers are added coherently and the highest peak is observed, the peak power of the OFDM signal is:

$$\begin{aligned}\underset{0\leq n\leq LN-1}{max}|x(n)|^2 &\leq \left(\frac{1}{N}\sum_{k=0}^{N-1}max|X_k|\right)\\ &= \left(\frac{AN}{N}\right)^2\\ &= A^2\end{aligned} \tag{6.14}$$

Using the Parseval's relationship for the DFT [38]:

$$\sum_{n=0}^{N-1}|x(n)|^2 = \frac{1}{N}\sum_{k=0}^{N-1}|X_k|^2 \tag{6.15}$$

In order to get average power in time domain both sides are divided by N:

$$\begin{aligned}\mathbb{E}\big(|x(n)|^2\big) &= \frac{1}{N}\mathbb{E}\big(|X_k|^2\big)\\ &= A^2/N\end{aligned} \tag{6.16}$$

Then using eq.6.14 and 6.16 the PAPR of OFDM signal can be written as:

$$
\begin{aligned}
PAPR\Big[x(n)\Big] &= \frac{\underset{0\leq n\leq\leq LN-1}{max}|x(n)|^2}{\mathbb{E}\big(|x(n)|^2\big)} \\
&\leq \frac{A^2}{A^2/N} \\
&\leq N
\end{aligned}
\tag{6.17}
$$

PAPR of MPSK-OFDM signal is always less than or equal to N [37].

MQAM-OFDM

Since in MQAM both amplitude and phase of the signal are varied, therefore MQAM-OFDM signal has different power levels:For square constellation M-QAM signal i.e. $\big(\pm mA, \pm mA\big)$ where $m = 1, 3, \ldots, \sqrt{M}-1$ assuming all the constellation points are equally probable, then the average transmitter power can be given by[39]:

$$
\begin{aligned}
\sigma_x^2 &= \frac{A^2}{M}\sum_{m=1}^{M}\big(a_{mc}^2 + a_{ms}^2\big) \\
&= \frac{1A^2}{M}\sum_{m=1}^{M}(a_{mc}^2) = \frac{8A^2}{M}\sum_{m=1}^{M/4}(a_{mc}^2) \\
&= \frac{8A^2}{M}\sqrt{\frac{M}{4}}\sum_{m=1}^{\sqrt{\frac{M}{4}}}\big(2m-1\big)^2 \\
&= \frac{2A^2(M-1)}{3}
\end{aligned}
\tag{6.18}
$$

Where (a_{mc}, a_{ms}) are the coordinates of the mth constellation Worst-case PAPR as in [21]:

$$\begin{aligned} \frac{\hat{P}_{min}}{\mathbb{E}(|x(n)|^2)} \leq PAPR_{max} \leq \frac{\hat{P}_{max}}{\mathbb{E}|x(n)|^2} \\ \frac{3N}{M-1} \leq PAPR_{max} \leq \frac{3N(\sqrt{M}-1)^2}{M-1} \end{aligned} \tag{6.19}$$

Where $\hat{P}_{min} = 2A^2$ and $\hat{P}_{max} = 2A^2(\sqrt{M}-1)^2$

6.4.4 Statistical Characteristics

Consider the case where all the sub symbols are i.i.d, then by CLT the real and imaginary parts of the N-point FFT output have Gaussain distribution with mean zero and variance σ^2 i.e. $\mathcal{N} \sim (0, \sigma^2)$. Therefore, the instantaneous power of the baseband OFDM signal $s(n)$ is:

$$p = \Re\{x(n)\}^2 + \Im\{x(n)\}^2 \tag{6.20}$$

Instantaneous power can be characterised as Chi-squared distribution with two DoF as follows[40]:

$$f(p) = \frac{1}{\sigma^2} \exp\big(-\frac{p}{\sigma^2}\big), \quad p \leq 0 \tag{6.21}$$

The CDF of PAPR is defined as:

$$\begin{aligned} Pr(p < p_0) &= \int_0^{p_0} f(p)dp \\ &= 1 - e^{-\frac{p_0}{\sigma^2}} \end{aligned} \tag{6.22}$$

If $\mathbb{E}[|x(n)|^2]$ is normalised to unity, then the CCDF of the PAPR is given by:

$$Pr(p > p_0) = 1 - \big(1 - e^{-\frac{p_0}{\sigma^2}}\big)^N \tag{6.23}$$

Table 6.1: Theoretical approximation to CCDF of PAPR values[21]

CCDF	Remarks	Reference
$Pr(p > p_0) \approx 1 - \left(1 - e^{-\frac{p_0}{\sigma^2}}\right)^{\alpha N}$	$\alpha = 2.8$ and $N \geq 64$	[41]
$Pr(p > p_0) \approx 1 - \exp\left(-\sqrt{\frac{\pi p_0}{3}} N e^{-p_0}\right)$		[42]
$Pr(p > p_0) \approx 1 - \exp\left(-\sqrt{\frac{\pi \log N}{3}} N e^{-p_0}\right)$		[43]
$Pr(p > p_0) \approx 1 - \exp\left(-\frac{2N}{\sqrt{3} e^{-\frac{p_0}{2}}}\right)$	N and p_0 are large	[44]

PAPR CDF for non-circular constellation is given by[45]:

$$Pr[p > p_0] = 1 - \left(1 - 2\exp(-p_0) + \exp\left(-\frac{2}{1+\mu_2^2} p_0\right)\right)^{\frac{N-2}{2}} \left\{\int_0^{\sqrt{p_0}} \frac{2}{\sqrt{2\pi}\sigma_r} \exp\left(-\frac{u^2}{2\sigma_r^2}\right)\left(1 - erfc\left(\sqrt{\frac{x-u^2}{2\sigma_i^2}}\right)\right)\right\}^2 \tag{6.24}$$

Where $\sigma_i^2 = (1-\mu_2)/2$, μ_2 mean power of the symbol constellation, $\sigma_r^2 = (1+\mu_2)/2$. For BPSK, $\mu_2 = 1, \sigma_r^2 = 1$ and $\sigma_r^2 = 0$, the CDP of PAPR can given mathematically:

$$Pr[p > p_0] = 1 - \left(1 - erfc\left(\sqrt{p_o/2}\right)\right)^2 \left(1 - e^{p_0}\right)^{\frac{N-2}{2}} \tag{6.25}$$

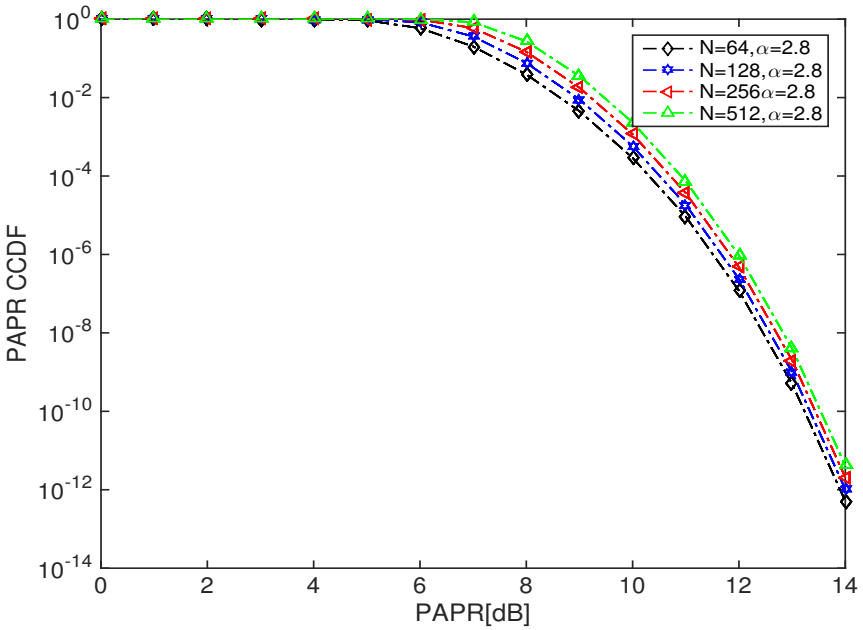


Figure 6.7: Peak-to-Average-Power-Ratio (PAPR) CCDF

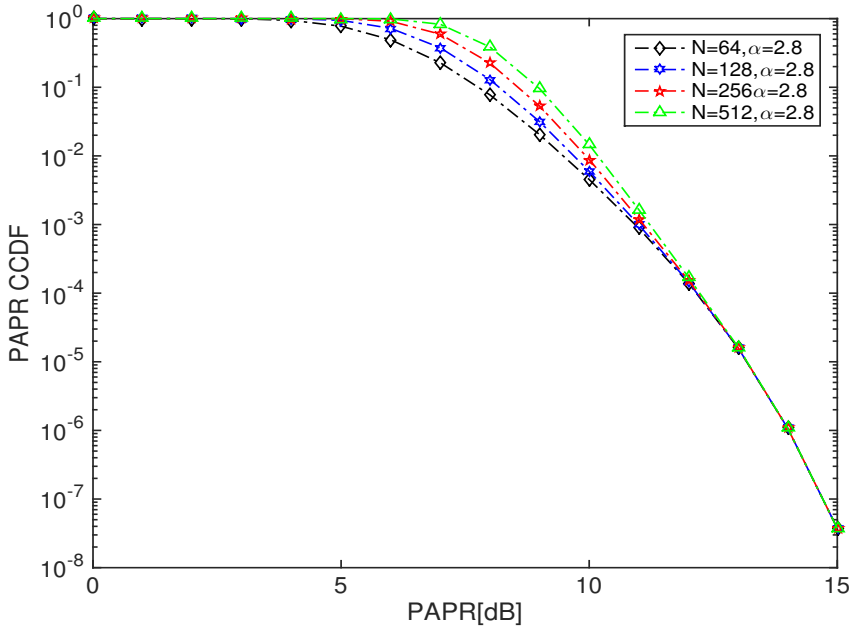


Figure 6.8: Peak-to-Average-Power-Ratio (PAPR) CCDF of BPSK

6.5 PAPR of NC-OFDM Signal

Using CLT for large number of carriers N, the OFDM signal is Gaussian distributed with zero mean and variance $\sigma^2 = N_u\sigma_D^2/N$ Where N_u is number of active subcarriers and σ_D^2 is input sequence variance [46]. Assuming the symbols are i.i.d, then by invoking CLT the real and imaginary parts of N-point IFFT output follow mutually independent Gaussian distribution function i.e $\mathcal{N}(0, \sigma^2)$. Thus instantaneous power of the baseband OFDM signal $s(n)$ is mathematically given by:

$$p = \Re\{x(n)\}^2 + \Im\{x(n)\}^2 \tag{6.26}$$

The instantaneous power follows Chi-squared distribution with two DoF:

$$f(p) = \frac{1}{\sigma^2}\exp\left(-\frac{p}{\sigma^2}\right) \quad \leq 0 \tag{6.27}$$

Therefore, CDF is given by:

$$Pr[p < p_0] = \int_0^{p_0} f(p)dp = 1 - e^{-\frac{p_0}{\sigma^2}} \tag{6.28}$$

If $\mathbb{E}[|x(n)|^2]$ is normalised to unity, then the CCDF of PAPR is given by:

$$Pr[p > p_0] = 1 - \left(1 - e^{-\frac{p_0}{\sigma^2}}\right)^N \tag{6.29}$$

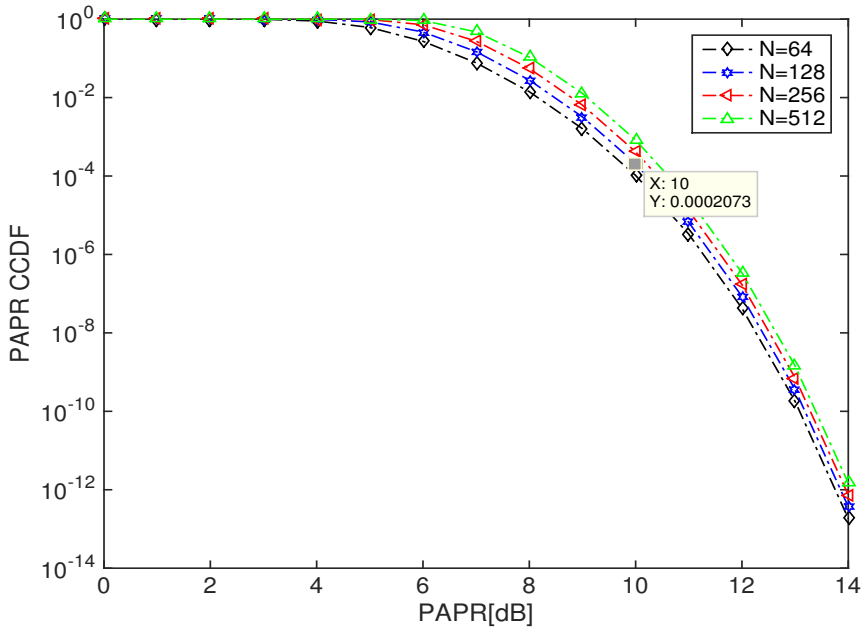


Figure 6.9: PAPR Distribution in NC-OFDM Signal $\alpha = 1$

In NC-OFDM system active subcarriers have three different locations as explained below:

Contiguously-spaced Active subcarriers

Data over continuously spaced active subcarriers with adjacent deactivated subcarriers can be given by:

$$A_k = \begin{cases} 0 & \text{for } k = 0, 1, \ldots, n_1 \\ c_k & \text{for } k = n_1, n_1 + 1, \ldots, n_2 \\ 0 & \text{for } k = n_2, n_2 + 1, \ldots, N \end{cases} \tag{6.30}$$

Where c_k are data symbols and $x_k \in \{\pm 1 \pm j\}$ for QPSK signalling and subcarrier through n_1 and n_2 are active.

Regularly-spaced Active subcarriers

The data over regularly spaced active subcarriers is given by:

$$A_k = \begin{cases} c_k & \text{for } k = 0, m, \ldots, N \\ 0 & \text{otherwise} \end{cases} \tag{6.31}$$

6.5.1 Maximum PAPR Distribution in NC-OFDM Signal

PAPR of an MPSK-OFDM signal is less than or equal to N[37].With p active subcarrier and input symbols chosen from MPSK constellation such that $|A_k|$. The peak power of the NC-OFDM signal is given by:

$$\begin{aligned} \underset{0\leq t\leq T}{max}|x(t)|^2 &= \left|\frac{1}{\sqrt{N}\sum_{k=0}^{N-1} A_k e^{j2\pi kt/T}}\right|^2 \\ &\leq \left(\frac{1}{\sqrt{N}}\sum_{k=0}^{N-1}\max|A_k|\right)^2 \\ &\leq \frac{p^2}{N} \end{aligned} \tag{6.32}$$

Moreover, using Parseval's relationship the average power of NC-OFDM signal is given by:

$$\begin{aligned} \mathbb{E}[|x(t)|^2] &= \mathbb{E}\left\{\left|\frac{1}{\sqrt{N}\sum_{k=0}^{N-1} A_k e^{j2\pi kt/T}}\right|^2\right\} \\ &= \frac{1}{N}\sum_{k=0}^{N-1}\mathbb{E}[|A_k|^2] \\ &= \frac{p}{N} \end{aligned} \tag{6.33}$$

Finally, the PAPR of the NC-OFDM signal is given as follows:

$$\begin{aligned} PAPR_{NC-OFDM} &= \frac{\max\limits_{0\leq t\leq T}|x(t)|^2}{\mathbb{E}[|x(t)|^2]} \\ &\leq \frac{p^2/N}{p/N} \\ &\leq p \end{aligned} \tag{6.34}$$

Hence, the maximum PAPR for MPSK-OFDM signal with p active subcarriers is p regardless of the total number of subcarriers N.

6.6 Sensing-throughput tradeoff in OFDM-based Cognitive Radio

The system model for OFDM based CR can written as follows:

$$\begin{aligned} \mathcal{H}_0: &\quad x_k(n) = w_k(n) \\ \mathcal{H}_1: &\quad x_k(n) = h_k e^{j\theta_k} s(n) + w(n) \quad n = 0, 1, \ldots, N-1 \end{aligned} \tag{6.35}$$

Moreover, the global test statistics at FC under the two hypothesis which are Gaussian distributed as follows[47]:

$$\begin{aligned} \mathcal{H}_0: &\quad T_k(x_k) \sim \mathcal{N}\big(\sigma^2, \sigma^2/KN\big) \\ \mathcal{H}_1: &\quad T_k(x_k) \sim \mathcal{N}\bigg(\sigma^2 + \frac{\sigma_s^2}{k}\sum_k h_k^2, \frac{\sigma^4}{kN} + \frac{2\sigma^2\sigma_s^2}{k^2 N}\sum_k h_k^2\bigg) \end{aligned} \tag{6.36}$$

Where σ^2 is noise variance, $\Omega = \mathbb{E}\big[h_k^2\big]$ average power in the channel and θ_k is kth channel phase. Therefore, the global P_{FA} and P_D at the FC can be written as[47]:

$$P_{FA}\big(\tau, N\big) = Q\bigg(\big(\frac{\tau}{\sigma^2} - 1\big)\sqrt{kN}\bigg) \tag{6.37}$$

$$P_D\big(\tau, N\big) = Q\bigg(\sqrt{\frac{kN}{1 + 2\gamma/k}}\bigg(\tau/\sigma^2 - 1 - \frac{\gamma}{k}\bigg)\bigg) \tag{6.38}$$

Similarly, average SNR γ is:

$$\gamma = \bar{\gamma}\sum_{k=0}^{K-1} h_k^2\,, \quad \bar{\gamma} = \sigma_s^2/\sigma^2 \tag{6.39}$$

Now probability of outage P_{out} is defined as:

$$P_{out} = Pr.\{P_{MD} > \epsilon\} = Pr.\{P_D \leq 1 - \epsilon\} \leq \alpha \tag{6.40}$$

Putting eq.6.40 into eq.6.38 and after some algebra P_{out} can be given as:

$$P_{out} = P\Big\{\big(N/k\big)\gamma^2 - 2\bigg(N\lambda + \frac{\epsilon_c^2}{k}\bigg)\gamma + \big(kN\lambda^2 - \epsilon_c\big) \leq 0\Big\} \tag{6.41}$$

Where $\epsilon_c = Q^{-1}(1-\epsilon)$,$\lambda = \big(\tau/\sigma^2 - 1\big)$. Let β be the largest root and minimum SNR below which outage occurs:

$$\beta\big(\tau, \epsilon_c, N\big) = k\lambda + \frac{\epsilon_c}{N}\Big[\epsilon_c + \sqrt{\epsilon_c^2 + kN\big(2\lambda + 1\big)}\,\Big] \tag{6.42}$$

Probability of outage in terms of instantaneous SNR

$$\begin{aligned} &Pr\bigg\{\gamma \leq \beta(\tau, \epsilon_c, N)\bigg\} = Pr\bigg\{\bar{\gamma}\sum_k h_k^2 \leq \beta(\tau, \epsilon_c, N)\bigg\} \\ &\implies Pr\bigg\{\sum_k h_k^2 \leq \frac{\beta(\tau, \epsilon_c, N)}{\bar{\gamma}}\bigg\} \end{aligned} \tag{6.43}$$

Where $h_k \sim$ Nakagami$(m, \frac{\Omega}{m})$ and has the following PDF:

$$f_{h_k}^2 = \bigg(\frac{m}{\Omega}\bigg)^m \frac{t^{m-1}}{\Gamma(m)} \exp\bigg(-\frac{mt}{\Omega}\bigg) \tag{6.44}$$

P_{out} is given by the CDF of the $f_{h_k}^2$ as:

$$P_{out} = 1 - \frac{\Gamma\bigg(km, \frac{m\beta(\tau, \epsilon_c, N)}{\Omega\bar{\gamma}}\bigg)}{\Gamma(km)} \tag{6.45}$$

Setting eq. 6.45 equal to α

$$1-\frac{\Gamma\left(km,\frac{m\beta(\tau,\epsilon_c,N)}{\Omega\bar{\gamma}}\right)}{\Gamma(km)}=\alpha \implies (1-\alpha)=\frac{\Gamma\left(km,\frac{m\beta(\tau,\epsilon_c,N)}{\Omega\bar{\gamma}}\right)}{\Gamma(km)}$$

$$\Gamma(km)(1-\alpha)=\frac{\Gamma\left(km,\frac{m\beta(\tau,\epsilon_c,N)}{\Omega\bar{\gamma}}\right)}{\Gamma(km)} \quad \text{if } X=\Gamma(\alpha,\beta) \implies Z=\Gamma^{-1}(\beta,X)$$

$$\implies \Gamma^{-1}(km,\Gamma(km)(1-\alpha))=\frac{m\beta(\tau,\epsilon,N)}{\Omega\bar{\gamma}}$$

$$\implies \beta(\tau,\epsilon_c,N)=\frac{\Omega}{m}\bar{\gamma}\Gamma^{-1}\Big(km,\Gamma(km)(1-\alpha)\Big) \tag{6.46}$$

Substituting $\beta(\tau,\epsilon_c,N)=\frac{\Omega}{m}\bar{\gamma}\Gamma^{-1}\Big(km,\Gamma(km)(1-\alpha)\Big)$ in eq.6.45, P_{out} can be given as:

$$P_{out}=1-\Gamma(km,\Gamma^{-1}(km,\Gamma(km)(1-\alpha))) \tag{6.47}$$

If $m=1$, them $\Omega=2\sigma_i^2$ and $\sigma_i^2=1$ for Rayleigh distribution:

$$\beta(\tau,\epsilon,N)=\frac{\Omega}{m}\bar{\gamma}\Gamma^{-1}(km,\Gamma(km)(1-\alpha)) \tag{6.48}$$

For $k=1$ non-cooperative case:

$$\beta(\tau,\epsilon_c,N)=-2\bar{\gamma}\ln(1-\alpha) \tag{6.49}$$

Critical Threshold

$$\tau(\epsilon_c,\alpha,N)=\sigma^2\Bigg\{1+\frac{\Omega\bar{\gamma}\Gamma^{-1}(km,\Gamma(km)(1-\alpha))}{km}+\frac{\epsilon_c}{Nk} \sqrt{N\bigg(\Big(\frac{\Omega}{m}\Big)\bar{\gamma}\Gamma^{-1}\big(km,km(1-\alpha)\big)+k\bigg)}\Bigg\} \tag{6.50}$$

After taking into consideration the critical threshold probability of false alarm P_{FA} and probability of detection P_D can be written as follows:

$$P_{FA}(\tau,N)=Q\bigg(\Big(\frac{\tau\big(\epsilon_c,\alpha,N\big)}{\sigma^2}-1\Big)\sqrt{kN}\bigg) \tag{6.51}$$

$$P_D(\tau, N) = Q\left(\sqrt{\frac{kN}{1+2\gamma/k}}\left(\frac{\tau(\epsilon_c, \alpha, N)}{\sigma^2} - 1 - \frac{\gamma}{k}\right)\right) \tag{6.52}$$

6.7 Average OFDM Cognitive Radio Throughput

The total average throughput for OFDM cognitive radio is sum of the throughput in presence and absence of the primary user. Hence,mathematically[47]:

$$\begin{aligned} R(N) = &\left(1 - N/M\right)\log_2\left(1 + \frac{\epsilon_c}{\sigma^2}\right)\left(1 - P_{FA}(\tau, N)\right)P(\mathcal{H}_0) + \\ &\left(1 - N/M\right)\log_2\left(1 + \frac{\epsilon_c}{\epsilon_p + \sigma^2}\right)\left(1 - P_D(\tau, N)\right)P(\mathcal{H}_1) \end{aligned} \tag{6.53}$$

Finally, the achievable throughput is the throughput of OFDM cognitive radio in absence of PU since the throughput for CR in presence of PU is very small as compared to throughput of the CR in absence of PU. Hence, eq. 6.53 can be written as follows:

$$R(N) = \left(1 - N/M\right)\log_2\left(1 + \frac{\epsilon_c}{\epsilon_p + \sigma^2}\right)\left(1 - P_D(\tau, N)\right)P(\mathcal{H}_1) \tag{6.54}$$

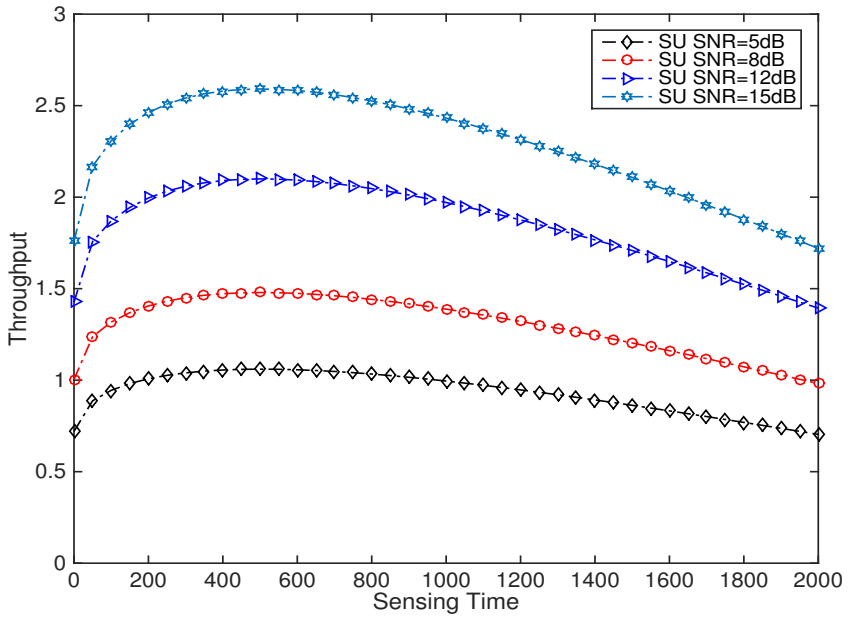


Figure 6.10: Throughput versus sensing time of OFDM based cognitive radio: $N_c = 8$,$N_d = 32$,$\lambda = 0.001$,$N_f = 100(N_c + N_d)$

6.8 Autocorrelation Based Sensing of CP-OFDM Signals

In order to detect the PU signals which are most of the time OFDM signals with cyclic prefix (CP) and known as CP-OFDM is useful method of detecting PUs[48]. Autocorrelation coefficient for CP-OFDM is non-zero at delays $\tau = \pm T_d$, where T_d is useful OFDM symbol. Moreover, of special interest is the low SNR regime because it is imperative to detect very weak PU signals so that SU should not introduce harmful interference. The performance of autocorrelation based detection scheme in AWGN and multipath fading in terms of P_{FA} and P_D is assessed.

6.8.1 Autocorrelation based spectrum sensing

Typically an OFDM signals is sum of narrowband subcarriers that are PSK or QAM modulated. The number of subcarrier is is passed through IFFT block and S/P blocks for transmission. If $c(0), c(1), \ldots, c(T_d - 1)$ are T_d complex PSK or QAM symbols then the output of the IFFT block can be written as follows:

$$c(t) = \frac{1}{\sqrt{T_d}} \sum_{f=0}^{T_d-1} C(f) e^{\frac{j2\pi tf}{T_d}} \quad t = 0, 1, \ldots, T_d - 1 \tag{6.55}$$

Where t is discrete time index and f is discrete frequency index. If T_c is number of symbols in CP i.e. $[c(T_d - T_c), \ldots, c(T_d - 1)]$ are added infront of the block as the CP to form an OFDM block $c(T_d - T_c), \ldots, c(T_d - 1), c(0), c(1), \ldots, c(T_d - 1)]$. A transmitted OFDM frame consists of such blocks. Let us represent symbols of transmitted OFDM frame by $s(t)$, $\mathcal{H}_0$ null-hypothesis and $\mathcal{H}_1$ an alternative hypothesis. Now hypothesis problem can be written as :

$$\begin{aligned} \mathcal{H}_0 : &\quad y(t) = w(t) \\ \mathcal{H}_1 : &\quad y(t) = s(t) + w(t) \end{aligned} \tag{6.56}$$

Where $y(t)$ is received complex OFDM signal and $w(t)$ is CSCG noise. For a large IFFT size and by invoking CLT such that

$$\begin{aligned} s(t) &\sim \mathcal{N}_c\Big(0, \sigma_s^2\Big) \\ s(t) &\sim \mathcal{N}_c\Big(0, \sigma_w^2\Big) \end{aligned} \tag{6.57}$$

Where $\mathcal{N}_c$ is complex Gaussian random variable. Since $y(t) = y_r(t) + y_i(t)$ therefore

$$\begin{aligned} y_r(t) &\sim \mathcal{N}_r\Big(0, \sigma_y^2/2\Big) \\ y_i(t) &\sim \mathcal{N}_r\Big(0, \sigma_y^2/2\Big) \end{aligned} \tag{6.58}$$

For CP-OFDM signals the autocorrelation coefficient can be given by:

$$\rho(\tau) = \mathbb{E}\Big(y(t)y^*(t+\tau)\Big) \Big/ \mathbb{E}\Big(y(t)y^*(t)\Big) \tag{6.59}$$

For lags at $\tau = \pm T_d$ under the two hypotheses

$$\begin{aligned} \mathcal{H}_0 : &\quad \rho(\pm T_d) = 0 \\ \mathcal{H}_1 : &\quad \rho(\pm T_d) = \rho_1 \end{aligned} \tag{6.60}$$

Where

$$\begin{aligned} \rho_1 &= \left(\frac{T_c}{T_d + T_c}\right)\left(\frac{\sigma_s^2}{\sigma_s^2 + \sigma_w^2}\right) \\ &= \left(\frac{T_c}{T_c + T_d}\right)\left(\frac{SNR}{1 + SNR}\right) \quad \therefore SNR = \left(\frac{\sigma_s^2}{\sigma_w^2}\right) \end{aligned} \tag{6.61}$$

Similarly, for multipath channel of order P and tap coefficients $g(l)$, $l = 0, 1, \ldots, P-1$ and $\delta = \sum_{l=0}^{P-1} \mathbb{E}\Big(|g(l)|^2\Big)$

$$\rho_2 = \left(\frac{T_c}{T_c + T_d}\right)\left(\frac{\delta\sigma_s^2}{\delta\sigma_s^2 + \delta\sigma_w^2}\right) \tag{6.62}$$

For AWGN case $\delta = 1$ and $\rho_1 = \rho_2$ and $0 < \rho_1 < 1$ and real-valued coefficient $\rho(\tau) = \rho(-\tau)$. From the observations of several OFDM symbols $y(0), y(1), \ldots, y(M + T_d - 1)$ two real random vectors can be formed from observations such that:

$$\begin{aligned} \mathbf{z}_1 &= \Big[y_r(0)y_i(0)y_r(1)y_i(1)\ldots y_r(M-1)y_i(M-1)\Big] \\ \mathbf{z}_2 &= \Big[y_r(T_d)y_i(T_d)y_r(T_d+1)y_i(T_d+1)\ldots y_r(M+T_d-1)y_i(M+T_d-1)\Big] \end{aligned} \tag{6.63}$$

Now, the two random variables are jointly Gaussian under both hypothesis with PDF [49]:

$$f\Big(z_1(t), z_2(t)|\mathcal{H}_0\Big) = \frac{\exp\left(-1/2\Big(\frac{z_1(t)^2 + z_2(t)^2}{\sigma_0^2}\Big)\right)}{2\pi\sigma_0^2} \tag{6.64}$$

and

$$f(z_1(t), z_2(t)|\mathcal{H}_1) = \frac{\exp\left(-\frac{1}{2(1-\rho_1^2)} \frac{\left(z_1(t)^2 - 2\rho_1 z_1(t) z_2(t) + z_2(t)^2 \right)}{\sigma_1^2} \right)}{2\pi\sigma_1^2\sqrt{1-\rho_1^2}} \tag{6.65}$$

Where $\sigma_1^2 = \frac{\sigma_s^2+\sigma_w^2}{2}$ and $\sigma_0^2 = \frac{\sigma_w}{2}$. Now the LR for hypothesis test is given as:

$$\Psi = \prod_{t=0}^{2M-1} \frac{f(z_1(t), z_2(t)|\mathcal{H}_1)}{f(z_1(t), z_2(t)|\mathcal{H}_0)} \tag{6.66}$$

$$\Psi = \frac{\sigma_0^{2M}}{\sigma_1^{2M}(1-\rho_1^2)^M} \exp\left(-\frac{1}{2}\left(\frac{1}{(1-\rho_1^2)\sigma_1^2} - \frac{1}{\sigma_0^2} \right) \sum_{t=0}^{2M-1} \left(z_1(t)^2 + z_2(t)^2 \right) + \frac{\rho_1 \sum_{t=0}^{2M-1} z_1(t) z_2(t)}{(1-\rho_1^2)\sigma_1^2} \right) \tag{6.67}$$

Since $z_1(t)$ and $z_2(t)$ are iid, therefore $\mathbb{E}(z_1^2(t)) = \mathbb{E}(z_2^2(t))$. Now $\hat{\sigma_z}^2$ is maximum likely estimate of $\mathbb{E}(z_1^2(t))$ based on $\mathbf{z}_1$ and $\mathbf{z}_2$ then $\hat{\sigma_z}^2$ is given as [49]:

$$\hat{\sigma_z}^2 = \frac{1}{4M} \sum_{t=0}^{2M-1} \left(z_1^2(t) + z_2^2(t) \right) \tag{6.68}$$

Equivalently, $\hat{\sigma_z}^2$ can be rewritten in terms of observations as $\left[y_r(t), y_i(t), \ldots, y_r(M+T_d-1), y_i(M+T_d-1) \right]$ as follows:

$$\begin{aligned} \hat{\sigma_z}^2 &= \frac{1}{2(M+T_d)} \sum_{t=0}^{M+T_d-1} y_r^2(t) + y_i^2(t) \\ &= \frac{1}{2(M+T_d)} \sum_{t=0}^{M+T_d-1} |y(t)|^2 \end{aligned} \tag{6.69}$$

Using low SNR approximation $\hat{\sigma_z}^2 \approx \sigma_1^2 \approx \sigma_0^2$ and substituting eq. 6.69 into 6.67:

$$\begin{aligned}\Psi &= \frac{\exp\left(-2M\left(\frac{1}{(1-\rho_1^2)}-1\right)+\frac{\rho_1\sum_{t=0}^{2M-1}z_1(t)z_2(t)}{(1-\rho_1^2)\sigma_z^2}\right)}{(1-\rho_1^2)^M} \\ &= \frac{\exp\left(-2M\left(\frac{\rho_1^2}{(1-\rho_1^2)}\right)+\frac{2M\rho_1\hat{\rho}_{ML}}{(1-\rho_1^2)}\right)}{(1-\rho_1^2)^M}\end{aligned} \tag{6.70}$$

Where $\hat{\rho}_{ML}$ is ML estimate of ρ from vectors $\bar{z_1}$ and $\bar{z_2}$ [49]:

$$\hat{\rho}_{ML} = \frac{1/2M\sum_{t=0}^{2M-1}z_1(t)z_2(t)}{\hat{\sigma_z}^2} \tag{6.71}$$

Equivalently, $\hat{\rho}_{ML}$ can be rewritten as in terms of observations: $\big[y_r(0), y_i(0), \ldots, y_r(M+T_d-1)y_i(M+T_d-1)\big]$ as:

$$\begin{aligned}\hat{\rho}_{ML} &= \frac{1/2M\sum_{t=0}^{M-1}y_r(t)y_r(t+T_d)+y_i(t)y_i(t+T_d)}{\hat{\sigma_z}^2} \\ &= \frac{1/M\sum_{t=0}^{M-1}\Re(y(t)y^*(t+T_d))}{\hat{\sigma_z}^2}\end{aligned} \tag{6.72}$$

For exponential distributions it's convenient to use LLR instead of LR. Therefore, the LLR is given by:

$$L = \log\Psi = -M\log(1-\rho_1^2)+\frac{2M\rho_1(\hat{\rho}_{ML}^2-\rho_1)}{(1-\rho_1)} \tag{6.73}$$

In addition $\mathcal{H}_1$ is decided if $L > \xi_1$ where ξ_1 is detector threshold and $\mathcal{H}_1$ is decided if

$$\hat{\rho}_{ML}^2 > \frac{(1-\rho_1^2)}{2M\rho_1}\left(\xi_1+M\log(1-\rho_1^2)\right)+\rho_1 \tag{6.74}$$

$\hat{\rho}_{ML}$ is required LLRT for hypothesis test. The probability density of $\hat{\rho}_{ML}^2$ under $\mathcal{H}_0$ based on $2M$ real symbols is [49]:

$$f_{2M}(\hat{\rho}_{ML}|\mathcal{H}_0) = \frac{\Gamma\Big(\frac{1}{2}\big(2M-1\big)\Big)}{\Gamma\Big(\frac{1}{2}\big(2M-2\big)\Big)\sqrt{\pi}}\Big(1-\hat{\rho_{ML}}^2\Big)^{(2M-4)/2} \tag{6.75}$$

Theorem 6.8.1 *If $\hat{\rho}_{ML}$ is correlation coefficient for $2M$ symbols from real-valued Gaussian distribution with correlation ρ, then $\frac{\sqrt{2M}(\hat{\rho}_{ML}-\rho)}{(1-\rho^2)}$ is asymptotically distributed according to $\mathcal{N}(0,1)$[49]:*

$$\mathcal{H}_0: \quad \lim_{M\to\infty}\sqrt{2M}\hat{\rho}_{ML} \xrightarrow{d} \mathcal{N}\Big(0,1\Big) \tag{6.76}$$

$$\mathcal{H}_1: \quad \lim_{M\to\infty}\sqrt{2M}\hat{\rho}_{ML} \xrightarrow{d} \mathcal{N}\Big(\sqrt{2M}\rho_1, \big(1-\rho_1^2\big)^2\Big) \tag{6.77}$$

Where $\rho_1 = \Big(\frac{T_c}{T_c+T_d}\Big)\Big(\frac{\sigma_s^2}{\sigma_s^2+\sigma_w^2}\Big)$ and $\xrightarrow{d}$ denotes distribution convergence. Test statistics for sufficiently large M can be approximated as:

$$\begin{aligned}\mathcal{H}_0: &\quad \hat{\rho}_{ML} \sim \mathcal{N}\Big(0, 1/2M\Big)\\ \mathcal{H}_1: &\quad \hat{\rho}_{ML} \sim \mathcal{N}\Big(\rho_1, \frac{(1-\rho_1^2)^2}{2M}\Big)\end{aligned} \tag{6.78}$$

It can be seen that this is classical detection problem with test statistics ρ_{ML}. Different detection strategies can be used for example Min-Max, Neyman-Pearson and Bayes depending upon the error constraints to be satisfied and extent of prior information available. For Neyman-Pearson selected false alarm rate to be satisfied at the detector. For example Gaussian random variable $r \sim \mathcal{N}(\mu_r, \sigma_r^2)$ it can be expressed as [50]:

$$Pr(r > \xi_r) = \frac{1}{2}erfc\Big(\frac{\xi_r - \mu_r}{\sqrt{2}\sigma_r}\Big) \tag{6.79}$$

Therefore, from above equation, the expression for P_{FA} is derived as follows:

$$P_{FA} = Pr(\hat{\rho}_{ML} > \xi_l | \mathcal{H}_0) = \frac{1}{2} erfc\big(\sqrt{M}\xi_i\big) \tag{6.80}$$

Where the threshold can be given by:

$$\xi_l = \frac{1}{\sqrt{M}} erfc^{-1}(P_{FA}) \tag{6.81}$$

Similarly, the P_D is given by:

$$P_D = Pr\big(\hat{\rho}^2_{ML} > \xi_l | \mathcal{H}_1\big) = \frac{1}{2} erfc\left(\sqrt{M}\left(\frac{\xi_l - \rho_1}{1 - \rho_1^2}\right)\right) \tag{6.82}$$

This requires knowledge about T_d such information is provided in different standards. Even if it is not given it can be extracted from the few possible available options. Figure 6.11 shows probability of detection versus SNR for DVB-T standard with parameters as enlisted in caption. It can be seen the probability of detection increases with the increase in SNR and it also increases with the increase in probability of false alarm which is in accord with our intuition developed in chapter 5.

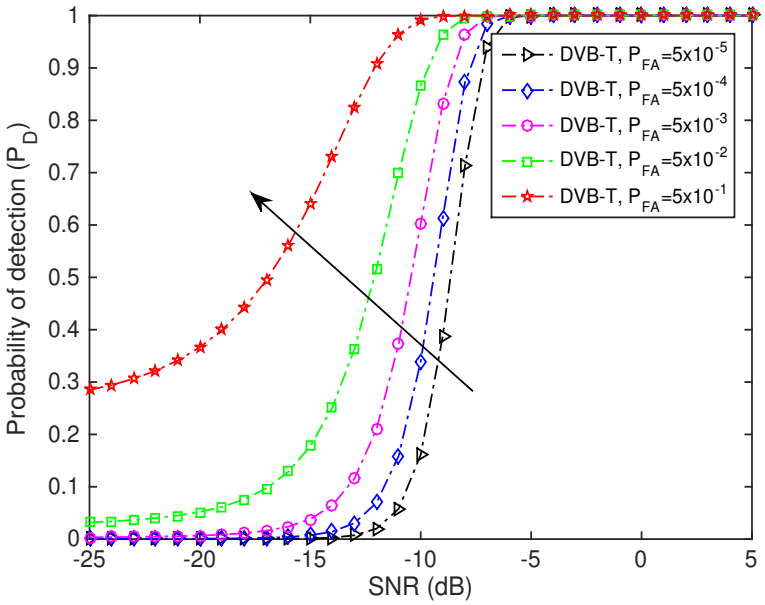


Figure 6.11: Probability of detection P_D versus SNR for DVB-T standard: $T_d = 8192$,$T_c = 1024$,$\mu = 0.111$

Figure 6.12 shows the ROC curves for DVB-T standard which parameters enlisted in caption. It is shown that the probability of detection increases as the probability of false alarm increases. It is also shown the probability of detection increases with the increase in SNR. For example at P_D is 0.05 at P_{FA} value of 0.05 for SNR of $-22dB$ and at the same $P_{FA} = 0.05$ it shoots up to P_D value of 0.88 for SNR of $-10dB$. It's shown that the P_D drops slowly for lower values of SNR as compared to the higher counterparts.

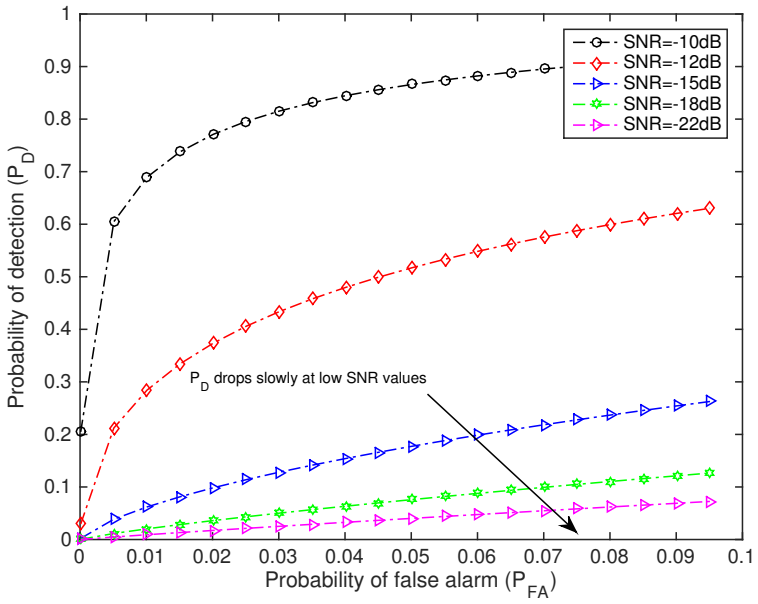


Figure 6.12: Receiver Operating Characteristic (ROC) curves for DVB-T standard: $T_d = 8192$,$T_c = 1024$,$\mu = 0.111$

Figure 6.13 shows the ROC curves of three different standards utilising OFDM-based communication system at SNR values of $-12dB$ and $-15dB$ with the parameters as enlisted in caption. It follows the same interpretation for ROC as shown in previous Fig. 6.12, but here it's shown that their relative ROC performance. It's also shown that ROC curves of WLAN at both SNR values outperform other two standards i.e. DVB-T and LTE-A. WLAN ROC curve at SNR of $-12dB$ shows almost excellent trajectory where it's seen that it nears the desirable performance i.e. at lower value of P_{FA} it gives maximum P_D value which is uncommon for rest of the standards.

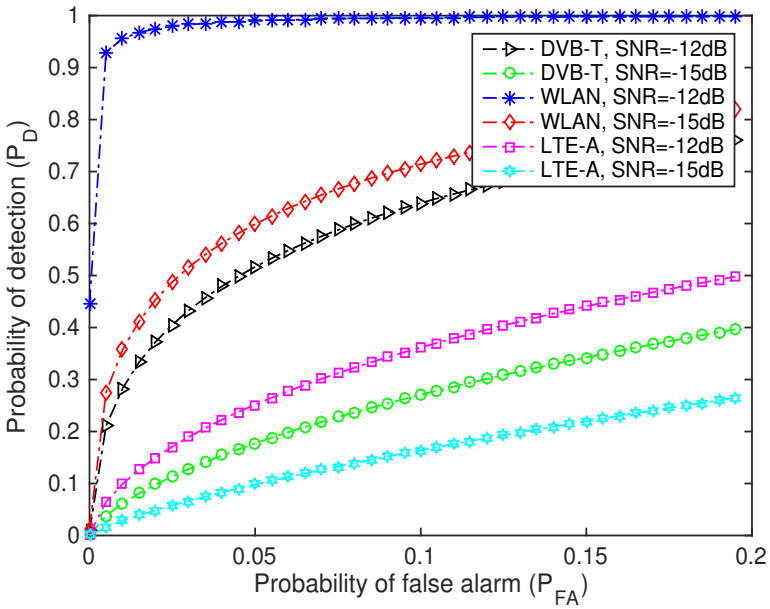


Figure 6.13: Receiver Operating Characteristic (ROC) curves for DVB-T, WLAN and LTE-A standards: $T_d = 8192, T_c = 1024, \mu = 0.111$; $T_d = 52, T_c = 13, \mu = 0.2$ and $T_d = 512, T_c = 36, \mu = 0.067$ respectively

6.9 Effect of Information of CP

If CP is known , then the performance can be improved. The ML estimate for autocorrelation can be rewritten as:

$$\begin{aligned} \hat{\rho}_{ML} &= \frac{\frac{1}{M}\sum_{t=0}^{M-1} \Re\{y(t)y^*(t+T_d)\}}{\hat{\sigma}_z^2} \\ &= \frac{\frac{1}{M}\sum_{n=0}^{N_s-1}\sum_{t=0}^{T_s-1} \Re\{y(nT_s+t)y^*(nT_s+T_d)\}}{\sigma_z^2} \end{aligned} \tag{6.83}$$

Where $N_s = M/T_s$ is number of OFDM blocks over which autocorrelation coefficient is estimated $Ts = Tc + Td$ is number of symbols in OFDM block. Thus in absence of CP information, numerator is obtained by summing the product over a sliding window of length $T_c + T_d$ for OFDM block and again adding these sums

for N_s blocks. Autocorrelation for this case is:

$$\hat{\rho}_c = \frac{\sum_{n=0}^{Ns-1} \sum_{t \in Cp} \Re\{y(nT_s + t)y^*(nT_s + t + T_d)\}}{M_1 \hat{\rho}_z^2} \tag{6.84}$$

$$\begin{aligned} \mathcal{H}_0 : \quad & \hat{\rho}_c \sim \mathcal{N}\left(0, \frac{1}{2M_1}\right) \\ \mathcal{H}_1 : \quad & \hat{\rho}_c \sim \mathcal{N}\left(\rho_c, \frac{(1-\rho_c^2)^2}{2M_1}\right) \end{aligned} \tag{6.85}$$

Where $\rho_c = SNR/(SNR+1)$, DVB-T and DVB-T2 have 4 and 6 different CP lengths respectively.

6.9.1 Detection Performance in Multipaths

Consider multipath channel P. Let us denote channel tap-coefficient by $g(l)\, l = 0, 1, \ldots, P-1$. Channel taps are assumed to be independent of transmitted signal $s(t)$ and noise $w(t)$. Under the hypothesis $\mathcal{H}_1$ received signal in multipath scenario is:

$$\begin{aligned} y(t) &= s(t) * g(t) + w(t) \\ &= \sum_{l=0}^{P-1} g(l)s(t-l) + w(l) \end{aligned} \tag{6.86}$$

Autocorrelation coefficient $\rho = \mathbb{E}\big(y(t)y^*(t+T_d)\big)/\mathbb{E}\big(y(t)y^*(t)\big)$ under two hypothesis is given by:

$$\begin{aligned} \mathcal{H}_0 : \quad & \rho = 0 \\ \mathcal{H}_1 : \quad & \rho = \rho_2 \end{aligned} \tag{6.87}$$

$$\begin{aligned}\rho_2 &= \frac{\mathbb{E}\Big(y(t)y^*(t+T_d)|\mathcal{H}_1\Big)}{\mathbb{E}\Big(y(t)y^*(t)|\mathcal{H}_1\Big)} \\ &= \left(\frac{T_c}{T_c+T_d}\right)\left(\frac{\delta\sigma_s^2}{\delta\sigma_s^2+\sigma_w^2}\right)\end{aligned} \tag{6.88}$$

Where $\delta = \sum_{l=0}^{P-1}\mathbb{E}\big(|g(l)|^2\big)$ and $s(t), g(t)$ and $w(t)$ are CSCG and also $y(t) = s(t)*$ $g(t) + w(t)$ is CSCG random variable. Similar to AWGN case, LLRT statistic for hypothesis testing problem in multipath scenario is gven by $\rho_{\hat{ML}}$. Using theorem 6.8.1, the asymptotic distribution of $\hat{\rho}_{ML}$ under two hypothesis are:

$$\begin{aligned}\mathcal{H}_0: &\quad \hat{\rho}_{ML} \sim \mathcal{N}\left(0, 1/2M\right) \\ \mathcal{H}_1: &\quad \hat{\rho}_{ML} \sim \mathcal{N}\left(\rho_2, \frac{(1-\rho_2)^2}{2M}\right)\end{aligned} \tag{6.89}$$

Using these distribution, the Neyman-Pearson detector is designed and hence P_{FA}, ξ_l and P_D respectively are as follows:

$$P_{FA} = Pr\left(\hat{\rho}_{ML} > \xi_l|\mathcal{H}_0\right) = \frac{1}{2}erfc\big(\sqrt{M}\xi_l\big) \tag{6.90}$$

$$\xi_l = \frac{1}{\sqrt{M}}erfc^{-1}\big(2P_{FA}\big) \tag{6.91}$$

$$P_D = Pr\left(\hat{\rho}_{ML} > \xi_l|\mathcal{H}_1\right) = \frac{1}{2}erfc\left(\sqrt{M}\frac{\xi_l-\rho_2}{1-\rho_2^2}\right) \tag{6.92}$$

6.10 Full-Duplex Communication CR

In this section the case of non-time slotted CRN is discussed where PUs and the SUs are not synchronised like the case in slotted CRN where PUs and SUs are synchronised. In multichannel non-slotted CRN PUs randomly arrive and leave the channel and they can reclaim the licensed sub-channels later on. In non-slotted

CRN PUs may sense busy channel since it can't distinguish between peer PUs traffic or SU traffic and thus goes into backoff stage and retransmit with persistent carrier sense multiple access (p-CSMA) which might result in collision and ultimately affect the PU throughput if the SU doesn't sense the PU reactivation and leave licensed PU sub-channel. In time-slotted CRN PU and SUs are synchronised and as in [51][52] cognitive MAC protocols have been proposed to maximise SU throughput in time-slotted CRN. Legacy half-duplex spectrum sensing (HDC-SS) schemes and half-duplex communication MAC (HDC-MAC) can't solve reactivation failure problem for non-time slotted CRN.

6.10.1 System Model

Figure 6.14 shows non-time-slotted multi-channel cognitive radio network model where PUs use their L licensed sub-channels and M SUs opportunistically contend for the PU licensed sub-channels.

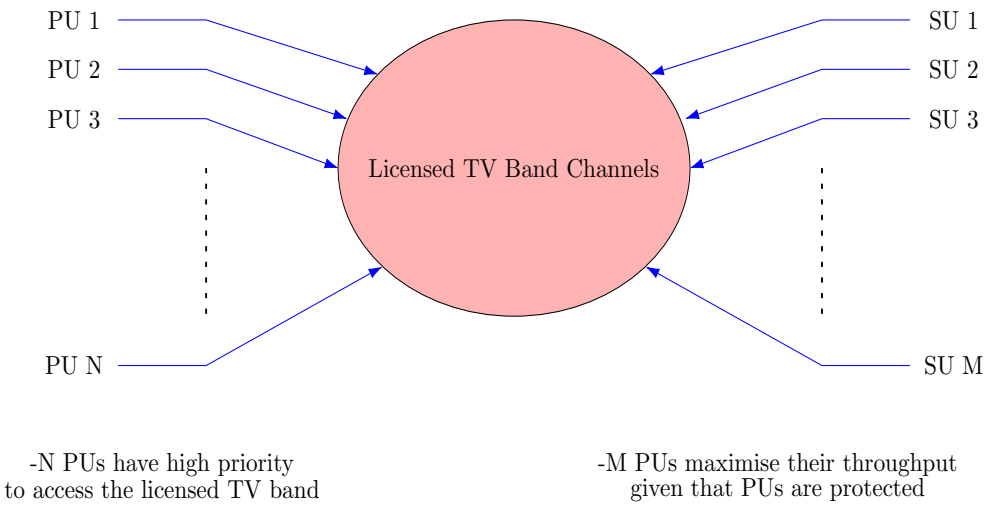


Figure 6.14: Multi-channel cognitive radio network model

Control model of non-time slotted CRN

In non-time-slotted PU traffic and the SU traffic is asynchronous in nature. Figure 6.15 shows the control model of the non-time-slotted and the time-slotted CRN.

On/off times of PU and SU to access and leave the channel for non-time-slotted CRN are different.

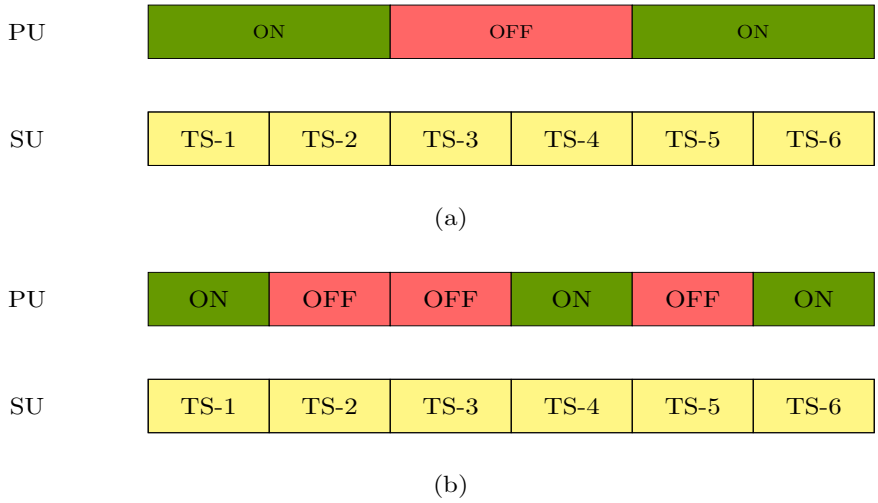
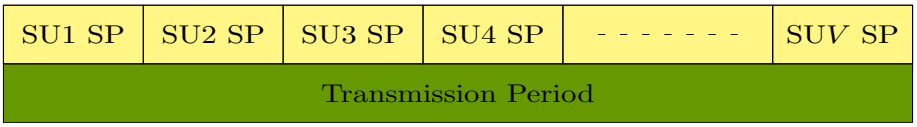


Figure 6.15: Control model of non-slotted multi-channel CRN and time-slotted CRN

Spectrum sensing in NTS-CRN

In NTS-CRN spectrum sensing and transmission is performed at the same time using two different antennas. Figure 6.16 shows that the total transmission time of NTS-CRN is divided into V sub-slots to do parallel sensing during transmission.



SU1 SP: Sensing Period of SU1

Figure 6.16: Spectrum sensing non-time slotted CRN (NTS-CRN)

FDC-SS scheme algorithm

FDC-SS algorithms as shown below is used for non-time slotted CRN:

Algorithm 1 FDC-Spectrum Sensing Scheme

1: Time-slotted SU sensing period (SP) is divided into V sub-periods
2: **if** SU attempts the idle channel **then**
3: SU uses legacy HDC-SS scheme within each sensing period
4: **else**
5: SU is using channel C_1
6: The SU senses the channel C_1 with FDC-SS within each sensing period
7: **end if**

6.11 FDC-SS System Model

The sampled output of CR employing energy-detector can be given as follows:

$$y(n) = \sqrt{k}hs(n) + w(n)\, n = 0, 1, 2, ..., N-1 \tag{6.93}$$

Where h is channel gain between PU and SU and has Rayleigh distribution. $s(n)$ is sampled PU signal, $w(n)$ is sampled AWGN with zero mean and variance σ^2 i.e. $\mathcal{N} \sim (0, \sigma^2)$ and k is self-interference introduced because of the simultaneous sensing and transmission that takes place in FDC-CR. When $k = 0$ means there maximum self-interference introduced and no self-interference for $k = 1$. The test statistics using FDC-SS at the output of the energy detector can be given by:

$$T_N(y) = \begin{cases} \frac{1}{N}\left(\sum_{n=0}^{u} \mid \sqrt{k}hs(n) + w(n) \mid^2 + \sum_{n=u+1}^{N} \mid w(n) \mid^2 \right), & \text{if}\, \mathcal{H}_{10} \\ \\ \frac{1}{N}\left(\sum_{n=0}^{v} \mid w(n) \mid^2 + \sum_{n=v+1}^{N} \mid \sqrt{k}hs(n) + w(n) \mid^2 \right), & \text{if}\, \mathcal{H}_{01} \end{cases} \tag{6.94}$$

Where hypothesis $\mathcal{H}_{10}$ means PU is active for first u samples and then becomes inactive for rest of the samples $n = u+1$ to N. and hypothesis $\mathcal{H}_{01}$ means the PU was inactive for the first v samples and then became active for rest of the samples

$n = v + 1$ to N. N is total number of samples for entire sensing period. Here PU signal $s(n)$ and noise $w(n)$ are considered as CSCG which represents signals with rich-ISI such as OFDM. For large number of samples N using CLT under hypothesis $\mathcal{H}_{10}$ and the PDF of the test statistics $T_N y$, $p_{10}(x)$ can be approximated by Gaussian distribution. Thus the P_D and P_{FA} of a PU for non-time slotted CRN respectively can be given mathematically as follows:

$$\begin{aligned} P_{FA}(\xi, N, u, k) &= Pr.\Big(T_N(y) > \xi \mid \mathcal{H}_{10}\Big) = \int_{\xi}^{\infty} p_{10}(x)dx \\ &= Q\left(\frac{\frac{\xi}{\sigma_u^2} - \frac{u}{N}k\gamma_{ps} - 1}{\sqrt{\frac{u}{N^2}\big(k\gamma_{ps}+1\big)^2 + \frac{N-u}{N^2}}}\right) \end{aligned} \tag{6.95}$$

$$\begin{aligned} P_D(\xi, N, v, k) &= Pr.\Big(T_N(y) > \xi \mid \mathcal{H}_{01}\Big) = \int_{\xi}^{\infty} p_{01}(x)dx \\ &= Q\left(\frac{\frac{\xi}{\sigma_u^2} - \frac{N-v}{N}k\gamma_{ps} - 1}{\sqrt{\frac{N-v}{N^2}\big(k\gamma_{ps}+1\big)^2 + \frac{v}{N^2}}}\right) \end{aligned} \tag{6.96}$$

Where ξ is the threshold of the energy detector employed in the receiver. Now by setting $u = 0, v = 0$ and $k = 1$ in above equations and the expressions for $P_{FA}(\xi, N, u, k)$ and $P_D(\xi, N, v, k)$ can be given as follows:

$$P_{FA}(\xi, N, u, k) = Q\left(\Big(\frac{\xi}{\sigma_u^2} - 1\Big)\sqrt{N}\right) \tag{6.97}$$

$$P_D(\xi, N, v, k) = \left(\Big(\frac{\xi}{\sigma_u^2} - \gamma_{ps} - 1\Big)\frac{\sqrt{N}}{\gamma_{ps}+1}\right) \tag{6.98}$$

From above two equations it can be seen that the P_{FA} and P_D for slotted CRN are special case of non-time slotted CRN. Figure 6.17 shows the probability of detection and energy-detection threshold for FDC-SS without self-interference i.e. $k = 1$. It can be seen that the probability of detection decreases as the threshold increases. It also decreases with the increase in number of samples for which PU is initially absent i.e from $v = 500$ to $v = 1500$. Figure 6.18 shows the probability

of missed detection versus threshold for FDC-SS with no self-interference. It can be seen that the probability of missed detection increases with the increase in threshold ϵ. It also increases with the increase in number of samples assigned to PU for which initially remains inactive.

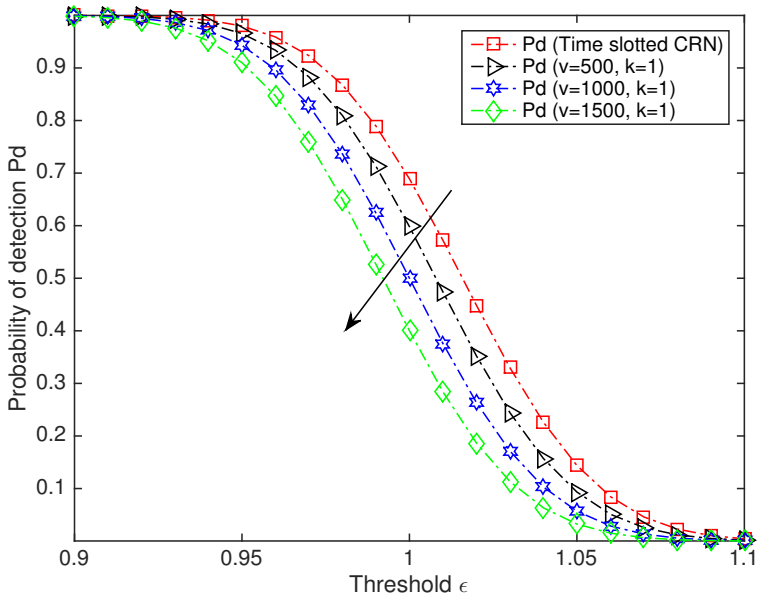


Figure 6.17: Probability of detection of time slotted and non-time slotted full-duplex cognitive radio without self-interference

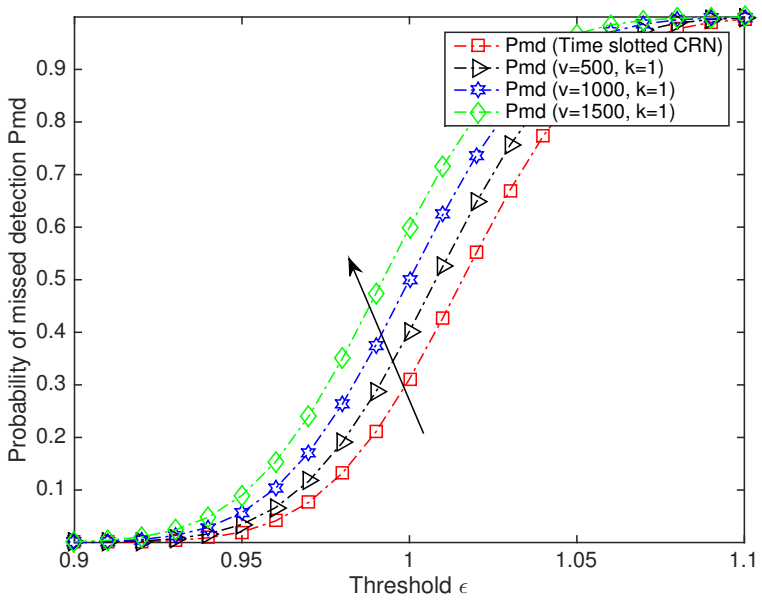


Figure 6.18: Probability of missed detection of time slotted and non-time slotted full-duplex cognitive radio without self-interference

Figure 6.19 shows the probability of detection of slotted and non-slotted CRN with HDC-SS and FDC-SS spectrum sensing scheme. Here the effect of self-interference is considered and the probability of detection with self-interference and without self-interference for FDC-SS is compared. It's shown that the P_D for time-slotted CRN outperforms all the cases of non-time slotted CRN. Moreover, the P_D decreases as the energy-detector threshold increases, it also decreases for the non-time slotted CRN with the self-interference and without self-interference. However, the P_D without self-interference is higher than the P_D with self-interference, but the performance gap is very small. Similarly, Fig. 6.20 shows the probability of missed detection which increases with the increase in energy-detection threshold. It also increases with the increase in number of initial sample values for which PU remains inactive. The probability of missed detection also increases with the increase in self-interference factor k. There is small performance gap between probability of missed detection with self-interference and without self-interference, but there is significant difference in probability of missed detection for slotted CRN and the probability of missed detection when the number of initial samples

for which PU is inactive increase to $v = 1500$. For example at energy-detection threshold of $\xi = 1$ the probability of missed detection is 0.2 which increases to P_{MD} value of 0.55 for PU which remains inactive for initial sample values of $v = 1500$. Summary of different values of P_D, P_{MD} and P_{FA} in the following table. Note that P_{FA} is calculated when he PU is active initially for u samples and then leave the channel for rest of the sample values.

Table 6.2: P_D, P_{MD} and P_{FA} values for non-time slotted CRN with self-interference and without self-interference

Threshold (ξ)	# of samples (v)	Self-interference (k)	P_D	P_{MD}	u	P_{FA}
1	500	1	0.68	0.32	500	0.70
1	500	0.9	0.65	0.35	500	0.68
1	1500	1	0.28	0.72	1500	0.92
1	1500	0.9	0.25	0.75	1500	0.90

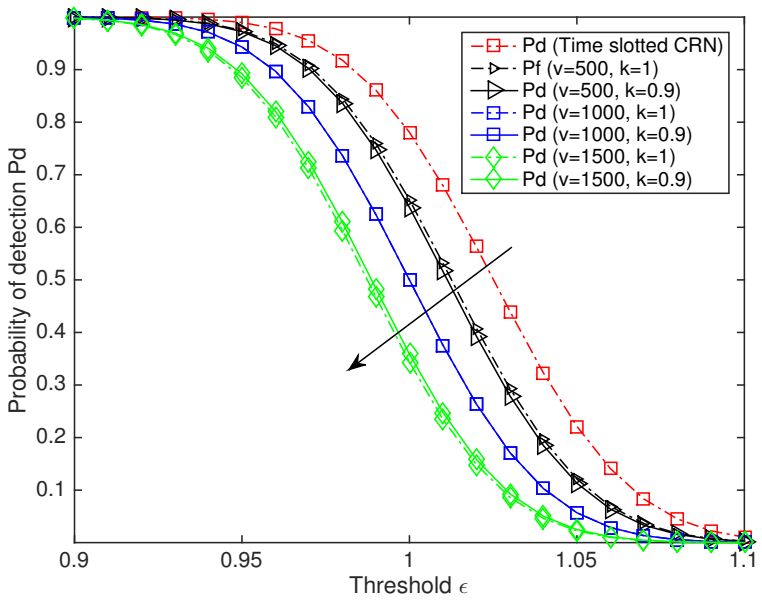


Figure 6.19: Probability of detection of time slotted and non-time slotted full-duplex cognitive radio with and without interference

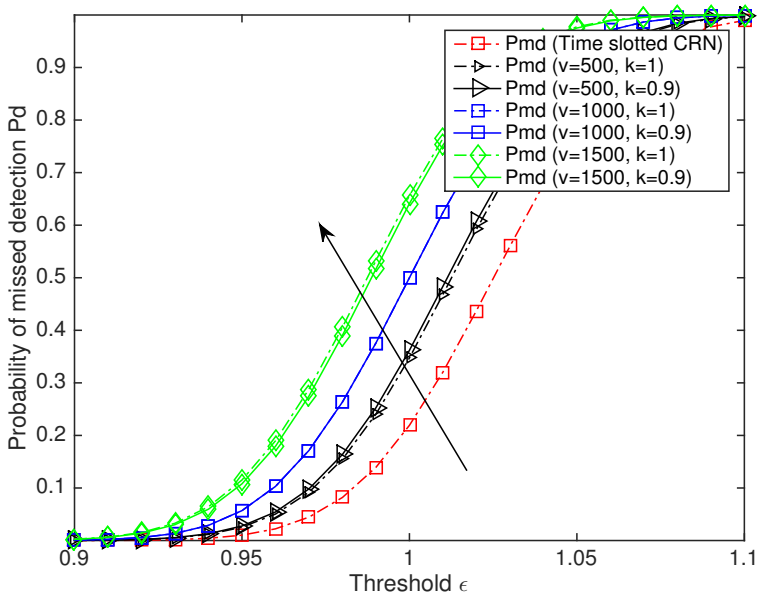


Figure 6.20: Probability of missed detection of time slotted and non-time slotted full-duplex cognitive radio with and without interference

Figure 6.21 and Fig. 6.22 show probability of false alarm versus threshold which follows our intuition developed after our earlier discussions on P_D and P_{MD} with and without self-interference for slotted and non time-slotted CRN. It's shown that the probability of false alarm of time-slotted CRN is less than the probability of false alarm for time-slotted CRN when the PU is initially active for $u = 500$ to $u = 1500$ samples and later leaves the channel empty. This is also true for the P_{FA} values with self-interference and without self-interference. For fixed sample values let us say $u = 500$ the P_{FA} with interference is little higher than the P_{FA} without self-interference i.e. $k = 0.9$, however the performance gap is very minutes and negligible. More degradation in P_{FA} is expected when the self-interference factor is increased from $k = 0.9$ to $k = 0.1$ where sever interference can be expected.

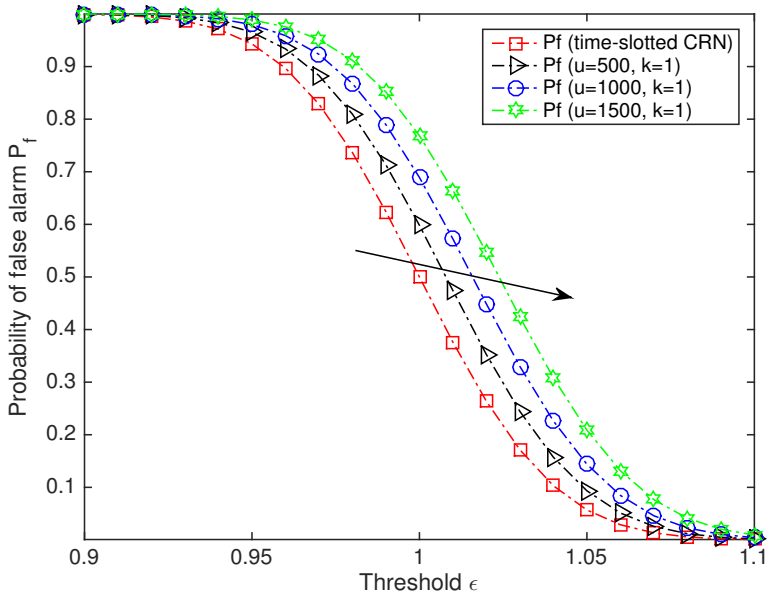


Figure 6.21: Probability of false alarm of time slotted and non-time slotted full-duplex cognitive radio without self-interference

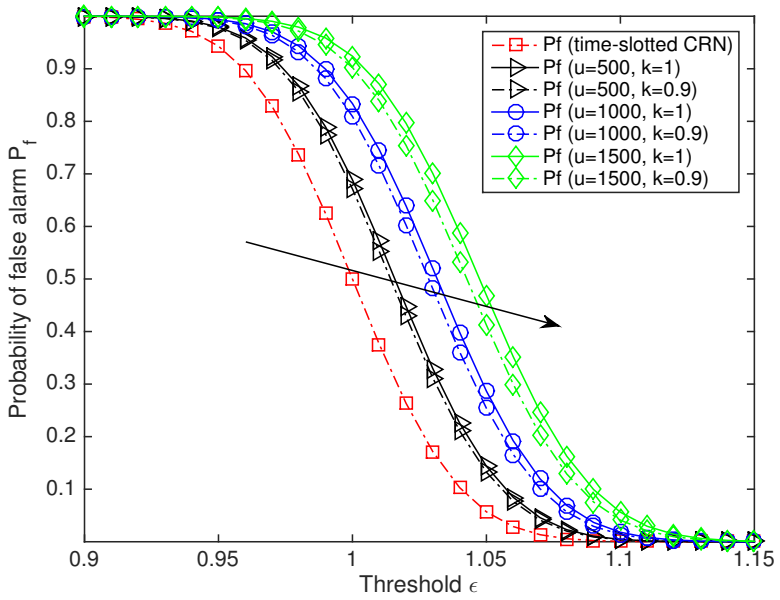


Figure 6.22: Probability of false alarm of time slotted and non-time slotted full-duplex cognitive radio with and without interference

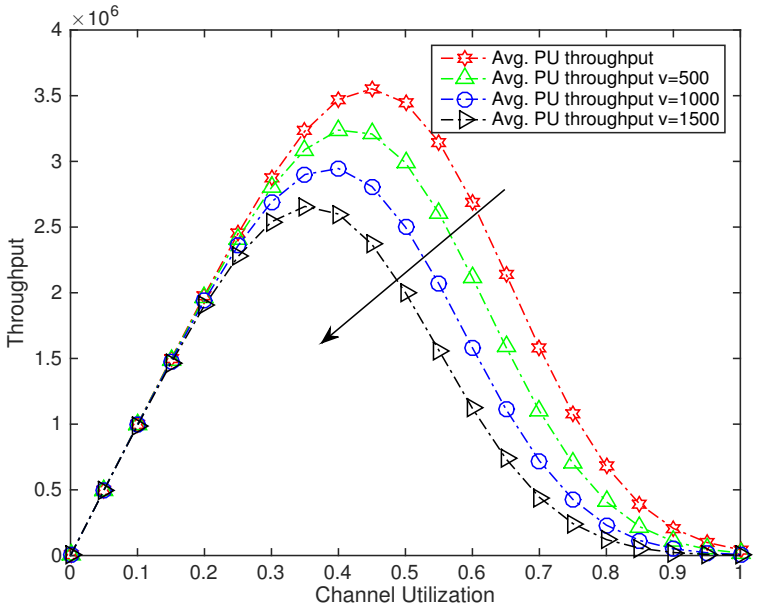


Figure 6.23: Average throughput of saturated full-duplex cognitive radio

Figure 6.23 shows the PU throughput as a function of channel utilisation for time slotted and non-time slotted FDC-CR. It can be seen that the throughput of time-slotted CR is higher than the throughput of non-time slotted CR. Moreover, the throughput of the PU decreases when the number of samples for which SU remains inactive increases.

6.12 Summary

OFDM is ubiquitous in many of the today's and legacy digital wireless communication systems. Therefore, OFDM has been taken into consideration for the throughout analysis of the cognitive radio enable SU. OFDM uses orthogonal subcarrier which are summed together before transmission over the channel this process gives rise to increased peak-to-average power ratio which degrades the performance of the receiver because it derives the RF amplifier of the receiver into saturation which results in signal clipping. Therefore, PAPR of MQAM and MPSK modulated NC-OFDM system is addressed by deriving the expressions for upper and lower bounds on PAPR. Additionally, sensing-throughput tradeoff is

studied for OFDM-based cognitive radio in fading fading environment in line with sensing-throughput discussions in previous chapters. After this autocorrelation based sensing of CP-OFDM signal is discussed and receiver operating characteristic curves are used to assess the performance of various standards for example DVB-T, WLAN and LTE-A. It's observed that for a given SNR value WLAN outperforms other two standards. Following this problem of reactivation failure in FDC-SS cognitive radio using HDC-SS is introduced. FDC-SS uses two antennas to perform simultaneous sensing and data transmission which results in self-interference between two colocated antennas. The performance of FDC-CR with FDC-SS is assessed with the help of probability of false alarm and probability of detection after discussing the system model and including the test-statistic expression. It's shown that with minimal self-interference the throughput of the FDC-CR with HDC-SS is higher than the throughput for HDC-CR using HDC-SS because the former gets increased data transmission time whereas the data transmission time is reduced for later because it performs spectrum sensing and data transmission with same antennas at different times.

Chapter 7

Conclusion and Future Work

7.1 Conclusion

Cognitive Radio is used to increase the under-utilised band efficiently in time-frequency and space. Underutilised bands are known as white space bands which can arise in every well-known band because of the changing user patterns. Digital dividend has given rise to generation of white space specially in VHF/UHF band which are known as TV white spaces. This part of the band gives favourable propagation and reasonably high capacity for deployment of the prospective cognitive radio network by ensuring maximum protection to incumbent users. Considering the maximum throughput requirement of SU and maximum protection of PU various aspects and strategies that are optimal for the roll-over of secondary CRN are used. For example one of the challenge is to find out optimal sensing time for maximising the throughput, and increasing the detection probability for given sensing time. Since the PU or SU signals are largely OFDM based with certain baseband and passband modulation, therefore the OFDM based system is used and the work on sensing-throughout is extended for OFDM modulated signals. Energy-detection scheme has been considered at the receiver because of its well-established literature and its cost-effectiveness and its inherent property of detecting signals without having complete knowledge of the PU signals. Detection of the signals is also considered using autocorrelation based sensing of CP-OFDM signals for WLAN and different TV standards for DVB-T, DAB-T etc using half-duplex

spectrum sensing scheme. Finally, this work has been concluded with full-duplex communication CR which senses and transmits at the same time, thereby increasing the transmission period for SU and increasing the detection of PU signals but subject to tolerable self-interference.

7.2 Full-duplex Green Cognitive Radio

Full-Duplex CR is the one which uses two collocated antennas for transmission and reception purpose on same frequency and same time. Therefore, such colocation of antennas create self-interference. It's well-known fact that the self-interference can be perfectly removed but can cancel it to some extent. An efficient Full-duplex green cognitive radio can be studied to cater the high demand for green wireless communication systems.

7.3 Multi-parameter Cognitive Radio

System capacity can be increased by deploying relays, femtocells, and massive MIMO and bandwidth-efficiency and energy-efficiency can be increased via green cognitive radio. Concept of full cognitive radio was proposed by Mitola[53], however it still remains at conceptual level. It's therefore necessary to incorporate various parameters that depict network status. For example transmit power-level, modulation type, constellation size, bandwidth efficiency, channel coding, code rate, network topology, and communication protocol strategies. Multi-parameter cognitive radio can gal into two categories cognitive radio with known statistics or cognitive radio with unknown statistics before cognition. CR with know statistics (noise statistics and interference level) before cognition solves multi-parameter problem with signal processing only. Till this day various machine learning algorithms have been proposed for parameter cognition in CR. For example in [54] support vector machine (SVM) based spectrum sensing engine was designed. Similarly, in [55] reinforced learning was used to reduce sensing overhead by releasing network congestion. Parameter prediction can also be done by learning traffic characteristics of PU by using neural network[56]. In [57][58][59] problem of mod-

ulation recognition and classification has been addressed using ML-based methods, statistical pattern-recognition based methods and over fading channels.

7.4 Cognitive Pilot-Channel LTE-CR

Cognitive radio has drawn a lot of attention for deployment in cellular network for example in LTE. One application of CR is dynamic spectrum access in multi-radio-access-technology (Multi-RAT) heterogenous networks as given in IEEE 1900.4 [60] and is included in ETSI's end-to-end efficiency (E3) project. LTE has been considered for use in unlicensed 5GHz and TVWS known as LTE-CR [61][62][63]. Cognitive Pilot-Channel (CPC) based network access is promising scheme for LTE-CR. LTE-CR should work on harnessed spectrum and the licensed band. Various network access schemes have been proposed in IEEE 802.22 and IEEE 1900.4 system and are classified sensing-based (without pilot) and pilot-based schemes. Sensing-based schemes are more spectral efficient than pilot-based schemes. In pilot-based sensing CR listens to pilot channel to gain network information. Pilot channel based scheme is fast and energy-efficient compared to sensing-based network access scheme. TVWS IEEE 802.22 standard works between 54MHZ and 862MHz using sensing-based scheme. However, IEEE 1900.4 system uses DSA for multi-RAT and scans a large band from 450MHz to 3GHz. Thus time and energy-consuming sensing-based network access is not preferred instead pilot-based network access should be used. In LTE-CR cognitive spectrum includes TVWS, ISM band, UNII band and spectrum used by GSM, WCDMA, and LTE[64][65][66][67].

Appendix A

A

A.1 Proof of $\rho_2 = \left(\left(\frac{T_c}{T_c+T_d}\right)\left(\frac{\delta\sigma_s^2}{\delta\sigma_s^2+\sigma_w^2}\right)\right)$

The received signal in multipath fading under the alternative or noise plus signal hypothesis can be given by:

$$\begin{aligned} x(t) &= s(t) * h(t) + w(t) \\ &= \sum_{l=0}^{P-1} h(l)s(t-l) + w(t) \\ &= y(t) + w(t) \end{aligned} \tag{A.1}$$

Where $y(t) = \sum_{l=0}^{P-1} h(l)s(t-l)$ and for independent signal $s(t)$ and channel taps $h(l)$:

$$\begin{aligned} \mathbb{E}[y(t)] &= \mathbb{E}\left[\sum_{l=0}^{P-1} h(l)s(t-l)\right] \\ &= \sum_{l=0}^{P-1} \mathbb{E}[h(l)]\mathbb{E}[s(t-l)] = 0 \end{aligned} \tag{A.2}$$

Now, by extending the same concept of signal $s(t)$ and channel taps independence $h(l)$ for $\mathbb{E}[s(t)s^*(t+T_d)] = (T_c/(T_c+T_d))$, it can be written:

$$\begin{aligned}
\mathbb{E}[y(t)y^*(t+T_d)] &= \mathbb{E}\left[\left(\sum_{l=0}^{P-1} h(l)s(t-l)\right)\left(\sum_{i=0}^{P-1} h^*(i)s^*(t+T_d-i)\right)\right] \\
&= \sum_{l=0}^{P-1}\sum_{i=0}^{P-1} \mathbb{E}[h(l)s(t-l)h^*(i)s^*(t+T_d-i)] \\
&= \sum_{l=0}^{P-1} \mathbb{E}[h(l)h^*(l)]\mathbb{E}[s(t-l)s^*(t+T_d-l)] \\
&= \delta\sigma_s^2\Big(\frac{T_c}{T_c+T_d}\Big)
\end{aligned} \tag{A.3}$$

Where $\delta = \sum_{l=0}^{P-1} \mathbb{E}[|h(l)|^2]$ and again using the independence of signal $s(t)$ and channel taps $h(l)$ for $\mathbb{E}[s(t)s^*(t)]$:

$$\begin{aligned}
\mathbb{E}[y(t)y^*(t)] &= \mathbb{E}\left[\left(\sum_{l=0}^{P-1} h(l)s(t-l)\right) \times \left(\sum_{l=0}^{P-1} h^*(i)s^*(t-i)\right)\right] \\
&= \sum_{l=0}^{P-1}\sum_{i=0}^{P-1} \mathbb{E}[h(l)s(t-l)h^*(i)s^*(t-i)] \\
&= \sum_{l=0}^{P-1} \mathbb{E}[h(l)h^*(l)]\mathbb{E}[s(t-l)s^*(t-l)] \\
&= \delta\sigma_s^2
\end{aligned} \tag{A.4}$$

For uncorrelated noise samples $w(t_1)$ and $w(t_1)$ for $t_1 \neq t_2$ and independent $y(t)$ and $w(t)$ it can expressed mathematically as:

$$\begin{aligned}
\mathbb{E}[x(t)x^*(t+T_d)|\mathcal{H}_1] &= \mathbb{E}[(y(t)+w(t))(y^(t+T_d)+w^*(t+T_d))] \\
&= \mathbb{E}[y(t)y^*(t+T_d)] \\
&= \delta\sigma_s^2\left(\frac{T_c}{T_c+T_d}\right)
\end{aligned} \tag{A.5}$$

Similarly, it can be written for $\mathbb{E}[x(t)x^*(t)$:

$$\begin{aligned}\mathbb{E}[x(t)x^*(t)|\mathcal{H}_1] &= \mathbb{E}[(y(t)+w(t))(y^*(t)+w^*(t))] \\ &= \mathbb{E}[y(t)y^*(t)] + \mathbb{E}[w(t)w^*(t)] \\ &= \delta\sigma_s^2 + \sigma_w^2\end{aligned} \tag{A.6}$$

Substituting A.5 and A.6 in autocorrelation coefficient in multipath scenario ρ_2 it can be written as:

$$\begin{aligned}\rho_2 &= \frac{\mathbb{E}x(t)x^*(t+T_d)|\mathcal{H}_1}{\mathbb{E}[x(t)x^*(t)]|\mathcal{H}_1} \\ &= \left(\frac{T_c}{T_c+T_d}\right)\left(\frac{delta\sigma_s^2}{\delta\sigma_s^2+\sigma_w^2}\right)\end{aligned} \tag{A.7}$$

Appendix B

B

B.1 PicoSDR Configuration Steps

Figures B.1 and B.2 represent the Nutaq's perseus blocks with FPGA token and perseus only examples respectively as loaded in Simulink library.

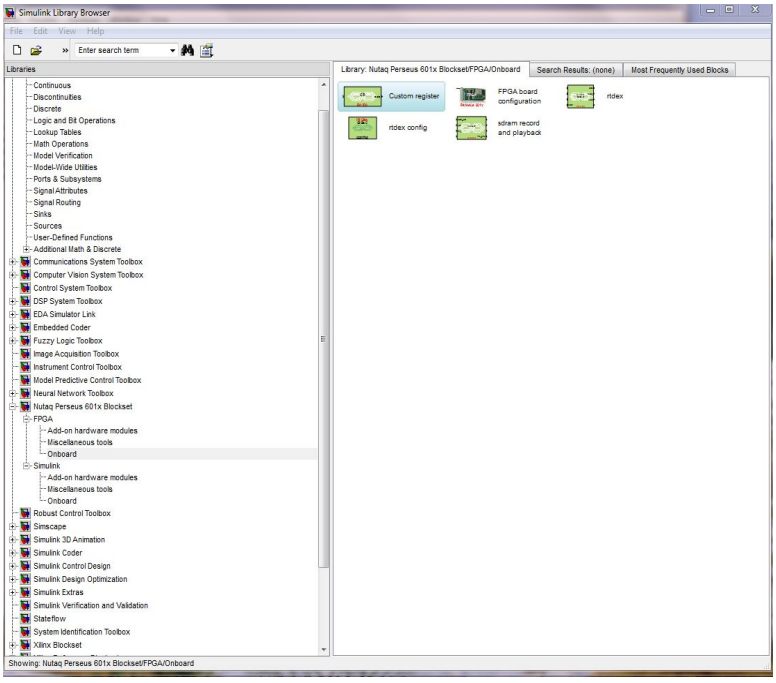


Figure B.1: Nutaq's Perseus 601x Blockset and FPGA board configuration

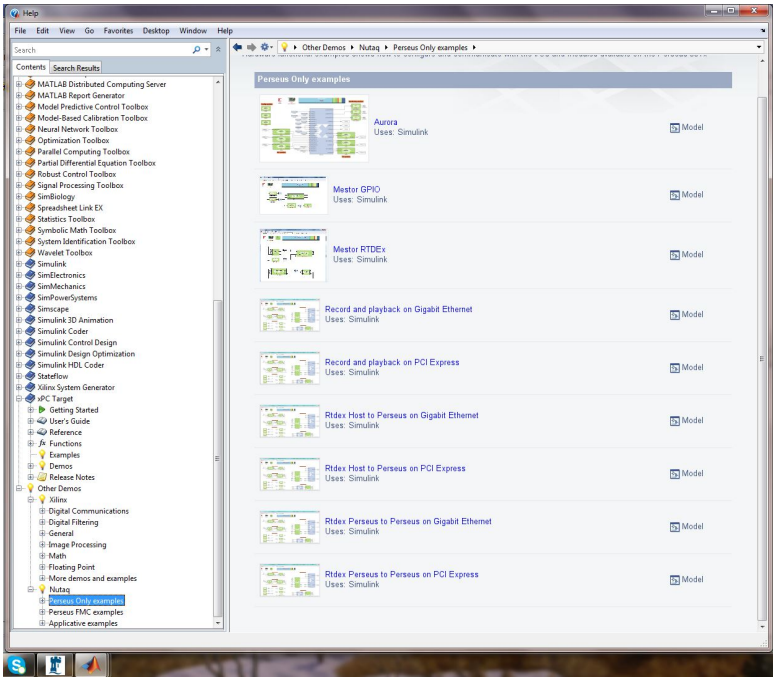


Figure B.2: A set of perseus only examples as loaded on MATLAB 2011b

Following figures show the sequence of very important steps where each subsequent figure differs by one step leading to the final set up of configuring the PicoSDR device for high definition video transmission between host and the PicoSDR Figure B.3 shows the complete OFDM communications system with QAM-64 modulation and Fig. B.4 shows configuration of the putty communication software. Figure B.5 shows the advance design platform (ADP) command line interface used to connect with perseus board with static IP address 192.168.0.101. Figure B.6 shows the complete path for launching OFDM model and Fig. B.7 shows the complete screen capture of the setup showing two putty configurations, ADP CLI and another CLI which shows the progress of video transmission.

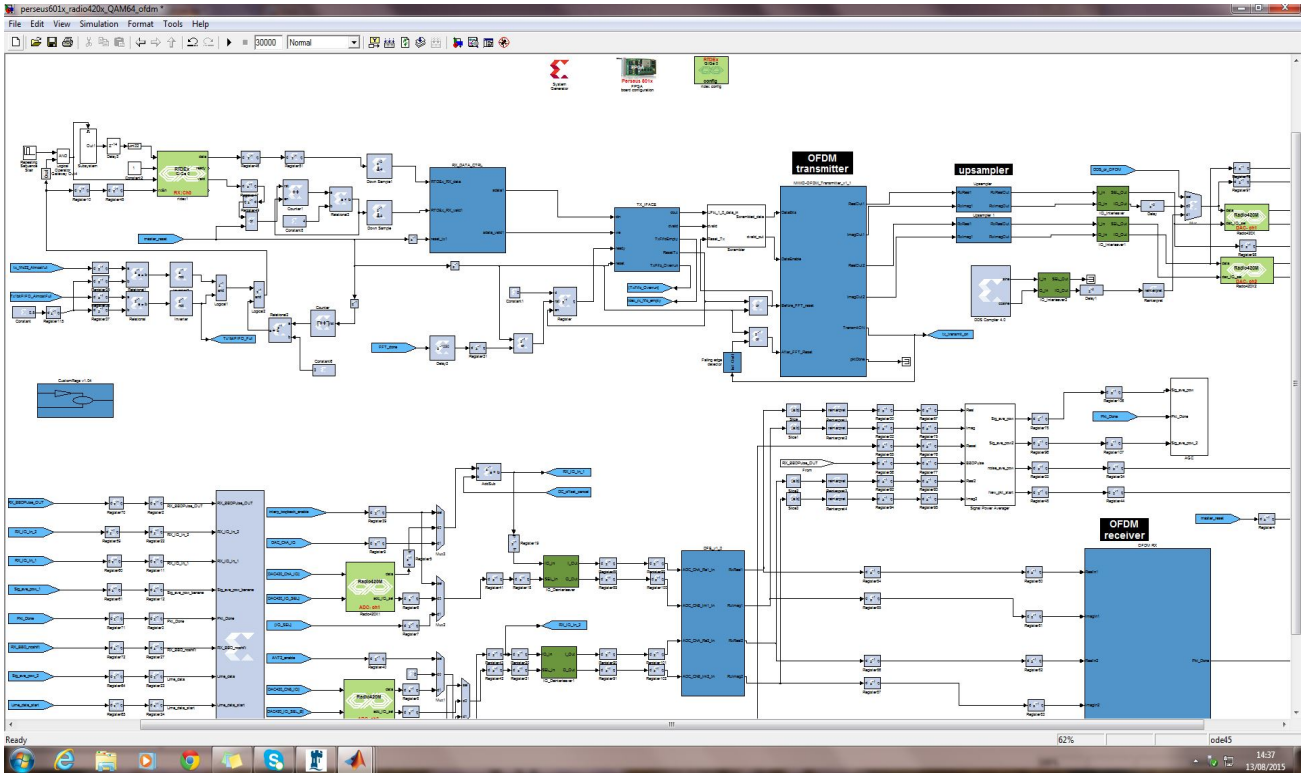


Figure B.3: Complete QAM-64 OFDM Transceiver in Simulink

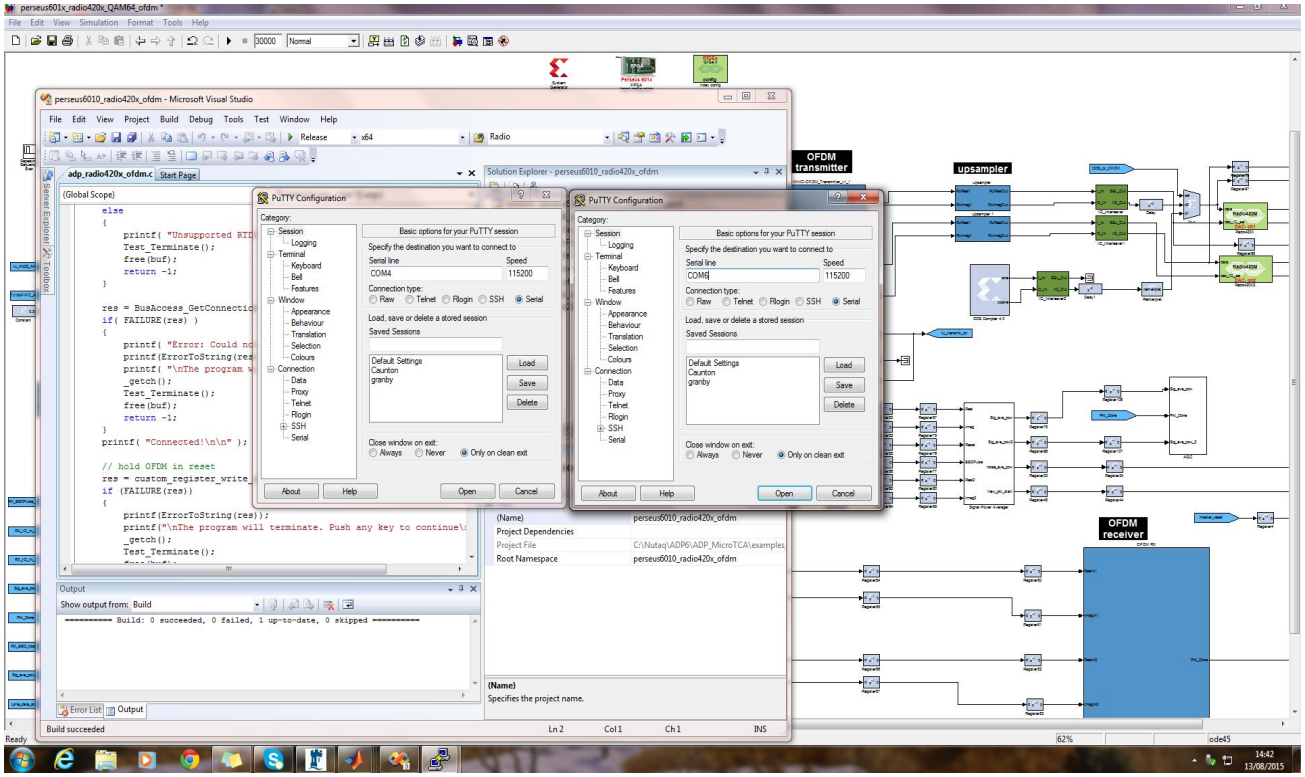


Figure B.4: Configuration of Putty communication software

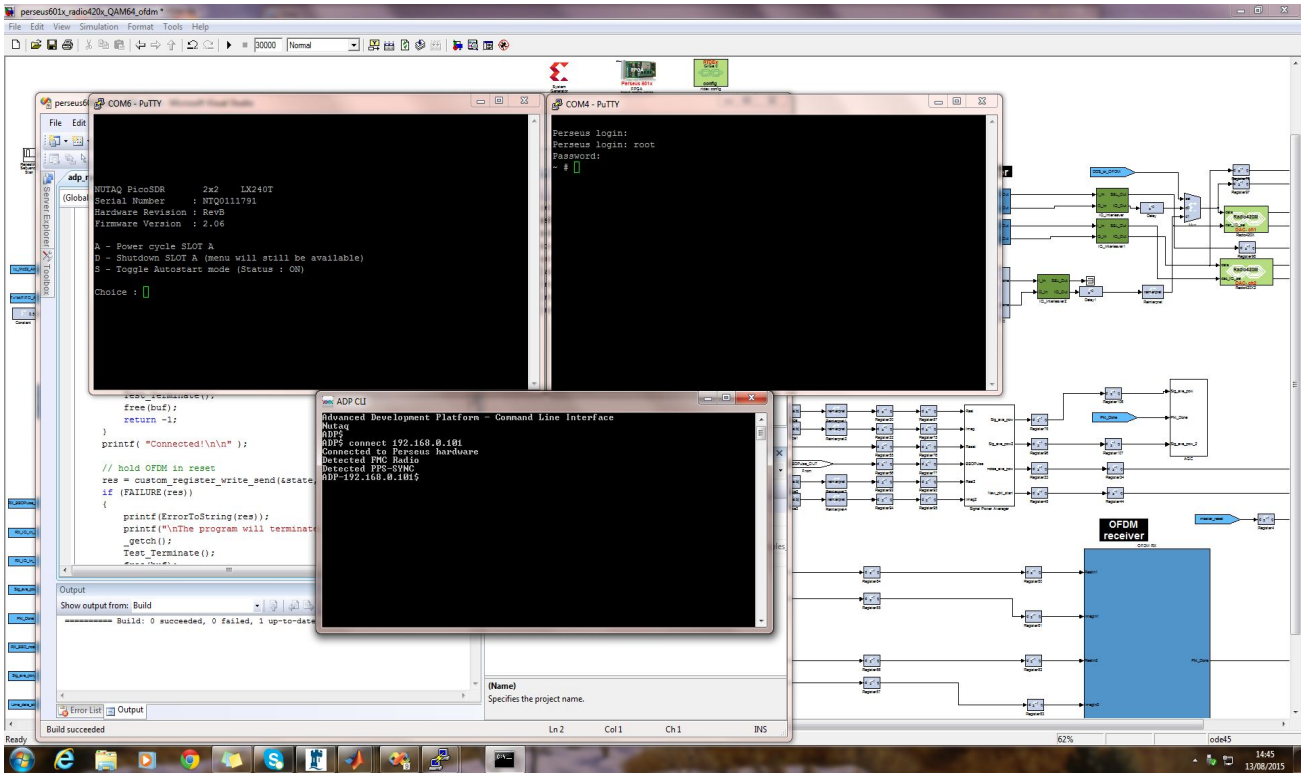


Figure B.5: Initiating ADP CLI and connecting with perseus board

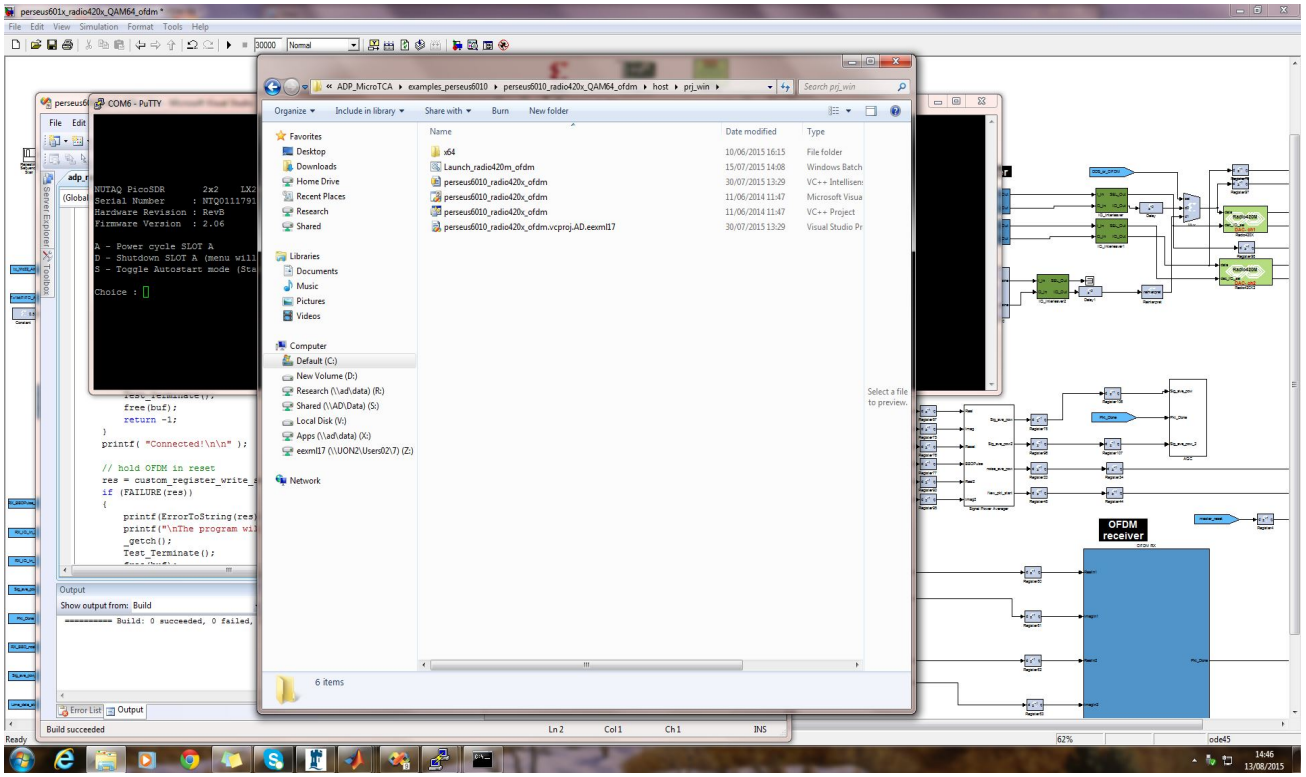


Figure B.6: Complete path for launching radio420m-ofdm OFDM model

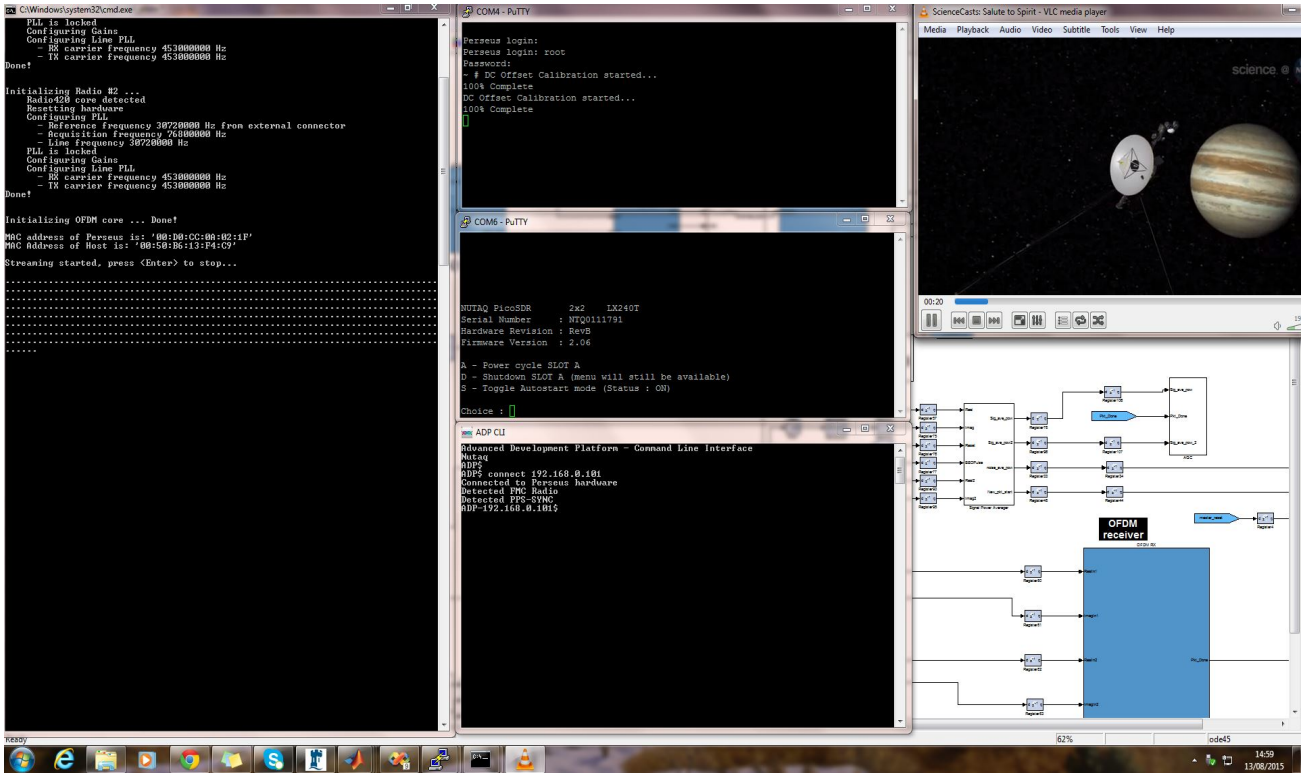


Figure B.7: Complete system screen capture showing video transmission from host PC to Nutaq's PicoSDR

Bibliography

[1] Adriana B Flores, Ryan E Guerra, Edward W Knightly, Peter Ecclesine, and Shishir Pandey. Ieee 802.11 af: a standard for tv white space spectrum sharing. *Communications Magazine, IEEE*, 51(10):92–100, 2013.

[2] Amir Ghasemi and Elvino S Sousa. Spectrum sensing in cognitive radio networks: requirements, challenges and design trade-offs. *Communications Magazine, IEEE*, 46(4):32–39, 2008.

[3] Joe Mitola. The software radio architecture. *Communications Magazine, IEEE*, 33(5):26–38, 1995.

[4] Joseph Mitola and Gerald Q Maguire Jr. Cognitive radio: making software radios more personal. *Personal Communications, IEEE*, 6(4):13–18, 1999.

[5] Simon Haykin. Cognitive radio: brain-empowered wireless communications. *Selected Areas in Communications, IEEE Journal on*, 23(2):201–220, 2005.

[6] Theodore S Rappaport et al. *Wireless communications: principles and practice*, volume 2. prentice hall PTR New Jersey, 1996.

[7] Rahul Tandra, Shridhar Mubaraq Mishra, and Anant Sahai. What is a spectrum hole and what does it take to recognize one? *Proceedings of the IEEE*, 97(5):824–848, 2009.

[8] Steven M Kay. Fundamentals of statistical signal processing, vol. ii: Detection theory. *Signal Processing. Upper Saddle River, NJ: Prentice Hall*, 1998.

[9] Rahul Tandra and Anant Sahai. Snr walls for signal detection. *Selected Topics in Signal Processing, IEEE Journal of*, 2(1):4–17, 2008.

[10] Anant Sahai, Niels Hoven, and Rahul Tandra. Some fundamental limits on cognitive radio. In *Allerton Conference on Communication, Control, and Computing*, pages 1662–1671. Monticello, Illinois, 2004.

[11] T Clancy and W Arbaugh. Measuring interference temperature. In *Virginia tech symposium on wireless personal communications*, pages 1–10, 2006.

[12] Ekram Hossain, Dusit Niyato, and Zhu Han. *Dynamic spectrum access and management in cognitive radio networks*. Cambridge University Press, 2009.

[13] Ojonav Hazarika. White rhino: A low-cost communications radar hardware platform. Thesis, 2013.

[14] Yutaka Ihara, Haris Kremo, Onur Altintas, Hiroya Tanaka, Masaaki Ohtake, Teruya Fujii, Chikara Yoshimura, Keisuke Ando, Kazuya Tsukamoto, Masato Tsuru, et al. Distributed autonomous multi-hop vehicle-to-vehicle communications over tv white space. In *Consumer Communications and Networking Conference (CCNC), 2013 IEEE*, pages 336–344. IEEE, 2013.

[15] Chin-Liang Wang, Han-Wei Chen, and Zong-Ying Tsai. Throughput maximization for cognitive radio networks with wideband spectrum sensing. In *Wireless Communications and Networking Conference (WCNC), 2012 IEEE*, pages 1293–1298. IEEE, 2012.

[16] Chin-Sean Sum, Ming-tuo Zhou, Liru Lu, Fumihide Kojima, and Hiroshi Harada. Performance and coexistence analysis of multiple ieee 802 wpan/wlan/wran systems operating in tv white space. In *Dynamic Spectrum Access Networks (DYSPAN), 2014 IEEE International Symposium on*, pages 145–148. IEEE, 2014.

[17] Ying-Chang Liang, Yonghong Zeng, Edward CY Peh, and Anh Tuan Hoang. Sensing-throughput tradeoff for cognitive radio networks. *Wireless Communications, IEEE Transactions on*, 7(4):1326–1337, 2008.

[18] Z Chair and Pramod K Varshney. Optimal data fusion in multiple sensor detection systems. *Aerospace and Electronic Systems, IEEE Transactions on*, (1):98–101, 1986.

[19] Harry Urkowitz. Energy detection of unknown deterministic signals. *Proceedings of the IEEE*, 55(4):523–531, 1967.

[20] Amir Ghasemi and Elvino S Sousa. Interference aggregation in spectrum-sensing cognitive wireless networks. *Selected Topics in Signal Processing, IEEE Journal of*, 2(1):41–56, 2008.

[21] Rakesh Rajbanshi et al. Ofdm-based cognitive radio for dsa networks, 2007.

[22] Timo Weiss, Joerg Hillenbrand, Albert Krohn, and Friedrich K Jondral. Mutual interference in ofdm-based spectrum pooling systems. In *Vehicular Technology Conference, 2004. VTC 2004-Spring. 2004 IEEE 59th*, volume 4, pages 1873–1877. IEEE, 2004.

[23] Samir Kapoor and Slobodan Nedic. Interference suppression in dmt receivers using windowing. In *Communications, 2000. ICC 2000. 2000 IEEE International Conference on*, volume 2, pages 778–782. Ieee, 2000.

[24] Ivan Cosovic, Sinja Brandes, and Michael Schnell. A technique for sidelobe suppression in ofdm systems. In *Global Telecommunications Conference, 2005. GLOBECOM'05. IEEE*, volume 1, pages 5–pp. IEEE.

[25] Sinja Brandes, Ivan Cosovic, and Michael Schnell. Sidelobe suppression in ofdm systems by insertion of cancellation carriers. In *Vehicular Technology Conference, 2005. VTC-2005-Fall. 2005 IEEE 62nd*, volume 1, pages 152–156. IEEE, 2005.

[26] Xiaodong Li and Leonard J Cimini Jr. Effects of clipping and filtering on the performance of ofdm. In *Vehicular Technology Conference, 1997, IEEE 47th*, volume 3, pages 1634–1638. IEEE, 1997.

[27] Jean Armstrong. Peak-to-average power reduction for ofdm by repeated clipping and frequency domain filtering. *Electronics letters*, 38(5):246–247, 2002.

[28] Hangjun Chen and Alexander M Haimovich. Iterative estimation and cancellation of clipping noise for ofdm signals. *Communications Letters, IEEE*, 7 (7):305–307, 2003.

[29] TA Wilkinson and AE Jones. Minimisation of the peak to mean envelope power ratio of multicarrier transmission schemes by block coding. In *Vehicular Technology Conference, 1995 IEEE 45th*, volume 2, pages 825–829. IEEE, 1995.

[30] Richard DJ Van Nee. Ofdm codes for peak-to-average power reduction and error correction. In *Global Telecommunications Conference, 1996. GLOBECOM'96.'Communications: The Key to Global Prosperity*, volume 1, pages 740–744. IEEE, 1996.

[31] Hyo-Joo Ahn, Yoan Shin, and Sungbin Im. A block coding scheme for peak-to-average power ratio reduction in an orthogonal frequency division multiplexing system. In *Vehicular Technology Conference Proceedings, 2000. VTC 2000-Spring Tokyo. 2000 IEEE 51st*, volume 1, pages 56–60. IEEE, 2000.

[32] Robert W Bäuml, Robert FH Fischer, and Johannes B Huber. Reducing the peak-to-average power ratio of multicarrier modulation by selected mapping. *Electronics Letters*, 32(22):2056–2057, 1996.

[33] Stefan H Müller and Johannes B Huber. Ofdm with reduced peak-to-average power ratio by optimum combination of partial transmit sequences. *Electronics letters*, 33(5):368–369, 1997.

[34] Homayoun Nikookar and Knut Sverre Lidsheim. Random phase updating algorithm for ofdm transmission with low papr. *Broadcasting, IEEE Transactions on*, 48(2):123–128, 2002.

[35] Serdar Sezginer and Hikmet Sari. Peak power reduction in ofdm systems using dynamic constellation shaping. In *Signal Processing Conference, 2005 13th European*, pages 1–4. IEEE, 2005.

[36] Brian Scott Krongold. *New techniques for multicarrier communication systems*. PhD thesis, University of Illinois at Urbana-Champaign, 2003.

[37] Jose Tellado. *Multicarrier modulation with low PAR: applications to DSL and wireless*, volume 587. Springer Science & Business Media, 2006.

[38] Alan V Oppenheim, Ronald W Schafer, John R Buck, et al. *Discrete-time signal processing*, volume 2. Prentice-hall Englewood Cliffs, 1989.

[39] John G Proakis. *Intersymbol Interference in Digital Communication Systems*. Wiley Online Library, 2001.

[40] Robert J Baxley and G Tong Zhou. Power savings analysis of peak-to-average power ratio in ofdm. *Consumer Electronics, IEEE Transactions on*, 50(3): 792–798, 2004.

[41] Richard Van Nee and Amout De Wild. Reducing the peak-to-average power ratio of ofdm. In *Vehicular Technology Conference, 1998. VTC 98. 48th IEEE*, volume 3, pages 2072–2076. IEEE, 1998.

[42] Hideki Ochiai and Hideki Imai. On the distribution of the peak-to-average power ratio in ofdm signals. *Communications, IEEE Transactions on*, 49(2): 282–289, 2001.

[43] Shuangqing Wei, Dennis L Goeckel, and Patrick E Kelly. A modern extreme value theory approach to calculating the distribution of the peak-to-average power ratio in ofdm systems. In *Communications, 2002. ICC 2002. IEEE International Conference on*, volume 3, pages 1686–1690. IEEE, 2002.

[44] Hua Yu, Min Chen, and Gang Wei. Distribution of par in dmt systems. *Electronics Letters*, 39(10):799–801, 2003.

[45] Hao Wang and Biao Chen. On the distribution of peak-to-average power ratio for non-circularly modulated ofdm signals. In *Global Telecommunications Conference, 2003. GLOBECOM'03. IEEE*, volume 1, pages 502–506. IEEE, 2003.

[46] Yao-Hong You, I-T Hwang, C-K Song, and Hyoung-Kyu Song. Apr analysis for multi-band ofdm signals. *Electronics Letters*, 41(5):55–56, 2005.

[47] Youssif Fawzi Sharkasi, Mounir Ghogho, and D McLernon. Sensing-throughput tradeoff for ofdm-based cognitive radio under outage constraints. In *Wireless Communication Systems (ISWCS), 2012 International Symposium on*, pages 66–70. IEEE, 2012.

[48] Toon Van Waterschoot, Vincent Le Nir, Jonathan Duplicy, and Marc Moonen. Analytical expressions for the power spectral density of cp-ofdm and zp-ofdm signals. *Signal Processing Letters, IEEE*, 17(4):371–374, 2010.

[49] Theodore Wilbur Anderson, Theodore Wilbur Anderson, Theodore Wilbur Anderson, and Theodore Wilbur Anderson. *An introduction to multivariate statistical analysis*, volume 2. Wiley New York, 1958.

[50] M Barkat. Signal detection and estimation. 2005. *Artech House, Boston, London*.

[51] Hang Su and Xi Zhang. Cross-layer based opportunistic mac protocols for qos provisionings over cognitive radio wireless networks. *Selected Areas in Communications, IEEE Journal on*, 26(1):118–129, 2008.

[52] Xi Zhang and Hang Su. Cream-mac: Cognitive radio-enabled multi-channel mac protocol over dynamic spectrum access networks. *Selected Topics in Signal Processing, IEEE Journal of*, 5(1):110–123, 2011.

[53] Joseph Mitola. Cognitive radio—an integrated agent architecture for software defined radio. 2000.

[54] Yuqing Huang, Hong Jiang, Hong Hu, and Yuancheng Yao. Design of learning engine based on support vector machine in cognitive radio. In *Computational Intelligence and Software Engineering, 2009. CiSE 2009. International Conference on*, pages 1–4. IEEE, 2009.

[55] Brandon F Lo and Ian F Akyildiz. Reinforcement learning-based cooperative sensing in cognitive radio ad hoc networks. In *Personal Indoor and Mobile Radio Communications (PIMRC), 2010 IEEE 21st International Symposium on*, pages 2244–2249. IEEE, 2010.

[56] Vamsi Krishna Tumuluru, Ping Wang, and Dusit Niyato. A neural network based spectrum prediction scheme for cognitive radio. In *Communications (ICC), 2010 IEEE International Conference on*, pages 1–5. IEEE, 2010.

[57] Ananthram Swami and Brian M Sadler. Hierarchical digital modulation classification using cumulants. *Communications, IEEE Transactions on*, 48(3): 416–429, 2000.

[58] Octavia A Dobre, Ali Abdi, Yeheskel Bar-Ness, and Wei Su. Survey of automatic modulation classification techniques: classical approaches and new trends. *Communications, IET*, 1(2):137–156, 2007.

[59] George Hatzichristos and Monique P Fargues. A hierarchical approach to the classification of digital modulation types in multipath environments. In *Signals, Systems and Computers, 2001. Conference Record of the Thirty-Fifth Asilomar Conference on*, volume 2, pages 1494–1498. IEEE, 2001.

[60] Soodesh Buljore, Hiroshi Harada, Stanislav Filin, Paul Houze, Kostas Tsagkaris, Oliver Holland, Klaus Nolte, Tim Farnham, and Vladimir Ivanov. Architecture and enablers for optimized radio resource usage in heterogeneous wireless access networks: the ieee 1900.4 working group. *Communications magazine, IEEE*, 47(1):122–129, 2009.

[61] RP-140481. New sid: Study on licensed-assisted access using lte. 2014.

[62] RP-140060. Summary of workshop on lte in unlicensed spectrum. 2014.

[63] RP-140057. On the primacy of licensed spectrum in relation to the proposal of using lte for licensed assisted access to unlicensed spectrum. 2014.

[64] Qixun Zhang, Zhiyong Feng, Fang Tian, and Zheng Hu. A novel mesh division scheme using cognitive pilot channel in cognitive radio environment. In *Vehicular Technology Conference Fall (VTC 2009-Fall), 2009 IEEE 70th*, pages 1–6. IEEE, 2009.

[65] Jordi Pérez-Romero, Oriol Sallent, Ramón Agustí, and Lorenza Giupponi. A novel on-demand cognitive pilot channel enabling dynamic spectrum allocation. In *New Frontiers in Dynamic Spectrum Access Networks, 2007. DySPAN 2007. 2nd IEEE International Symposium on*, pages 46–54. IEEE, 2007.

[66] Zhi Quan, Shuguang Cui, Ali H Sayed, and H Vincent Poor. Wideband spectrum sensing in cognitive radio networks. In *Communications, 2008. ICC'08. IEEE International Conference on*, pages 901–906. IEEE, 2008.

[67] Ling Liu, Yiqing Zhou, Lin Tian, and Jinglin Shi. Cpc-based backward-compatible network access for lte cognitive radio cellular networks. *Communications Magazine, IEEE*, 53(7):93–99, 2015.